A timer gene network is spatially regulated by the terminal system in the *Drosophila* embryo

Erik Clark[1,2,3*†], **Margherita Battistara**[1,4], **Matthew A. Benton**[1,5*‡]

***For correspondence:** ec491@cam.ac.uk (EC); matthewabenton@gmail.com (MAB)

Present address: †Department of Genetics, University of Cambridge, UK; ‡Developmental Biology Unit, EMBL, Heidelberg, Germany

[1]Department of Zoology, University of Cambridge, UK; [2]Department of Systems Biology, Harvard Medical School, USA; [3]Department of Genetics, University of Cambridge, UK; [4]Department of Physiology, Development and Neuroscience, University of Cambridge, UK; [5]Developmental Biology Unit, EMBL, Heidelberg, Germany

Abstract In insect embryos, anteroposterior patterning is coordinated by the sequential expression of the "timer" genes *caudal*, *Dichaete* and *odd-paired*, whose expression dynamics correlate with the mode of segmentation. In *Drosophila*, the timer genes are expressed broadly across much of the blastoderm, which segments simultaneously, but their expression is delayed in a small "tail" region, just anterior to the hindgut, which segments during germband extension. Specification of the tail and the hindgut depends on the terminal gap gene *tailless*, but beyond this the regulation of the timer genes is poorly understood. We used a combination of multiplexed imaging, mutant analysis, and gene network modelling to resolve the regulation of the timer genes, identifying 11 new regulatory interactions and clarifying the mechanism of posterior terminal patterning. We propose that a dynamic Tailless expression gradient modulates the intrinsic dynamics of a timer gene cross-regulatory module, delineating the tail region and delaying its developmental maturation.

Introduction

Insect segments are patterned by a relatively conserved gene regulatory network including gap genes, pair-rule genes and segment-polarity genes (reviewed in ***Nasiadka et al., 2002***; ***Hughes and Kaufman, 2002***; ***Clark et al., 2019***). Within and across species, embryonic development depends on these network components being activated at the right times and in the right places. Locally, the maturation of any given segment involves segmentation genes being activated in a conserved temporal sequence (e.g., primary pair-rule genes before secondary pair-rule genes and segment-polarity genes; ***Akam, 1987***; ***Baumgartner and Noll, 1990***; ***Schroeder et al., 2011***; ***Clark and Akam, 2016***). Globally, the relative timing of segmentation across the anteroposterior (AP) axis correlates with the specific developmental mode of each species, ranging from predominantly sequential, germband-based patterning in the cricket *Gryllus bimaculatus* or the beetle *Tribolium castaneum*, to more-or-less simultaneous, blastoderm-based patterning in the fruit fly *Drosophila melanogaster* (reviewed in ***Davis and Patel, 2002***).

Previously, we have proposed that segment patterning is coordinated by an underlying framework of "timer gene" (alternatively, "timing factor") expression, which broadly regulates segmentation gene expression in time and space (***Clark and Peel, 2018***; ***Clark et al., 2019***). We identified the timer genes (not necessarily exhaustively) as *caudal* (*cad*; ***Mlodzik et al., 1985***; ***Macdonald and Struhl, 1986***), *Dichaete* (*D*; ***Russell et al., 1996***; ***Nambu and Nambu, 1996***), and *odd-paired* (*opa*;

Benedyk et al., 1994), all of which code for transcription factors. The expression dynamics of these genes correlate with the progression of segmentation: in *Drosophila* they are expressed sequentially within the blastoderm, while in *Tribolium* the same expression sequence occurs in cells emerging from the segment addition zone into the segmented germ band (*Schulz et al., 1998*; *Copf et al., 2004*; *El-Sherif et al., 2014*; *Clark and Peel, 2018*). In addition, the protein products of these genes are known to directly regulate many segmentation genes in *Drosophila* (*Rivera-Pomar et al., 1995*; *Schulz and Tautz, 1995*; *La Rosee, 1997*; *Häder et al., 1998*; *Ma et al., 1998*; *Clark and Akam, 2016*; *Vincent et al., 2018*; *Soluri et al., 2020*; *Koromila et al., 2020*).

However, we currently do not understand how the timer genes themselves are spatiotemporally regulated within the embryo. What accounts for their local sequential activation in segmenting tissues, and why are these dynamics so deeply conserved across species? How is their expression globally regulated along the AP axis, and why is this regulation so evolutionarily flexible?

Here, we investigate these issues in the *Drosophila* embryo, exploiting the fact that segmentation in this model species is not quite so simultaneous as it is often described. Although most of the *Drosophila* blastoderm is patterned simultaneously before gastrulation, the most posterior part of the segmental ectoderm is not patterned until germband extension (*Kuhn et al., 2000*). This "tail" region (see *Box 1*) is located posterior to abdominal segment 8 (A8) and anterior to the prospective hindgut, and eventually gives rise to a set of ectodermal structures known as the embryonic terminalia (*Turner and Mahowald, 1979*; *Sato and Denell, 1986*; *Jürgens, 1987*). Consistent with the timer gene hypothesis, the tail exhibits *cad*, *D*, and *opa* expression dynamics which differ from those in the rest of the trunk (*Macdonald and Struhl, 1986*; *Russell et al., 1996*; *Clark and Akam, 2016*; *Clark and Peel, 2018*), correlating with the difference in segmentation dynamics.

The patterning of the tail region is dependent on the posterior terminal system (reviewed in *Perkins and Perrimon, 1991*), and, in particular, on its downstream effector, Tailless (Tll; *Strecker et al., 1986*; *Pignoni et al., 1990*). Tll has well-characterised effects on gap gene expression (*Jaeger, 2011*; *Janssens et al., 2013*), but its contribution to timer gene regulation is relatively unexplored. As a consequence, the specific regulatory interactions that mediate tail patterning remain unknown (*Casanova, 1990*; *Wu and Lengyel, 1998*; *Smits and Shvartsman, 2020*).

In this study, we discover that *Drosophila* timer gene expression is shaped by a combination of cross-regulatory interactions and extrinsic spatiotemporal inputs. Using multiplexed hybridisation chain reaction in situ hybridisation (HCR ISH; *Choi et al., 2016*; *Trivedi et al., 2018*; *Choi et al., 2018*), we first show that the tail region gives rise to two sets of parasegment-like boundaries after gastrulation, clarifying its segmental nature. We then characterise timer gene expression in wild-type embryos, timer gene mutants, and terminal system mutants, uncovering 11 new regulatory interactions within the *Drosophila* AP patterning network. Using a simple logical model, we show that the revised network both explains wild-type patterning dynamics and recapitulates the mutant phenotypes we examined. We conclude by discussing which aspects of timer gene regulation are likely to be conserved or divergent across species.

Results

Two parasegment-like boundaries form sequentially from the *Drosophila* tail region after gastrulation

The *Drosophila* embryo is well-known for its simultaneous mode segmentation, in which a segmental pattern is laid down at the end of the blastoderm stage, prior to significant morphogenetic movements. 14 prospective parasegment boundaries appear at this stage, marked by segmental stripes of segment-polarity gene expression (*DiNardo, 1985*; *Baumgartner et al., 1987*; *Baker, 1988*; *Lee et al., 1992*; *Grossniklaus et al., 1992*).

Sandwiched in between parasegment boundary 14 (PSB14; see *Box 1*) and the broad posterior domain of *wg* (thought to correspond to prospective hindgut; *Baker, 1988*) are about 4 cell rows of ectoderm that remain unpatterned by segment-polarity genes at the end of the blastoderm stage

Box 1: Notes on terminology

Morphological segments are offset from the initial metameric subdivisions of the embryo, the **parasegments**, by about 2/3 of a segment repeat (***Martinez-Arias and Lawrence, 1985***; ***Lawrence et al., 1985***; ***Ingham et al., 1985***; also see ***Figure 1***C). The *n*th **parasegment boundary** (PSB*n*) refers to the anterior boundary of parasegment *n*.

Segment-polarity stripes are conventionally numbered according to the parasegment they are located within (***Baker, 1987***; also see ***Figure 1***A,C). Thus, the first *en* stripe is en1, because it marks the anterior of parasegment 1, and the 14th *en* stripe is en14. The first *wingless* (*wg*) stripe, expressed just anterior to en1, is wg0, and the 14th wg stripe, expressed just anterior to en14, is wg13.

The term **telson** has been used to refer to the posterior region of the *Drosophila* embryo/larva (usually everything posterior to A8, sometimes everything posterior to A7; ***Lohs-Schardin et al., 1979***; ***Sato and Denell, 1986***; ***Nusslein-Volhard et al., 1987***; ***Perkins and Perrimon, 1991***). As "telson" generally refers to a terminal non-segmental region of an animal (***Snodgrass, 1935***), or at least its most posterior segment, it is non-standard to use this word to refer to a region that contains more than one segment. We therefore use the more neutral term **tail** (***Jürgens, 1987***) to refer to the region posterior to PSB14 and anterior to the hindgut.

(***Figure 1***A, stage 6). This "tail" region (see ***Box 1***) goes on to form the most terminal structures of the larva (***Turner and Mahowald, 1979***; ***Jürgens, 1987***), including a 15th parasegment boundary (***Kuhn et al., 1995***, ***2000***), various sensory organs (***Sato and Denell, 1986***; ***Jürgens, 1987***; ***Kuhn et al., 1992***) and the anal pads (external organs involved in ion transport; ***Jarial, 1987***).

The segmental nature of the tail is unclear. The tissue just posterior to PSB15 is abdominal segment 10 (A10; ***Figure 1***C). Some authors consider the region to contain a cryptic 11th abdominal segment as well (***Jürgens, 1987***; ***Baumgartner et al., 1987***), but most do not (see The segmental character of the *Drosophila* tail) and to the best of our knowledge a 16th parasegment boundary has not been described. To investigate this issue, we used multiplexed HCR ISH to re-examine the expression of the parasegment boundary markers *wingless* (*wg*; ***Baker, 1987***; ***Rijsewijk et al., 1987***), *engrailed* (*en*; ***Kornberg et al., 1985***; ***Fjose et al., 1985***), *sloppy-paired* (*slp*; ***Grossniklaus et al., 1992***), and *even-skipped* (*eve*; ***Macdonald et al., 1986***) during germband extension and extended germband stages (***Figure 1***; ***Figure 1—figure Supplement 1***).

wg and *en* expression in the tail

The *wg* and *en* stripes associated with PSB15 emerge during germband extension (***Figure 1***A, stages 8.3-8.4). In contrast to published descriptions of *wg* expression (***Baker, 1987***, ***1988***), we identified an additional *wg* stripe, wg15, which appeared after germband extension (***Figure 1***A, stage 11.1). During subsequent development, a medial patch of *en* expression appeared posteriorly adjacent to wg15 (***Figure 1***A, stage 11.2). This "en16" domain is clearly not a full stripe as found in parasegment boundaries 1-15. However, the domain marks the median neuroblast lineage of abdominal segment 10 (***Birkholz et al., 2013***), and median neuroblasts always originate from posterior segment compartments (***Bate, 1976***; ***Doe, 1992***; ***Biffar and Stollewerk, 2014***). wg15 and en16 therefore seem to correspond to a vestigial 16th parasegment boundary within the *Drosophila* embryo (***Figure 1***C).

slp and *eve* expression in the tail

In the simultaneously-segmenting region of the embryo (here, termed the "trunk"), segment-polarity domains are initially patterned by stripes of pair-rule gene expression (***DiNardo and O'Farrell, 1987***; ***Jaynes and Fujioka, 2004***; ***Clark, 2017***). In the tail, PSB15 is prefigured by pair-rule gene stripes slp14 and eve15, which appear after gastrulation (***Macdonald et al., 1986***; ***Grossniklaus et al., 1992***; ***Kuhn et al., 2000***). We found that slp14 and eve15 emerged simultaneously early in germband extension (***Figure 1***B, stage 8.1), at around the same time as the polarised cell divisions of mitotic domain 4

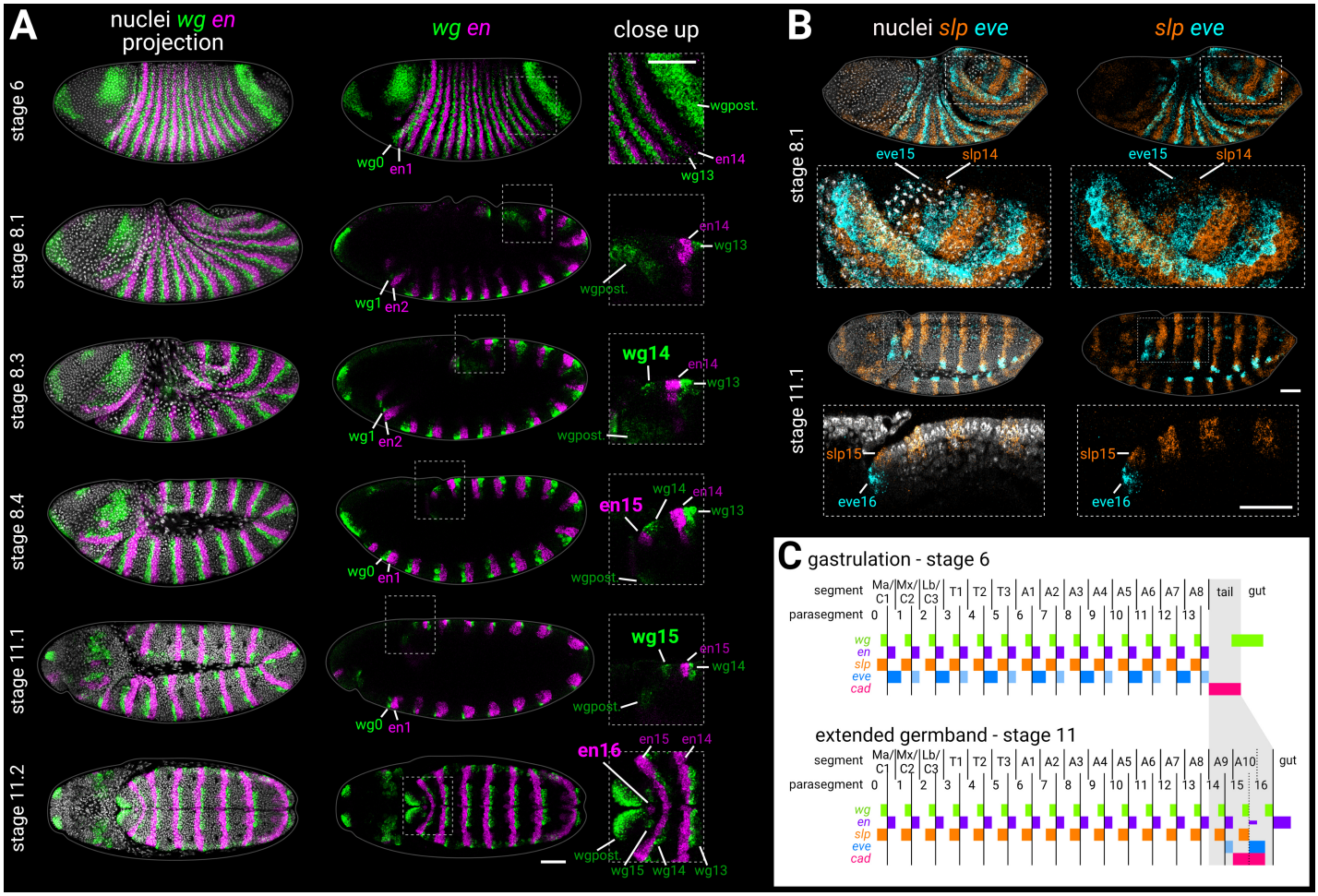

Figure 1: Segmentation of the tail region after gastrulation. **A**: *wg* and *en* expression from gastrulation to extended germband. Left column shows merged maximum projections of *wg*, *en*, and DAPI (nuclei). Middle column shows merged *wg* and *en* expression, either maximum projections (stage 6, stage 11.2), or sagittal sections (stage 8.1 to stage 11.1). Enlarged close-ups of the boxed regions are shown in the right column. Key expression domains are annotated with labels; newly-established domains are shown in large font; wgpost = *wg* posterior domain. Stages 6-11.1 show lateral views, stage 11.2 is a "dorsal" view which actually mainly shows the ventral side of the posterior germband, due to germband extension. **B**: *slp1* (*slp*) and *eve* expression during the division of mitotic domain 4 (stage 8.1) and at extended germband (stage 11.1). Both stages show dorsolateral views. Left column shows a merge with DAPI (nuclei); right column shows gene expression alone. Enlarged close-ups of the boxed regions are shown below the whole embryo views; see ***Appendix 2*** for details of how the close-up for stage 11.1 was re-sliced. Key expression domains are annotated with labels. **C**: schematic diagram showing the expression of key segmentation genes before tail segmentation (stage 6) and after tail segmentation (stage 11). The tail region is shaded in grey; note the expansion of the region due to morphogenesis, and the refinement of the *cad* domain. PSB16 is shown as a dotted line due to its vestigial nature; en16 is also depicted as narrower than the other domains. Lighter shading for *eve* domains represents weaker or decaying expression. C1-3 = gnathal segments; T1-3 = thoracic segments; A1-10 = abdominal segments; Ma = mandibular segment; Mx = maxillary segment; Lb = labial segment. All embryos are anterior left, dorsal up. Scale bars = 50 μm; grey lines show embryo outlines.

Figure 1—figure supplement 1. Single channel images.

(***Foe, 1989***; ***da Silva and Vincent, 2007***) . At the end of germband extension, we were surprised to find that an additional set of abutting *slp* and *eve* stripes, slp15 and eve16, emerged posterior to PSB15 (***Figure 1***B, stage 11.1), in the same region as wg15 and en16. This finding supports our conclusion that wg15 and en16 are segmental in nature.

To the best of our knowledge, the slp15 domain has not been described previously. Persistent

eve expression at the posterior of the embryo is well-known, although it has been described as a remnant of eve15 (***Macdonald et al., 1986***; ***Frasch et al., 1987***; ***Sackerson et al., 1999***; ***Kuhn et al., 2000***) or the 7th *eve* pair-rule stripe (***Singer et al., 1996***) rather than a separate domain. [Note that eve15 is described by some authors (e.g., ***Sackerson et al., 1999***) as the 8th stripe of *eve*, not counting the seven "minor" *eve* stripes that appear at even-numbered parasegment boundaries just before gastrulation.]

In summary, we propose that two parasegment-like boundaries form sequentially from the tail region of the *Drosophila* embryo after gastrulation (***Figure 1***C). In both cases, segment-polarity gene expression is preceded by a template of abutting *slp* and *eve* expression, similar to the odd-numbered parasegment boundaries of the trunk; (***Lawrence et al., 1987***; ***Cadigan et al., 1994***). Unlike in the trunk, however, the resolved segmental *eve* stripes appear de novo and are not preceded by a pair-rule phase of expression.

Timer gene expression differs between the trunk and the tail

Given that *Drosophila* shows distinct segmentation dynamics in the trunk and the tail, we examined the expression of the timer genes (*cad*, *D* and *opa*) in these regions during blastoderm stages and early germband extension (for an earlier survey using an inferior in situ hybridisation method, see ***Clark and Peel, 2018***). To account for the movement of nuclei/cells during blastoderm (***Keränen et al., 2006***) and gastrulation stages, we co-stained the timer genes with *wg* and used the posterior *wg* domain as a fiducial marker. (The posterior *wg* domain appears to be stable relative to nuclei, as nuclear transcription foci are not offset anteriorly or posteriorly relative to cytoplasmic transcripts.) To aid with fine scale staging of embryos, we have divided stage 5, which lasts ~40 minutes at 25° C, into 5 timeclasses based on gene expression and morphology (see ***Appendix 1***).

Timer gene expression in the trunk

In the trunk, *cad*, *D*, and *opa* transcripts are expressed sequentially over stages 4-6; first *cad*, then *D*, then *opa* (***Figure 2***; ***Figure 2—figure Supplement 2***). Despite some AP intensity modulation (presumably downstream of gap and pair-rule genes), similar temporal dynamics are present across the whole trunk region, consistent with its simultaneous mode of segmentation. *cad*, which is maternally deposited and then zygotically expressed, clears from the trunk by stage 5.4 (***Levine et al., 1985***; ***Mlodzik et al., 1985***; ***Hoey et al., 1986***; ***Macdonald and Struhl, 1986***; ***Mlodzik and Gehring, 1987a***; ***Schulz and Tautz, 1995***). *D*, which is detectable from stage 4.1 (nuclear cycle 10), reaches appreciable levels at stage 4.4 (nuclear cycle 13), rapidly reaches a very high peak at stage 5.2, then declines sharply, with residual expression clearing by stage 6, replaced ventrally by persistent expression in the neuroectoderm (***Russell et al., 1996***; ***Nambu and Nambu, 1996***). Finally, *opa* appears at stage 5.1, rapidly builds to high levels, then tapers off during germband extension (***Benedyk et al., 1994***; ***Clark and Akam, 2016***).

Cad, D, and Opa protein dynamics broadly match their respective transcript dynamics, albeit with time-lags for synthesis and decay (***Figure 2—figure Supplement 3***; ***Figure 2—figure Supplement 4***). Cad levels decrease steadily in the trunk over stage 5 (see Figure 2B in ***Surkova et al., 2008***). D levels rise and fall gradually from stage 4.4 to stage 6, peaking at mid stage 5 (***Figure 2—figure Supplement 3***; ***Figure 2—figure Supplement 4***C). Finally, Opa levels increase throughout stage 5 and into stage 6 (***Figure 2—figure Supplement 4***B; see also the live quantification of llama-tagged Opa in ***Soluri et al., 2020***). Segmentation stages in the trunk are therefore characterised temporally by decreasing Cad levels, increasing Opa levels, and a pulse of D expression in between (***Figure 2—figure Supplement 4***D).

Timer gene expression in the tail

In the tail, a similar *cad*/*D*/*opa* expression sequence is evident, but delayed with respect to the trunk (***Figure 2***). *cad* is expressed continuously in the tail region throughout stage 5 and into germband extension. In contrast, *D* and *opa* expression in the tail region remains either low (*D*) or absent (*opa*)

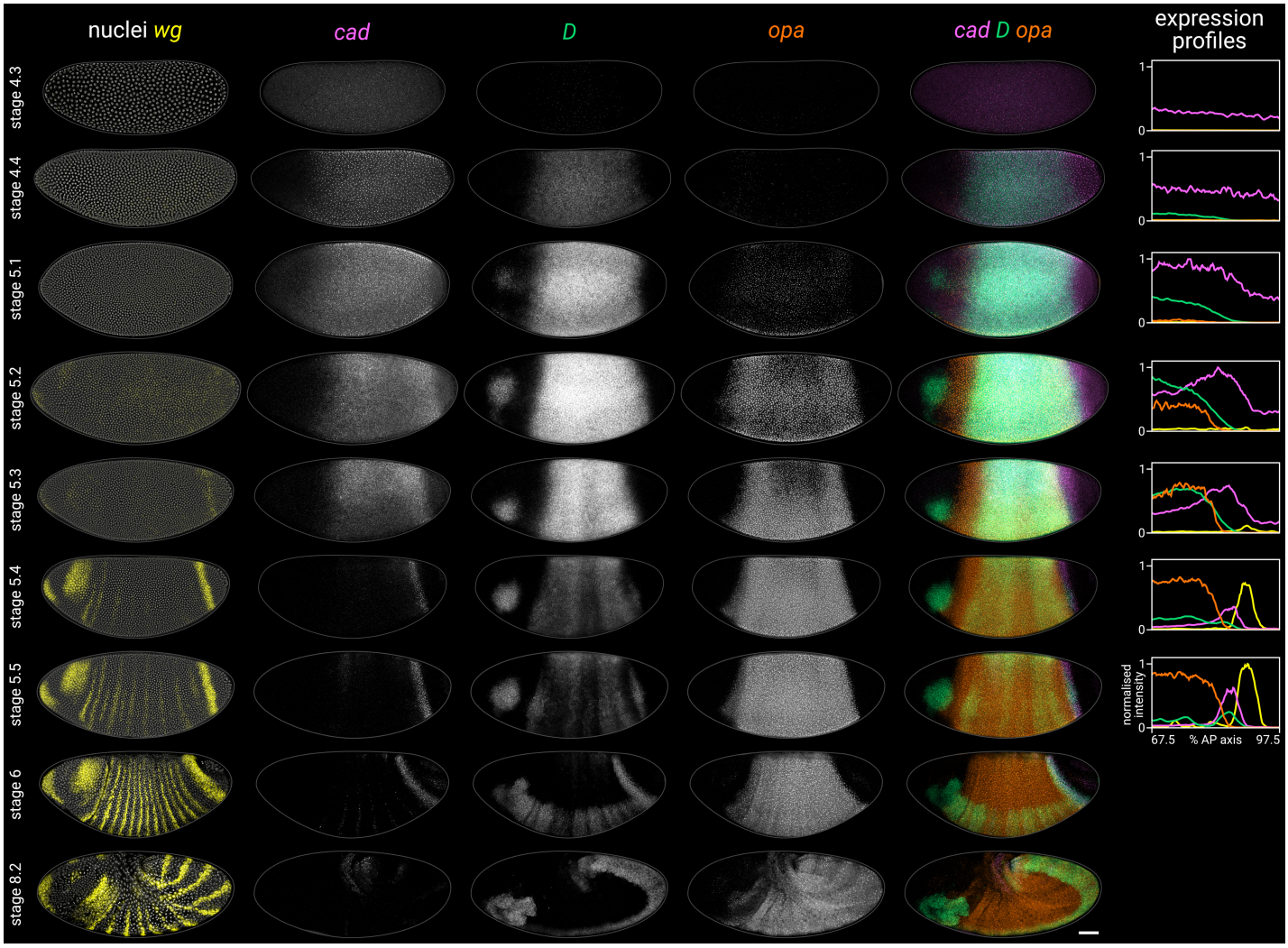

Figure 2: Timer gene expression dynamics in wild-type embryos. Column 1 shows a two-channel *wg* and DAPI (nuclei) merge for embryos of gradually increasing age; columns 2-4 show *cad*, *D*, and *opa* channels from the same embryos; column 5 shows a three-channel *cad* / *D* / *opa* merge. The plots at the right show quantitative expression traces (67.5-97.5% AP axis; all measurements from the anterior pole) for all four genes, extracted from the embryos pictured to the left (see ***Appendix 2***). The stage 4.3, stage 4.4 and stage 5.1 embryos are from a different scanning session compared to the rest of the figure. All embryos are anterior left, dorsal up. Stages 4.3-6 show lateral views; stage 8.2 is dorsolateral. Scale bar = 50 μm; grey lines show embryo outlines.

Figure 2—source data 1. Expression trace source data.

Figure 2—figure supplement 1. Additional single channel images.

Figure 2—figure supplement 2. Additional early stage embryos.

Figure 2—figure supplement 3. D antibody staining in embryos from stage 4 to stage 6.

Figure 2—figure supplement 4. Expression dynamics of timer gene transcripts and proteins.

Figure 2—figure supplement 4—source data 1. Expression trace source data

through most of stage 5. At stage 5.4, a *D* tail domain emerges within the lateral part of the *cad* tail domain, rapidly strengthening and extending dorsoventrally. D protein becomes prominent in the tail domain at stage 6 (***Figure 2—figure Supplement 3***; ***Figure 2—figure Supplement 4***C), again reflecting a modest time-lag for protein synthesis. Finally, *opa* expression expands into the tail region from late stage 5 (described below).

High-resolution close-ups of nascent transcripts, mature transcripts, and synthesised protein (***Figure 3***; ***Figure 3—figure Supplement 1***) reveal subtle posterior shifts. The *cad* tail domain is

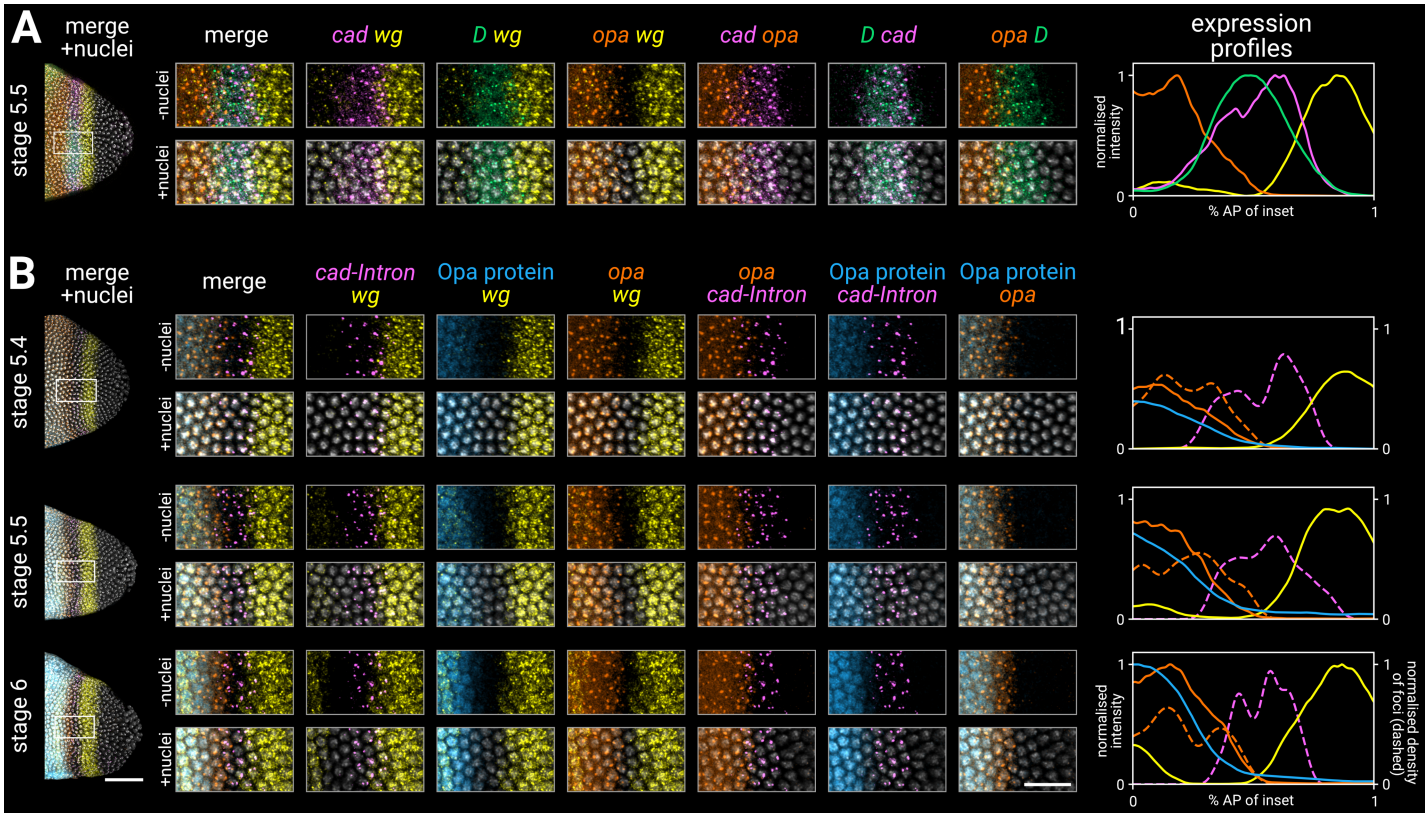

Figure 3: Timer gene expression in the tail region of wild-type embryos at high resolution. **A**, **B**: leftmost column shows the posterior ends of the selected embryos, each with a boxed region of interest in the tail; middle columns show high-resolution close-ups of the boxed region without and with DAPI signal ("-nuclei" vs "+nuclei"); rightmost column shows quantitative expression traces along the x-axis of the boxed region. **A**: timer gene expression, as in ***Figure 2***. **B**: *wg* and *opa* expression (as in A), combined with a *cad* intronic probe (*cad-Intron*, showing intranuclear transcription foci) and an antibody stain for Opa protein. Solid lines in the expression plots show the average intensity of *wg*, *opa*, and Opa protein; dashed lines show the normalised density of *cad* and *opa* transcription foci (see ***Appendix 2***). Note the staggered AP distributions of Opa protein, *opa* transcript, and *opa* transcription foci, the shrinking gap between the posterior *wg* domain and the *opa*/Opa signal, and the refinement of the *cad-Intron* domain over time. All embryos are anterior left, dorsal up, lateral view. Scale bars = 50 μm (embryo posteriors), 20 μm (boxed close-ups). For the high-resolution close-ups, the curvature of the tissue was straightened prior to z-projection (see ***Appendix 2***).

Figure 3—figure supplement 1. Single channel images.

mostly anterior to the *wg* posterior domain, with an overlap of a single cell row (***Figure 3***A *cad*/*wg* merge). At stage 5.4, *cad* is actively transcribed in a domain 3-4 cells wide, but this shrinks to 2-3 cells wide by stage 6, with transcription ceasing at the anterior edge (*cad* intronic probe, ***Figure 3***B). Throughout this period, the domain of active *opa* transcription, marked by prominent intranuclear foci, extends about one cell row posterior to the Opa protein domain (***Figure 3***B Opa/*opa* merge), and also overlaps the *cad* domain by about one cell row (***Figure 3***A *cad*/*opa* merge; ***Figure 3***B *opa*/*cad-Intron* merge). This suggests that *opa* transcription gradually invades the *cad* tail domain from the anterior edge, with *cad* transcription then ceasing in these cells as Opa levels increase (***Figure 3***B Opa/*cad-intron* merge). Supporting this interpretation, we confirmed that a posterior expansion of Opa expression is evident in published live-imaging data (***Soluri et al., 2020***).

In summary, we find that timer gene expression differs sharply between the trunk and the tail, although both regions express *cad*, *D*, and *opa* in the same temporal sequence. The difference in timer gene expression between the trunk and the tail correlates with the difference in simultaneous versus sequential segmentation dynamics described above.

The timer genes are patterned by cross-regulation

The relative spatiotemporal expression dynamics of the timer genes are suggestive of cross-regulation. To investigate this possibility, we examined timer gene expression in *opa*$^{-}$, *D*$^{-}$ and *cad*$^{-}$ mutants (***Figure 4***; ***Figure 4—figure Supplement 1***), and discovered a variety of cross-regulatory effects. As *cad* is expressed maternally as well as zygotically, we examined *cad* maternal mutants (*cad*$^{m-z+}$) and *cad* zygotic mutants (*cad*$^{m+z-}$) in addition to *cad* null mutants (*cad*$^{m-z-}$), in order to disentangle maternal and zygotic effects (***Figure 4—figure Supplement 3***). We also examined timer gene expression in *wg*$^{-}$ mutants, but did not observe any aberrant expression in these embryos during our stages of interest (***Figure 4—figure Supplement 4***).

Timer gene expression in *opa*$^{-}$ mutants

In *opa*$^{-}$ mutants, trunk expression of *D* persisted longer than usual, resulting in a more prominent stripy pair-rule pattern, while the tail domain was stronger and extended further anterior than normal (***Figure 4***A,B; ***Figure 4—figure Supplement 1***B; ***Figure 4—figure Supplement 5***). The *cad* tail domain looked similar to wild-type at stage 5.5 (***Figure 4***A,B; ***Figure 4—figure Supplement 1***B), but was broader at stage 6 (***Figure 4—figure Supplement 5***), suggesting it failed to retract posteriorly as in wild-type. *opa* transcription and the posterior *wg* domain looked normal.

Timer gene expression in *D*$^{-}$ mutants

In *D*$^{-}$ mutants, *cad* expression persisted abnormally in the trunk, with marked AP modulation, and the *cad* tail domain extended further anterior than normal (***Figure 4***A-C; ***Figure 4—figure Supplement 1***B). The *D* allele we used had very low transcript levels (presumably due to nonsense-mediated decay, S. Russell pers. comm.), but the residual expression indicated that both the clearance of *D* expression from the trunk and the appearance of the *D* tail domain may have been delayed. The posterior *wg* domain, the posterior border of the *cad* tail domain, and the posterior border of the *opa* domain were all modestly anteriorly shifted relative to wild-type (***Figure 4***B; ***Figure 4—figure Supplement 1***A; ***Figure 4—figure Supplement 2***); even after allowing for this shift, the gap between the *wg* domain and the *opa* domain was slightly larger in *D*$^{-}$ embryos than in wild-type (***Figure 4—figure Supplement 1***B).

Timer gene expression in *cad*$^{m-z-}$ mutants

In *cad*$^{m-z-}$ mutants, *cad* expression persisted abnormally in the trunk (***Figure 4***A-C), though without the AP modulation seen in *D*$^{-}$ mutants. *D* expression levels were weaker than normal at early stage 5 (***Figure 4***C, stage 5.2), the *D* neuroectodermal expression domain appeared precociously (***Figure 4***C, stage 5.4), and the *D* tail domain was only expressed in the ventral half of the embryo (arrowhead in ***Figure 4***A). The posterior *wg* domain was generally absent (arrowhead in ***Figure 4***A; ***Wu and Lengyel, 1998***), although weak expression was observed in some embryos, consistent with the variability of the *cad*$^{m-z-}$ larval phenotype (***Macdonald and Struhl, 1986***). The *opa* domain showed strong pair-rule modulation in the anterior trunk (arrowheads in ***Figure 4***A; ***Figure 4—figure Supplement 2***).

Timer gene expression in *cad*$^{m+z-}$ and *cad*$^{m-z+}$ mutants

One copy of maternal *cad* (*cad*$^{m+z-}$ embryos) largely rescued the *cad*$^{m-z-}$ phenotype, except that the *D* tail domain was lost prematurely, during germband extension (***Figure 4—figure Supplement 3***B). The posterior *wg* domain was present, conflicting with a previous report (***Wu and Lengyel, 1998***).

One copy of zygotic *cad* (*cad*$^{m-z+}$ embryos) rescued the *D* tail domain fully, and partially rescued the *wg* posterior domain (***Figure 4—figure Supplement 3***C), but the blastoderm dynamics of *D* and *cad* expression were still perturbed.

Other observations from *cad*$^{m-z-}$ mutants

We wondered whether the premature neuroectodermal expression of *D* in *cad*$^{m-z-}$ mutants might indicate a more general pattern of precocious neuroectoderm development. To investigate this,

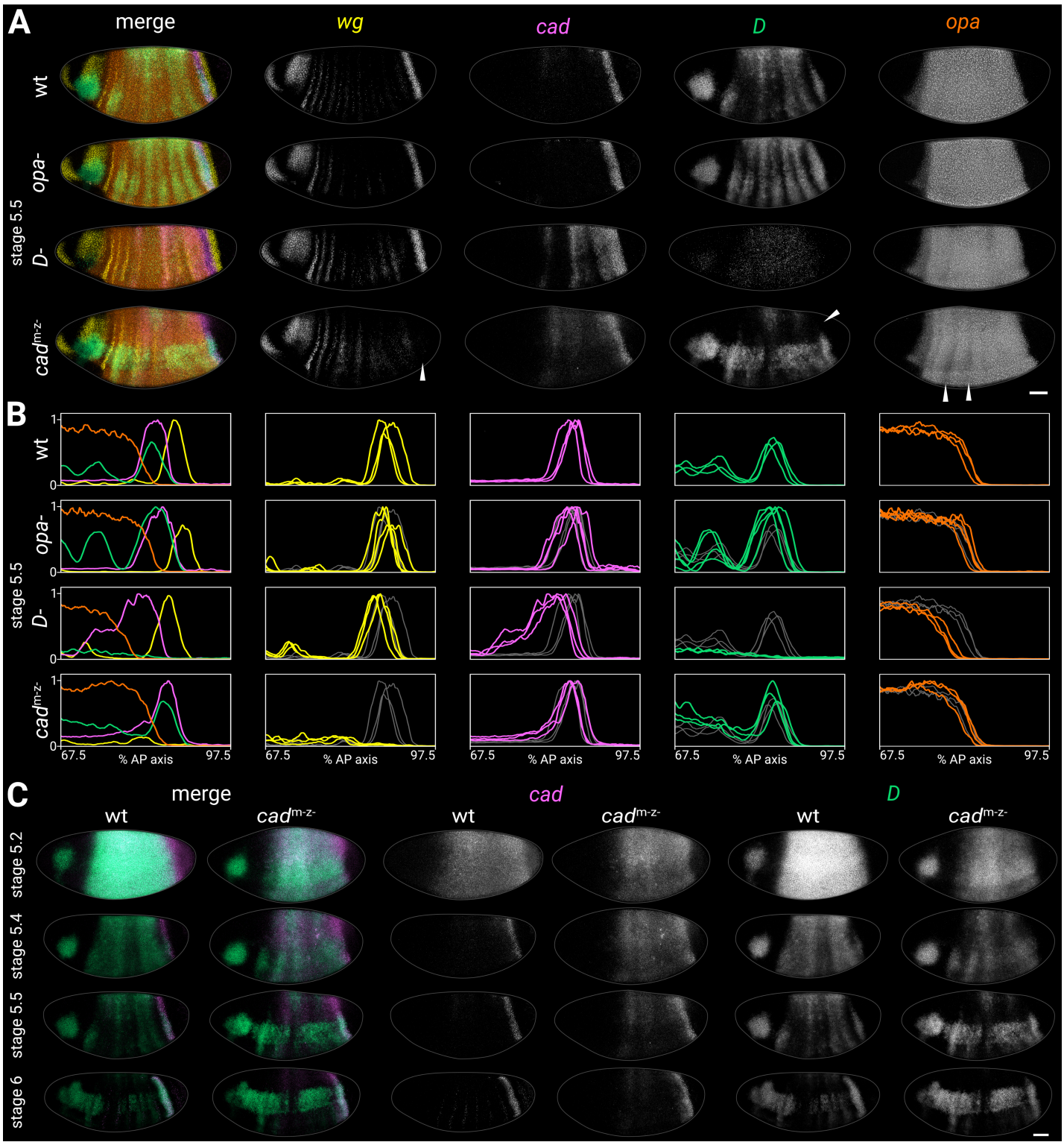

Figure 4: Timer gene expression in timer gene mutants. **A**: Timer gene expression in wild-type, *opa*$^{-}$ mutants, *D*$^{-}$ mutants, and *cad*$^{m\text{-}z\text{-}}$ mutants at stage 5.5. The leftmost column shows a four-channel merge and the other columns show individual channels. In the *cad*$^{m\text{-}z\text{-}}$ embryo, note the absence of the *wg* posterior domain (arrowhead in *wg* channel), the dorsal loss of the *D* tail domain (arrowhead in *D* channel), and the AP modulation of the *opa* trunk domain (arrowheads in *opa* channel). The brightness and contrast of the *D* channel was adjusted for the *D*$^{-}$ embryo to reveal the very weak residual signal. (Caption continued on next page.)

Figure 4: Timer gene expression in timer gene mutants (continued). **B**: quantitative expression traces (67.5-97.5% AP axis) from the individual embryos in A (multi-channel traces in leftmost column) or multiple stage 5.5 embryos (single-channel traces in other columns). All traces are individually normalised; mutant traces are overlaid on wild-type traces (grey) for ease of comparison. **C**: *cad* and *D* expression in wild-type and *cad*$^{m-z-}$ mutant embryos of gradually increasing age; left column shows a two-channel merge. In the *cad*$^{m-z-}$ embryos, note that *cad* transcript takes longer to clear from the trunk, while *D* is initially expressed at lower intensity and its neuroectodermal expression domain emerges earlier. All embryos are anterior left, dorsal up, lateral view. Scale bar = 50 μm; grey lines show embryo outlines.

Figure 4—source data 1. Expression trace source data.

Figure 4—figure supplement 1. Timer gene expression traces from timer gene mutants, relative to wild-type.

Figure 4—figure supplement 2. Full-length *opa* expression traces from timer gene mutants.

Figure 4—figure supplement 3. Additional characterisation of *cad*$^{m-z-}$, *cad*$^{m-z+}$, and *cad*$^{m+z-}$ mutants.

Figure 4—figure supplement 4. Timer gene expression in *wg*$^{-}$ mutants at stage 6.

Figure 4—figure supplement 5. Timer gene expression in *opa*$^{-}$, *tll*$^{-}$, and *tll*$^{-}$ *opa*$^{-}$ embryos at stage 6.

Figure 4—figure supplement 6. Morphological differences between wild-type and *cad*$^{m-z-}$ blastoderms.

Figure 4—figure supplement 6—source data 2. Measurements of wild-type and *cad*$^{m-z-}$ blastoderms.

we examined the expression of *muscle segment homeobox* (*msh*, also known as *Drop*; ***Lord et al., 1995***), a key neuroectoderm patterning gene expressed outside the *D* neuroectodermal domain. We found that *msh* was also expressed prematurely in *cad*$^{m-z-}$ mutants, particularly in posterior parts of the embryo (***Figure 4—figure Supplement 3***A).

Fixed and mounted *cad*$^{m-z-}$ embryos had a different range of shapes and sizes compared to wild-type embryos (***Figure 4—figure Supplement 6***). We did not investigate whether this was specifically due to the loss of Cad expression or an artefact of the "FLP-DFS" technique for generating germline clones (***Chou and Perrimon, 1996***). Given the robustness of AP patterning to variation in embryonic geometry (***Huang et al., 2020***), this minor morphological effect is unlikely to be the cause of the gene expression changes we observed.

In summary, our investigation of timer gene mutant phenotypes provides strong evidence for timer gene cross-regulation. *cad* is derepressed in *D*$^{-}$ mutants, and *D* is derepressed in *opa*$^{-}$ mutants. *cad*$^{m-z-}$ embryos have a complex phenotype in which the early expression of *D* is reduced, neuroectodermal gene expression is activated prematurely, the posterior *wg* domain is lost, and the *D* tail domain fails to activate dorsally. Finally, *opa* expression is fairly normal across all the mutants, except that its posterior border is anteriorly shifted in *D*$^{-}$ mutants.

These phenotypes, in combination with the expression dynamics described in the previous section, suggest that Opa represses *D* and *cad*, D represses *cad*, and Cad activates *D* (see ***Appendix 3*** for detailed reasoning). In addition, Cad is required for the expression of posterior *wg*, and D has a modest but concerted effect on the entire posterior fate map. Finally, most of the *cad*$^{m-z-}$ phenotype is mediated by maternal Cad, but zygotic Cad has specific late effects on *D* in the tail.

Tll and Hkb expression dynamics correlate with timer gene patterning in the posterior of the embryo

We next wanted to understand why timer gene expression differs between the trunk, tail, and prospective gut regions; i.e., how the timer gene network is spatially regulated. We therefore examined how timer gene expression relates to the expression domains of the zygotic terminal system genes *tll* (***Jürgens et al., 1984***; ***Strecker et al., 1986***; ***Pignoni et al., 1990***) and *huckebein* (*hkb*; ***Weigel et al., 1990***; ***Bronner and Jackle, 1991***), the obvious candidates for providing this spatial information.

tll and *hkb* expression dynamics

tll and *hkb*, which both code for repressive transcription factors, are expressed in nested domains at the posterior pole, with *tll* expression extending further from the pole than *hkb* expression (***Fig-***

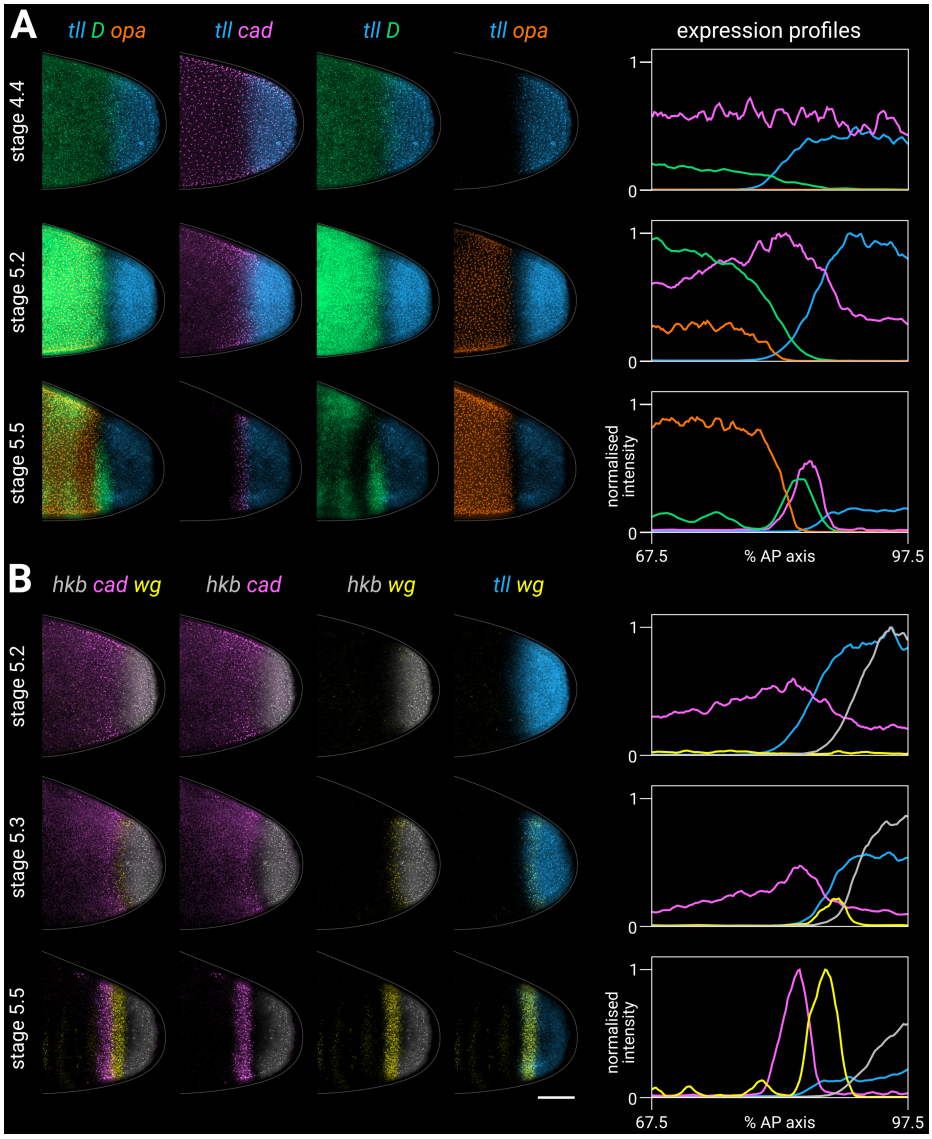

Figure 5: Timer gene expression relative to posterior terminal gene expression in wild-type embryos. **A**, **B**: timer and terminal gene expression in embryos of increasing age; only the posterior end of each embryo is shown. Left columns show either three-channel or two-channel merges; right column shows quantitative expression traces (67.5-97.5% AP axis) of all four genes in the stain (see ***Appendix 2***). **A**: timer gene expression relative to *tll*; note the posterior regression and changing intensity of the *tll* domain and the different spatial relationships with *opa*, *D*, and *cad*. **B**: *cad* and *wg* expression relative to *hkb* and *tll*; note how the posterior *wg* domain emerges within the *tll*-positive gap that opens up between *cad* and *hkb*. All embryos are anterior left, dorsal up, lateral view. Scale bar = 50 μm; grey lines show embryo outlines.

Figure 5—source data 1. Expression trace source data.

Figure 5—source data 2. Measurements of the size of the posterior *tll* expression domain at stage 5.2 versus 5.5.

Figure 5—figure supplement 1. Expression of *tll* and *hkb* in wild-type embryos from stage 2 to stage 6.

Figure 5—figure supplement 2. Single channel images.

Figure 5—figure supplement 3. Expression dynamics of *tll* and *hkb* transcripts.

Figure 5—figure supplement 3—source data 3. Expression trace source data.

Figure 5—figure supplement 4. Relative expression dynamics of Tll protein and *tll* transcript.

Figure 5—figure supplement 4—source data 4. Expression trace source data.

Figure 5—figure supplement 5. Relative expression dynamics of Hkb, Tll and Opa proteins.

Figure 5—figure supplement 5—source data 5. Expression trace source data.

Figure 5—figure supplement 6. Examples of source imaging data for supplementary plots.

ure 5; ***Figure 5—figure Supplement 1***; ***Pignoni et al., 1990***; ***Bronner and Jackle, 1991***). *tll* is transcribed at low levels from as early as nuclear cycle 9 (***Pignoni et al., 1992***), and we detected similar early transcription for *hkb*. Transcript levels in both domains peak at around stage 5.2 and then decline, with *tll* expression fading by stage 6 and *hkb* persisting at low levels after gastrulation (***Figure 5***; ***Figure 5—figure Supplement 1***; ***Figure 5—figure Supplement 3***). Previous studies (***Pignoni et al., 1990***, ***1992***) reported retraction of the *tll* border by about 5% egg length between stage 4.4 (nuclear cycle 13) and stage 5 (nuclear cycle 14); we noticed that this border also retracts by about 3-4 nuclear diameters over the course of stage 5 (***Figure 5—source data 2***). [Note that the absolute (% AP axis) shifts in ***Figure 5—figure Supplement 3*** appear smaller than this, because the posterior retraction of gene expression across nuclei is partially cancelled out by the anterior flow of nuclei away from the pole (***Keränen et al., 2006***).]

Tll and Hkb protein dynamics (***Figure 5—figure Supplement 4***; ***Figure 5—figure Supplement 5***) are spatiotemporally similar to *tll*/*hkb* transcript dynamics, albeit with a slight time lag, with the Tll protein border therefore lying slightly anterior to the *tll* transcript border during the second half of stage 5 (***Figure 5—figure Supplement 4***A). Our Tll antibody data closely resembles that collected by the Reinitz group, who noted that "*in contrast to the posterior domains of the other gap genes, the [Tll] posterior domain does not shift position with time*" (***Surkova et al., 2008***). We interpret the same data as providing evidence for a modest posterior retraction of the Tll domain over time, which does indeed contrast with the anterior shifts of the trunk gap genes, and is partially masked by anterior nuclear flow.

tll and *hkb* expression dynamics relative to the timer genes

The *tll* and *hkb* anterior borders correlate closely with the resolving expression boundaries of *cad*, *D*, *opa* and *wg* (***Figure 5***). At stage 4.4 (nuclear cycle 13), the graded *tll* border overlaps the graded posterior edge of the *D* domain (***Figure 5***A, top row). By mid stage 5, a narrow gap of low expression opens between the *tll* domain and the trunk domains of *D* and *opa* (***Figure 5***A, middle row), which is then filled by the *cad* and *D* tail domains at late stage 5 (***Figure 5***A, bottom row). *cad* is expressed ubiquitously throughout the posterior of the embryo at stage 4.4 (***Figure 5***B, top row), then fades from the *hkb* domain by mid stage 5 (***Figure 5***B, middle row), with a narrow gap of low expression opening up between the *cad* and *hkb* domains by late stage 5 (***Figure 5***B, bottom row). The *wg* posterior domain initiates at the border between *cad* and *hkb* expression present at mid stage 5 (***Figure 5***B, middle row), and by late stage 5 the *wg* posterior domain neatly demarcates the strip of *tll*-positive *hkb*-negative cells (***Figure 5***B, bottom row).

In summary, the spatiotemporal expression dynamics of Tll and Hkb make them good candidates for patterning the timer gene boundaries and the posterior *wg* domain, because they are differentially expressed across the various terminal regions. Specifically, from posterior to anterior, the prospective posterior midgut experiences strong expression of both Tll and Hkb, the prospective hindgut experiences strong expression of Tll but weak/transient expression of Hkb, the tail region experiences weak/transient expression of Tll, and the trunk is consistently free of Tll and Hkb expression.

The terminal system interacts with the timer gene network to pattern the posterior of the embryo

To determine whether Hkb and Tll spatially regulate the timer genes, we investigated timer gene expression in *hkb*$^{-}$ mutants, *tll*$^{-}$ mutants, and *torso* (*tor*$^{-}$) mutants (***Figure 6***). Tor (***Klingler et al., 1988***; ***Sprenger et al., 1989***; ***Casanova and Struhl, 1989***) is a maternally provided receptor necessary for transducing the extracellular signal-regulated kinase (ERK) signal that specifies the poles of the embryo (reviewed in ***Duffy and Perrimon, 1994***; ***Li, 2005***; ***Goyal et al., 2018***), and therefore *tor*$^{-}$ mutants express neither *hkb* nor *tll* (***Bronner and Jackle, 1991***; ***Pignoni et al., 1992***).

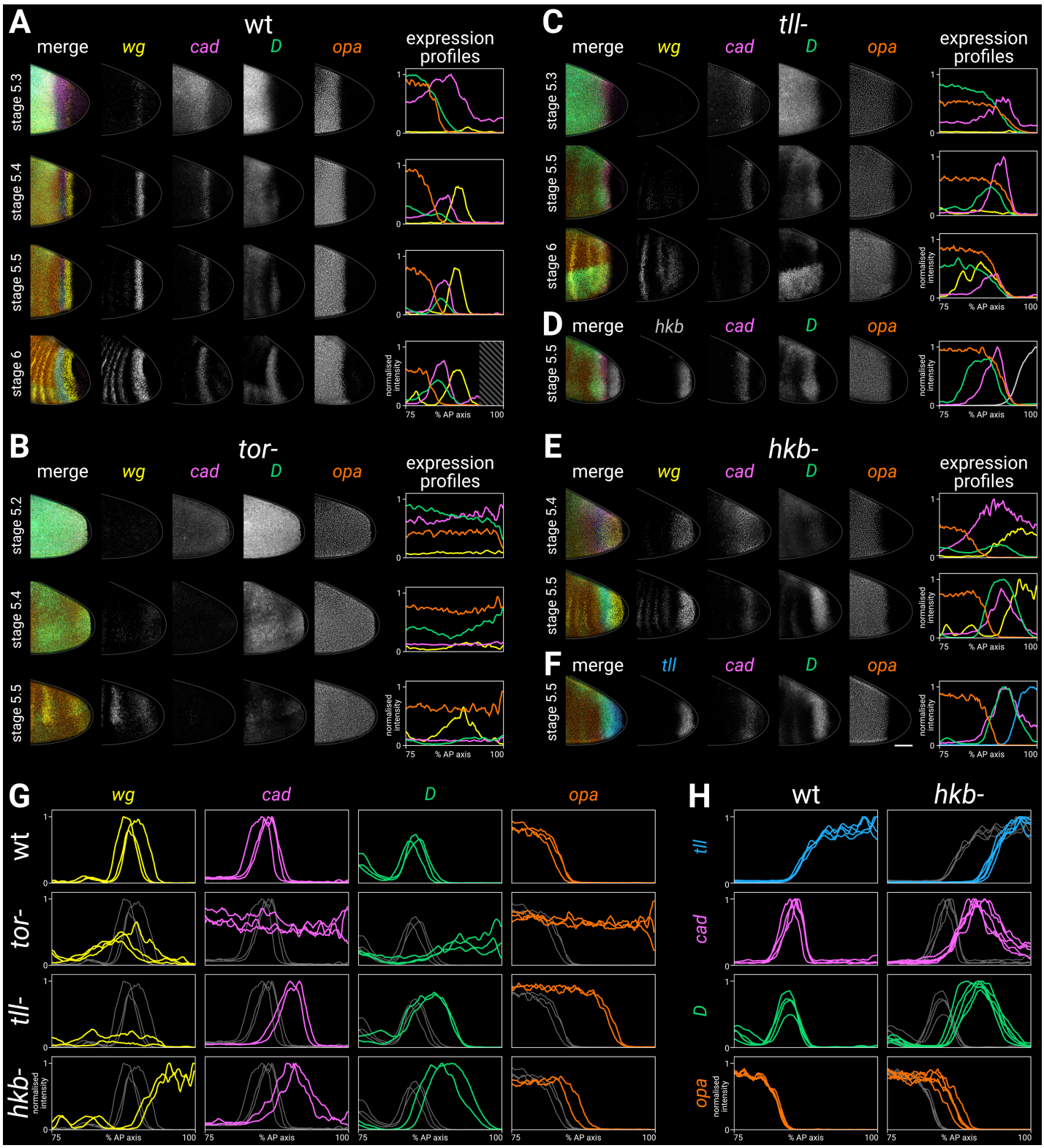

Figure 6: Timer gene expression in terminal system mutants. **A**-**F**: gene expression in wild-type and mutant embryos of increasing ages. The leftmost column shows a four-channel merge; the middle columns show individual channels; the rightmost column shows quantitative expression traces (75-100% AP axis) from the embryos shown to the left. **A**: timer gene expression in wild-type. The AP axis is truncated in the expression plot for the stage 6 embryo (diagonally shaded area) due to proctodaeal invagination. **B**: timer gene expression in *tor*⁻ mutants. Note how the timer gene expression expands all the way to the posterior pole (excluding the pole cells). (Caption continued on next page.)

Figure 6: Timer gene expression in terminal system mutants (continued). The broad posterior *wg* domain seen at stage 5.4-5.5 is mispatterned segmental expression; the posterior *wg* domain seen in wild-type embryos is absent. **C**: timer gene expression in *tll*$^-$ mutants, relative to *wg* expression. Note that the *cad*, *D*, and *opa* domains share a similar posterior border, the *cad* domain fades over time, and the *wg* posterior domain is absent. (Some mispatterned segmental *wg* expression is seen near the posterior of the embryo, similar to *tor*$^-$ mutants). **D**: timer gene expression in *tll*$^-$ mutants, relative to *hkb* expression. Note that the posterior borders of *cad*, *D* and *opa* all abut the *hkb* expression domain. **E**: timer gene expression in *hkb*$^-$ mutants, relative to *wg* expression. Note that *cad* is not repressed from the posterior pole until stage 5.5, and the posterior *wg* domain extends to the posterior pole. **F**: timer gene expression in *hkb*$^-$ mutants, relative to *tll* expression. Note that the *tll* domain is small, and it preserves normal relationships with the *cad*, *D* and *opa* domains. **G,H**: single-channel quantitative expression traces (75-100% AP axis) from multiple wild-type and mutant stage 5.5 embryos. Note the absence of spatial patterning in *tor*$^-$ mutants and the posteriorly shifted expression boundaries in *tll*$^-$ and *hkb*$^-$ mutants. All embryos are anterior left, dorsal up, lateral view. Scale bar = 50 μm; grey lines show embryo outlines. All traces are individually normalised; mutant traces are overlaid on wild-type traces (grey) for ease of comparison.

Figure 6—source data 1. Expression trace source data.

Figure 6—figure supplement 1. Timer gene expression traces from terminal system mutants, relative to wild-type.

Figure 6—figure supplement 2. Expression of *tll* in wild-type and *hkb*$^-$ embryos from stage 5.5 to stage 7.

Timer gene expression in *tor*$^-$ mutants

In *tor*$^-$ mutants (***Figure 6***B,G), all posterior spatial patterning of the timer genes was lost, and their temporal expression dynamics resembled those seen in the trunk of wild-type embryos. Thus *cad*, *D*, and *opa* were all expressed to the very posterior of the embryo at the beginning of stage 5, with first *cad* and then *D* expression turning off as stage 5 progressed. The posterior domain of *wg* was absent, and the region of segmental *wg* expression expanded posteriorly, as described previously (***Mohler, 1995***). Loss of the *cad* tail domain in *tor*$^-$ and *torso-like* (*tsl*$^-$) mutants has also been described previously (***Mlodzik and Gehring, 1987b***; ***Schulz and Tautz, 1995***).

Timer gene expression in *tll*$^-$ and *tll*$^-$ *opa*$^-$ mutants

In *tll*$^-$ mutants (***Figure 6***C,D,G; ***Figure 6—figure Supplement 1***A), the posterior *wg* domain was absent (***Wu and Lengyel, 1998***), and the *cad*, *D* and *opa* domains were expanded posteriorly to abut the *hkb* domain, which looked similar to wild-type (***Figure 7***B). Normal expression of *hkb* in *tll*$^-$ mutants has been previously reported (***Bronner and Jackle, 1991***; ***Bronner et al., 1994***; ***Ashyraliyev et al., 2009***).

A posteriorly-shifted *cad* tail domain was transiently expressed (***Figure 6***C,G; ***Figure 4—figure Supplement 5***). This finding conflicts with previous reports that the *cad* tail domain was either unaffected (***Reinitz and Levine, 1990***) or completely absent (***Mlodzik and Gehring, 1987b***) in *tll*$^-$ mutants.

The pattern of *D* expression in the trunk was abnormal (presumably caused by feedback from the segmentation genes, which are misregulated in *tll*$^-$ mutants; ***Mahoney and Lengyel, 1987***; ***Casanova, 1990***; ***Janssens et al., 2013***), and a persistent posterior *D* domain did not emerge (***Figure 6***C; ***Figure 4—figure Supplement 5***).

tll$^-$ *opa*$^-$ double mutants showed similar patterning dynamics to *tll*$^-$ single mutants, except that tail-like expression of *D* was rescued and persisted into germband extension (***Figure 4—figure Supplement 5***).

Timer gene expression in *hkb*$^-$ mutants

In *hkb*$^-$ mutants (***Figure 6***E-H), the *wg* posterior stripe became a posterior cap (***Mohler, 1995***), and *cad* expression persisted longer than normal at the posterior pole. The relative phasing of the *cad*, *D*, *opa* and *wg* domains was preserved, but the whole terminal pattern was posteriorly shifted/expanded into territory that would normally express *hkb* (***Figure 6***H).

In contrast to previous reports that *tll* expression is unaffected in *hkb*$^-$ mutants (***Bronner and Jackle, 1991***; ***Bronner et al., 1994***; ***Bronner and Jackle, 1996***), we found that the *tll* domain was

smaller than normal, thereby preserving the correlation between *tll* levels and timer gene expression boundaries seen in wild-type embryos (***Figure 6***F,H; ***Figure 6—figure Supplement 1***B). Expression of *tll* persisted throughout stages 6 and 7, rather than fading at stage 6, and ectopic expression appeared at the anterior pole (***Figure 6—figure Supplement 2***).

In summary, all posterior spatial patterning of the timer genes is dependent on the terminal system, via *tor*. Expression boundaries associated with the tail and hindgut are perturbed in *tll*$^{-}$ mutants, while expression boundaries associated with the posterior midgut are perturbed in *hkb*$^{-}$ mutants. In addition, there is a concerted posterior shift of the fate map in *hkb*$^{-}$ mutants, which we attribute to the reduced size of the *tll* domain.

Our observations from this and the previous section suggest that Tll strongly represses *D* and *opa* and weakly represses *cad*, while Hkb represses *wg*, *cad*, *D*, and *opa* (see ***Appendix 3*** for detailed reasoning). Hkb is also necessary for activation of *tll* at normal levels (an interaction that is presumably indirect, since Hkb acts as a repressor; ***Goldstein, 1999***), and for timely repression of *tll* after stage 5.

Fkh demarcates the tail / hindgut border and activates posterior *wg*

Having found that Tll is necessary for patterning both the tail region and the posterior *wg* domain (prospective hindgut), we next asked how these regions are distinguished from each other. Forkhead (Fkh) is a zygotic transcription factor which is expressed in the posterior of the embryo from stage 4.4 (nuclear cycle 13) downstream of Tor (***Weigel et al., 1989***, ***1990***) and is required for the specification of hindgut identity (***Jürgens and Weigel, 1988***; ***Weigel et al., 1989***; ***Kuhn et al., 1995***; ***Hoch and Pankratz, 1996***).

fkh expression in *cad*$^{m-z-}$, *hkb*$^{-}$ and *tll*$^{-}$ mutants

We examined the expression of *fkh* relative to other terminal genes in wild-type embryos and in mutant genotypes in which tail or hindgut patterning is perturbed (***Figure 7***A,B).

In wild-type embryos at stage 5.4, the posterior *fkh* domain had a fairly sharp border, which lined up with the anterior border of the posterior *wg* domain and the posterior border of the *cad* tail domain.

In *cad*$^{m-z-}$ mutants, *fkh* expression was strongly reduced (***Wu and Lengyel, 1998***), contrasting with the *tll* and *hkb* domains in these embryos, which looked normal (***Figure 7—figure Supplement 1***; ***Wu and Lengyel, 1998***; ***Olesnicky et al., 2006***).

In *hkb*$^{-}$ mutants, the *fkh* domain was reduced in size (***Weigel et al., 1990***; ***Gaul and Weigel, 1991***), correlating with the reduced size of the *tll* domain and the posteriorly shifted *wg* and *cad* borders in this genotype.

The *fkh* domain was also reduced in *tll*$^{-}$ mutants (***Weigel et al., 1990***; ***Gaul and Weigel, 1991***). The reduced domain was the same size as the *hkb* domain, and it abutted the posteriorly shifted *cad* tail domain.

Timer gene expression in *fkh*$^{-}$ mutants

In *fkh*$^{-}$ mutants (***Figure 7***C,D), the posterior *wg* domain was largely absent (***Wu and Lengyel, 1998***), although there was some residual posterior *wg* expression, particularly in ventral tissue. *cad*, *D*, and *opa* expression was essentially normal throughout stage 5, although the *cad* posterior border appeared to be slightly posteriorly expanded relative to the *D* tail domain.

A stronger effect on *cad* expression was seen after gastrulation, when new *cad* transcription appeared posteriorly abutting the *cad* tail domain, rather than several cells away (posterior to *wg*) as in wild-type embryos (***Figure 7—figure Supplement 3***). Our findings contrast with a previous report, which described *cad* expression as being normal in *fkh*$^{-}$ mutants (***Jürgens and Weigel, 1988***).

Abnormal morphogenesis in *fkh*$^{-}$ and *cad*$^{m-z-}$ mutants

Morphogenesis was abnormal in *fkh*$^{-}$ mutants, in that proctodaeal invagination was delayed until after stage 7 (***Figure 7—figure Supplement 4***). This finding contrasts with previous reports that

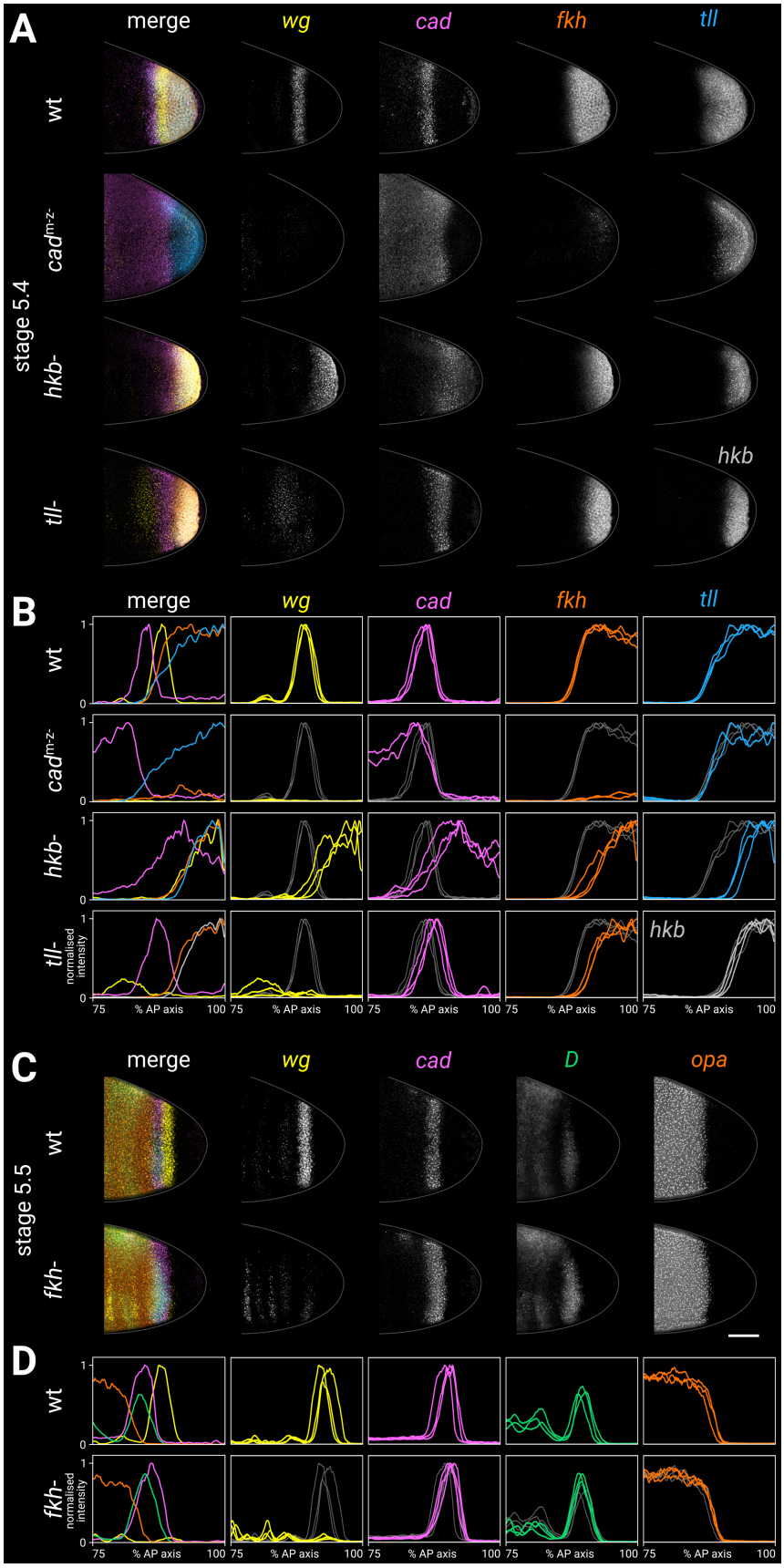

Figure 7: Spatial regulation of *fkh*, and timer gene expression in *fkh*⁻ mutants. (Caption continued on next page.)

Figure 7: Spatial regulation of *fkh*, and timer gene expression in *fkh*$^-$ mutants (continued). **A,B**: terminal gene expression (*wg*, *cad*, *fkh*, and *tll*/*hkb*) in wild-type and mutant embryos. In *cad*$^{m-z-}$, note the loss of *wg* and *fkh* expression. In *hkb*$^-$, note the posterior fate map shift and the delayed repression of posterior *cad*. In *tll*$^-$, note the loss of the posterior *wg* domain, the posteriorly shifted *cad* domain, and the reduced size of the *fkh* domain. **C,D**: timer gene expression in wild-type and *fkh*$^-$ mutant embryos. Note the extremely reduced posterior *wg* domain in *fkh*$^-$. **A, C**: individual stage 5.4 (A) or stage 5.5 (B) embryos; the leftmost column shows a four-channel merge, other columns show individual channels. All embryos are anterior left, dorsal up, lateral view. Scale bar = 50 μm; grey lines show embryo outlines. **B,D**: quantitative expression traces (75-100% AP axis); the leftmost column shows multi-channel traces from the individual embryos in A/C, other columns show single-channel traces from multiple stage 5.4-5 embryos (B) or stage 5.5 embryos (D). All traces are individually normalised; mutant traces are overlaid on wild-type traces (grey) for ease of comparison.

Figure 7—source data 1. Expression trace source data.

Figure 7—figure supplement 1. Terminal gene expression traces from *cad*$^{m-z-}$, *tll*$^-$ and *hkb*$^-$ mutants, relative to wild-type.

Figure 7—figure supplement 2. Timer gene expression traces from *fkh*$^-$ mutants, relative to wild-type.

Figure 7—figure supplement 3. *wg* and *cad* expression in *fkh*$^-$ mutants at stages 6 and 7.

Figure 7—figure supplement 4. Abnormal morphogenesis in *cad*$^{m-z-}$ and *fkh*$^-$ mutants.

morphogenesis in *fkh*$^-$ mutants is normal until the end of the extended germband stage (***Weigel et al., 1989***; ***Wu and Lengyel, 1998***).

cad^{m-z-} mutants (which have severely reduced *fkh* expression) show a similar morphogenetic delay (***Figure 7—figure Supplement 4***) as well as other defects in posterior invagination (***Wu and Lengyel, 1998***). Posterior invagination is dependent on Fog signalling (***Costa et al., 1994***; ***Sweeton et al., 1991***; ***Parks and Wieschaus, 1991***), which is known to be reduced in *cad*$^{m-z-}$ mutants (***Wu and Lengyel, 1998***). As Fkh is known to activate Fog signalling in other developmental contexts (***Chung et al., 2017***), the reduction in Fog signalling may be mediated by the reduction in Fkh.

In summary, we found a consistent pattern across wild-type, *cad*$^{m-z-}$, *hkb*$^-$, and *tll*$^-$ genotypes, in which the *fkh* border abutted the posterior border of the *cad* tail domain, and posterior *wg* was only expressed in *fkh*-positive *hkb*-negative territory. Accordingly, in *fkh*$^-$ mutants, the posterior *wg* domain was largely lost.

These results are consistent with previously proposed regulatory interactions: that Fkh activates *wg* (***Wu and Lengyel, 1998***), that Cad activates *fkh* (***Wu and Lengyel, 1998***), and that Tll and Hkb indirectly enable *fkh* to be expressed (***Weigel et al., 1990***; ***Casanova, 1990***; ***Goldstein, 1999***; ***Moran and Jimenez, 2006***). Accordingly, the activation of *wg* by Cad (***Wu and Lengyel, 1998***) appears to be indirect, via Fkh (see ***Appendix 3*** for detailed reasoning). In addition, it is possible that Fkh represses *cad*, but current evidence is inconclusive (see ***Appendix 3***).

Inferred regulatory interactions collectively form a network that can be formalised and simulated

From looking at how gene expression is affected in various mutant genotypes, we have inferred a network of regulatory interactions between the timer genes and the posterior terminal genes (***Figure 8***A; ***Appendix 3***). Most (11/18) of these proposed interactions originate from this study, although we also find support for previously proposed interactions related to the patterning of *tll*, *hkb*, *fkh* and *wg* (***Figure 8***B). (For a recent quantitative model of posterior gut specification using a network similar to ***Figure 8***B, see ***Keenan et al., 2022***.)

We now formalise the regulatory network in ***Figure 8***A as a logical model, and see whether it reproduces the patterning dynamics that we observed in the embryo. For the purposes of this study, we are aiming for a minimal, qualitative explanation of timer gene patterning, commensurable with the essentially qualitative developmental genetic paradigm we have been working within. We are interested in the relative ordering of gene expression domains in time and space, abstracted away from specific domain sizes, expression levels or expression kinetics. To the extent that the model is able to recapitulate the essential features of both wild-type and mutant genotypes, our

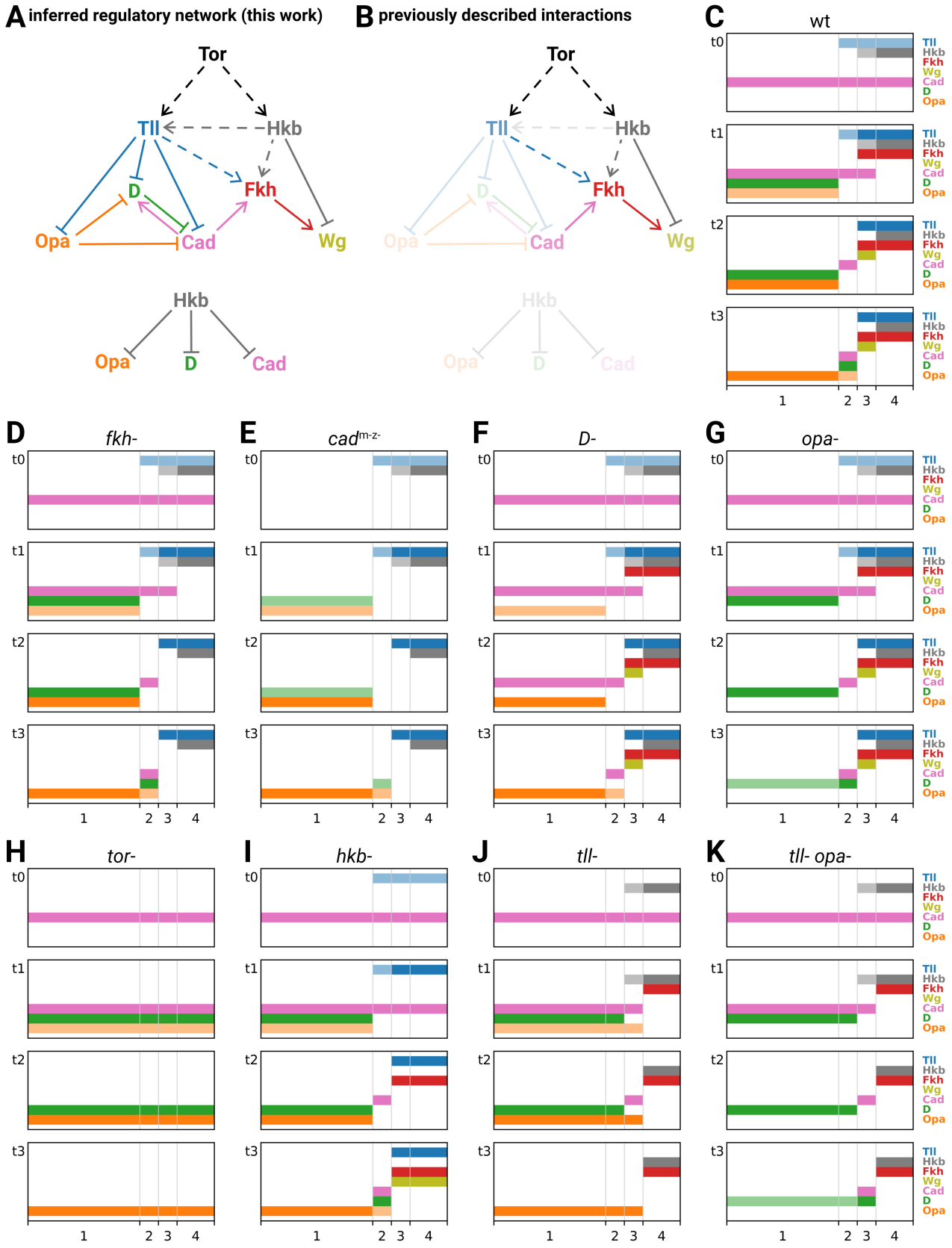

Figure 8: Inferred regulatory network for posterior terminal patterning and output of resulting model. (Caption continued on next page.)

Figure 8: Inferred regulatory network for posterior terminal patterning and output of resulting model (continued). **A**: arrow diagram showing the regulatory interactions we have inferred from the experiments described in this work. Pointed arrowheads indicate activation; flat arrowheads indicate repression. Solid lines indicate interactions that are presumed to be direct; dashed lines indicate interactions that are presumed to be indirect. The diagram is laid out so that the factors are arranged in approximately the same order left to right as their expression along the AP axis, and causation mainly flows from top to bottom (with exceptions for Opa and Cad). To avoid arrow crossovers, the repression of Opa, D and Cad by Hkb is shown separately from the main network. **B**: the same network as in A, highlighting the interactions described in the existing literature. **C-K**: simulation output for a logical model of posterior terminal patterning, for wild-type and eight mutant genotypes (see main text for details). Each set of plots shows the expression patterns of the logical variables `Tll`, `Hkb`, `Fkh`, `Wg`, `Cad`, `D` and `Opa` (y-axis) across AP regions 1-4 (x-axis), at timepoints $t0$-$t3$. For `Tll`, `Hkb`, `D`, and `Opa`, a light colour shade represents weak expression and a dark colour shade represents strong expression. Mutant genotypes never express the relevant protein; *tor*$^-$ mutants were simulated as *tll*$^-$ *hkb*$^-$ double mutants.

Figure 8—figure supplement 1. Simulation of a hypothetical timer gene network for sequential segmentation.

confidence in the network will be increased.

The modelling framework we have chosen is very simple (for a full description see ***Appendix 4***). Briefly, Hkb and Tll are assumed to be extrinsic inputs to the system (we ignore the cross-regulation of *tll* by Hkb), and we model how Fkh, Wg, Cad, D, and Opa are expressed in response. Each of these 7 factors is modelled as a logical variable, some of which (`Hkb`, `Tll`, `D`, `Opa`) may take one of three levels of expression (off/weak/strong), while the others (`Fkh`, `Wg`, `Cad`) may take only two (off/on). The AP axis is modelled as four discrete regions, 1-4 (corresponding to trunk, tail, hindgut, and posterior midgut, respectively), which differ in their hard-coded `Hkb` and `Tll` inputs over time. (Note that we do not include any dorsoventral input to the system, nor attempt to model the *D* neuroectodermal domain.) Each simulation consists of 4 time points, $t0$-$t3$ (corresponding to nuclear cycle 13, early stage 5, mid stage 5, and stage 6, respectively). At $t0$, `Cad` is on in all regions, and the other output factors are off. Expression at subsequent timepoints is computed from expression at $t(n-1)$, according to factor-specific logical rules (which remain the same for all timepoints). Mutants are simulated by keeping the relevant factor(s) turned off for all timepoints.

The regulatory network explains the patterning dynamics of each genotype

We simulated the patterning model for the wild-type condition (***Figure 8***C) and eight mutant genotypes examined in this study (*fkh*$^-$, *cad*$^{m\text{-}z\text{-}}$, *D*$^-$, *opa*$^-$, *tor*$^-$, *hkb*$^-$, *tll*$^-$, and *tll*$^-$ *opa*$^-$; ***Figure 8***D-K). A genotype-by-genotype explanation of the simulated expression dynamics is provided in ***Appendix 4***, along with a table cross-referencing the simulated expression data with the corresponding observations from real embryos. Allowing for the simple, qualitative nature of the model, the simulations were remarkably accurate at recapitulating the patterning dynamics of each genotype.

Recapitulation of wild-type patterning

Regions 1-4 generate different gene expression as a result of their different inputs from `Tll` and `Hkb`. Across regions 3 and 4, the nested domains of strong `Tll` and `Hkb` expression specify abutting domains of hindgut (`Fkh` + `Wg`) and posterior midgut (`Fkh` only) fates (***Weigel et al., 1990***; ***Casanova, 1990***), specifically by repressing the timer genes (both regions), activating `Fkh` (both regions), and differentially regulating `Wg` (repressed by `Hkb` in region 4). In region 1 (trunk), where `Tll` and `Hkb` are not expressed, gene expression is shaped by the intrinsic dynamics of the timer gene network: as `D` is activated and the level of `Opa` builds up, first `Cad` and then `D` are repressed. Finally, in region 2 (tail), these dynamics are modulated by transient expression of `Tll`, which delays the activation of `D` and `Opa`, and thereby prolongs the expression of `Cad`. Crucially, this `Tll` expression is weaker than in region 3, and so does not activate `Fkh` and (therefore) `Wg`.

Recapitulation of mutant phenotypes

Simulated mutants of the "outputs" Fkh, Cad, D and Opa (***Figure 8***D-G) have perturbed gene expression within specific regions, but the overall spatial organisation of the tissue is unaffected. In the *fkh*$^{-}$ mutant, Wg is never activated in region 3. In the *D*$^{-}$ and *opa*$^{-}$ mutants, the turnover of timer gene expression in region 1 is perturbed: the repression of cad is delayed in *D*$^{-}$, and the repression of D is delayed in *opa*$^{-}$. Finally, in the *cad*$^{m\text{-}z\text{-}}$ mutant, widespread effects on gene expression coexist with fairly normal spatial organisation: in regions 3 and 4, Fkh and (therefore) Wg are not expressed, while in regions 1 and 2 the activation of D is reduced. [Although we modelled mutants as deficiencies and therefore did not recapitulate the delayed *cad* repression seen in *cad*$^{m\text{-}z\text{-}}$ embryos (***Figure 4***A), we can interpret this delay as a knock-on effect of the reduced D expression, since D represses Cad.]

In contrast, simulated mutants involving the "inputs" Tll and Hkb (*tor*$^{-}$, *hkb*$^{-}$, *tll*$^{-}$, *tll*$^{-}$ *opa*$^{-}$; ***Figure 8***H-K) show more serious spatial effects, which tend to resemble homeotic transformations. The *tor*$^{-}$ mutant, which removes all expression of Tll and Hkb, transforms regions 2-4 into region 1. The *hkb*$^{-}$ mutant essentially transforms region 4 (posterior midgut) into region 3 (hindgut). The *tll*$^{-}$ mutant transforms region 2 into region 1 but produces novel expression dynamics in region 3: D expression is transiently repressed (as in wild-type region 2) but Opa is not, producing a posteriorly shifted, transient Cad stripe and precluding any late expression of D. Finally, in the *tll*$^{-}$ *opa*$^{-}$ mutant, the repression from Opa on D and Cad seen in the *tll*$^{-}$ mutant is removed, and region 3 is fully transformed into region 2.

Discrepancies with real embryos

The discrepancies with real patterning stem from the simple, qualitative nature of the model. The activation of Fkh and (therefore) Wg is spuriously delayed in the *hkb*$^{-}$ simulation (***Figure 8***I), owing to the discrete implementations of time, Tll expression and Fkh regulation. The model cannot recapitulate the subtle shifting dynamics with the tail region (***Figure 3***), because the tail is modelled as a single, discrete block. Similarly, the model cannot recapitulate the concerted fate map shifts seen in *hkb*$^{-}$ and *D*$^{-}$ mutants (***Figure 6***E-H; ***Figure 4***B), because there is no representation of region size. That said, if we extrapolate from the existing results, we can interpret the posterior shifting dynamics within the tail region as resulting from the posterior retraction of Tll expression over time (***Figure 5—figure Supplement 3***; ***Figure 5—figure Supplement 4***), interpret the posterior fate map shift in *hkb*$^{-}$ mutants as resulting from (indirect) cross-activation of *tll* by Hkb (***Figure 6***H), and interpret the anterior fate map shift in *D*$^{-}$ mutants as resulting from potential cross-repression of *tll* by D.

In summary, the genetic interactions we uncovered in this study are able to explain the qualitative aspects of timer gene patterning in both wild-type and mutant genotypes. In particular, our model explains how a graded Tll domain delineates both the anterior and posterior boundaries of the tail region, and explains why transient expression of Tll within the tail region is important for producing its characteristic timer gene dynamics. The model also explains the posteriorly shifted tail-like expression domains seen in *tll*$^{-}$ and *tll*$^{-}$ *opa*$^{-}$ mutants as the result of graded and dynamic Hkb expression. For insight into quantitative phenomena such as the fate map shifts in *hkb*$^{-}$ and *D*$^{-}$ mutants, it will be necessary to analyse quantitative models incorporating zygotic cross-regulation of *tll*.

Discussion

In this study we have used mutants, multiplexed imaging and modelling to elucidate how the blastoderm expression dynamics of the *Drosophila* timer genes *cad*, *D*, and *opa* arise from a combination of cross-regulatory interactions and spatially localised inputs from the posterior terminal system. This work has four main implications. First, we have demonstrated that timer gene expression is partially driven by intrinsic network dynamics. Second, we have uncovered more evidence that the

timer genes have broad effects on developmental timing, through our discovery that *cad*$^{m-z-}$ embryos precociously express genes associated with neural differentiation. Third, we have produced a coherent model for the patterning of the posterior terminal region. Fourth, we have clarified the segmental nature of the *Drosophila* tail. These findings increase our understanding of *Drosophila* development and have evolutionary significance for the mechanisms of axial patterning in other species.

Timer gene expression is regulated by intrinsic network dynamics and extrinsic spatiotemporal inputs

This work provides evidence for a set of cross-regulatory interactions between *cad*, *D*, and *opa* that helps generate dynamic, sequential expression. In particular, we find that Cad activates *D* (i.e., promotes the expression of the next gene in the sequence), while D represses *cad* and Opa represses *cad* and *D* (i.e., both inhibit the previous genes in the sequence). Opa is not cross-regulated, however, making it an "input-only" component of the three gene network (at least in the blastoderm context).

Timer gene expression is also shaped by extrinsic spatiotemporal regulation. In this work, we show how the timer gene network interacts with the posterior terminal system: most notably, Tll differentially represses *cad*, *D* and *opa* in the tail region, indirectly allowing *cad* expression to be maintained. The localised inputs from the posterior terminal system are overlaid on global temporal regulation provided by the nuclear:cytoplasmic ratio (which is particularly important for regulating the onset of *opa* transcription; ***Lu et al., 2009***) as well as the levels of maternal factors such as Tramtrack (***Harrison and Travers, 1990***; ***Brown et al., 1991***; ***Read et al., 1992***), Zelda (***Liang et al., 2008***; ***Harrison et al., 2011***; ***Nien et al., 2011***; ***McDaniel et al., 2019***), Stat92e (***Yan et al., 1996***; ***Hou et al., 1996***; ***Tsurumi et al., 2011***) and GAGA Factor/Trithorax-like (***Farkas et al., 1994***; ***Bhat et al., 1996***; ***Moshe and Kaplan, 2017***; ***Gaskill et al., 2021***). Ironically, precisely because these maternal factors are so crucial to development, their patterning roles remain less well understood than those of the zygotic patterning genes, which are less pleiotropic and therefore easier to study.

Timer gene expression has broad effects on developmental timing

Recent work in the *Drosophila* blastoderm has demonstrated the extensive effects of timer genes on developmental gene expression. Opa has been shown to act as a pioneer factor, reshaping gene expression genome-wide by opening chromatin at hundreds of target enhancers (***Soluri et al., 2020***; ***Koromila et al., 2020***). Cad and D are also known to regulate expression across the genome (***Li et al., 2008***; ***MacArthur et al., 2009***; ***Aleksic et al., 2013***). Here, we have found that early Cad expression appears to be necessary for the correct timing of later developmental events, because neuroectodermal gene expression turns on precociously in *cad*$^{m-z-}$ embryos. The vertebrate Cad ortholog Cdx4 has also been shown to temporally regulate neural differentiation, in the developing spinal cord (***Joshi et al., 2019***), a tissue in which D and Opa orthologs play key developmental roles (reviewed in ***Graham et al., 2003***; ***Merzdorf, 2007***; ***Houtmeyers et al., 2013***; ***Stevanovic et al., 2021***). More generally, comparative evidence suggests that Cad/Cdx plays a deeply conserved role in the formation of the posterior body and the patterning of the posterior gut (***Copf et al., 2004***; ***Wu and Lengyel, 1998***; ***van Rooijen et al., 2012***; ***Zhong et al., 2020***). In this context, *Drosophila cad*$^{m-z-}$ mutants offer a rare opportunity to study the genome-wide effects of a total loss of Cad/Cdx function without also catastrophically perturbing early developmental events.

A revised picture of posterior terminal patterning in *Drosophila*

In this work we have investigated blastoderm gene expression downstream of the posterior terminal system, revisiting a patterning network that was most intensely studied in the late 1980s and early 1990s (***Strecker et al., 1986***; ***Mahoney and Lengyel, 1987***; ***Mlodzik and Gehring, 1987b***; ***Strecker et al., 1988***; ***Jürgens and Weigel, 1988***; ***Weigel et al., 1990***; ***Casanova, 1990***; ***Bronner and Jackle, 1991***; ***Wu and Lengyel, 1998***). The modern availability of marked balancers and multiplexed

imaging techniques has allowed us to clarify the topology and spatiotemporal dynamics of the network, and incorporate genes (*D* and *opa*) that had not been cloned at the time most of the original work was completed. All told, we have identified 11 new regulatory interactions involved in *Drosophila* AP patterning, put forward the first formalised model (to our knowledge) for the patterning of the tail, and provided a solid foundation for future quantitative analyses of this system.

Although simple, our model provides new insights into how the tail and hindgut regions are specified in the early embryo. Both regions, along with segment A8, have long been known to depend on Tll expression (***Strecker et al., 1986***; ***Diaz et al., 1996***). *tll* alleles can be arranged into a coherent phenotypic series in which the most posterior structures within the Tll-dependent region are the most sensitive to *tll* perturbation and the most anterior structures are the least (***Strecker et al., 1986***; ***Diaz et al., 1996***), suggesting that this part of the blastoderm fate map is patterned by a gradient of Tll activity (***Casanova, 1990***). However, it has not been clear at the network level how graded Tll activity would be transduced into a specific series of boundaries and domains.

We found that *tll* expression was strong and persistent within the hindgut region, but weaker and transient in the tail region, with the anterior border of the expression domain retracting posteriorly across nuclei over time. We additionally found that Tll effectively patterned both the anterior and posterior boundaries of the tail region, by differentially repressing *D* and *opa* relative to *cad*. Crucially, *D* and *opa* were repressed even where Tll expression was transient and weak, but *cad* was not repressed (and *fkh* was not activated) unless Tll expression was stronger, helping explain the transition from tail fate to hindgut fate as Tll levels increase. Furthermore, the retraction of the Tll domain over time explains the posterior shifting dynamics we found for the timer genes within the tail region, which contrasts with the anterior shifting dynamics previously described for the pair-rule and gap genes (***Jaeger et al., 2004***; ***Keränen et al., 2006***; ***Surkova et al., 2008***; ***Lim et al., 2018***).

We also discovered, to our surprise, that there is a concerted posterior fate map shift in hkb^- embryos, apparently mediated by a reduction in the size of the *tll* domain. (A subtle anterior fate map shift additionally occurs in D^- embryos, which might also be mediated by Tll.) Although further research is necessary to determine the mechanism by which Hkb cross-regulates *tll*, the phenotype implies that the size of the *tll* domain is not an unmediated response to terminal signalling. (Indeed, there are hints in the existing literature that *tll* and *hkb* may be zygotically cross-regulated by other AP patterning genes as well, see ***Casanova et al., 1994***; ***Greenwood and Struhl, 1997***; ***de las Heras and Casanova, 2006***.) These findings may complicate the interpretation of recent studies that have characterised the input:output relationships between terminal signalling and *tll* and *hkb* expression using optogenetics (***Johnson and Toettcher, 2019***; ***Johnson et al., 2020***; ***Keenan et al., 2020***).

The segmental character of the *Drosophila* tail

The ancestral insect body plan has 11 true abdominal segments plus the periproct/telson, but this number has been reduced in many extant insect lineages (***Snodgrass, 1935***; ***Demerec, 1950***; ***Matsuda, 1976***; ***Chapman et al., 2013***). In *Drosophila*, the most common view has been that the embryo makes 10 abdominal segments (i.e., 15 parasegment boundaries), with the anal pads located in PS15/A10 (***Turner and Mahowald, 1979***; ***DiNardo, 1985***; ***Sato and Denell, 1986***; ***Perkins and Perrimon, 1991***; ***Kuhn et al., 1992***; ***Schmidt-Ott et al., 1994***). In particular, territories corresponding to A8, A9, and A10 are visible at the morphological level during embryogenesis (***Turner and Mahowald, 1979***), and surveys of *en*, *wg*, *hh* and *slp* staining have found evidence for (at most) 15 parasegment boundaries (***DiNardo, 1985***; ***Baker, 1987***, ***1988***; ***Kuhn et al., 1992***; ***Grossniklaus et al., 1992***; ***Mohler and Vani, 1992***; ***Tabata et al., 1992***; ***Lee et al., 1992***; ***Tashiro et al., 1993***; ***Kuhn et al., 1995***). However, fate mapping experiments (***Jürgens, 1987***) and surveys of *gooseberry* expression (***Baumgartner et al., 1987***; ***Gutjahr et al., 1993***) have suggested that the embryo makes 16 parasegment boundaries, with the anal pads located in PS16/A11. There is also some evidence for A11 from patterns of gene expression in adult genital discs (***Freeland and Kuhn, 1996***).

Given the small size of the tail region within the embryo, the fact that it is covered by am-

nioserosa during key stages of patterning, and the fact that it later undergoes complicated morphogenetic rearrangements and fusions that obscure its metameric nature, it is perhaps unsurprising that the number of *Drosophila* segments has not been unambiguously resolved. In this study, we present evidence for a vestigial 16th parasegment boundary in the embryo, by identifying additional domains of *slp* and *wg* expression and reinterpreting previously described domains of *eve* and *en*. These observations suggest that the anal pads are located in PS16. (Whether the tissue between PSB16 and the anus should be classified as a true 11th abdominal segment or a non-segmental periproct/telson is beyond the scope of this paper.) However, PSB16 appears extremely dorsoventrally restricted and may have little functional significance in the organism. As the number of abdominal segments varies across insects (***Matsuda, 1976***), the mechanistic basis of this evolutionary reduction would be interesting to study within a comparative developmental framework.

Our findings suggest that the *Drosophila* embryo sequentially patterns two parasegment boundaries after gastrulation, and that in both cases the new boundary is patterned by abutting stripes of *slp* and *eve*. In PS15 and PS16, the relative arrangement of *slp*, *eve*, *wg* and *en* expressing cells is the same, conserved pattern that is found at parasegment boundaries in the *Drosophila* trunk and throughout the arthropod phylum (reviewed in ***Clark et al., 2019***). However, tail segmentation differs from trunk segmentation in that resolved, stable *eve* stripes emerge de novo and with single-segmental periodicity, rather than from a dynamic and double-segmental phase of pair-rule gene expression.

Intriguingly, a remarkably similar switch from double-segment to single-segment periodicity occurs towards the end of segmentation in the centipede *Strigamia maritima*, where stable, resolved *eve* stripes start appearing de novo in the anterior segmentation zone instead of emerging from posterior oscillatory expression (***Brena and Akam, 2013***). A possible switch from double-segmental to single-segmental patterning has also been reported for terminal segments in the beetle *Tribolium* (***Janssen, 2014***). These observations hint that terminal and trunk segments may be homonomous at the level of segment-polarity gene expression but derived from distinct ontogenetic programs. More work is needed to determine how such a developmental switch — if present — is controlled, as well as its relationship to the more general problem of terminating axial development.

Comparative analysis and evolutionary implications

We end this study by assessing the relevance of our findings from *Drosophila* to the development of other insect species. Which aspects of the *Drosophila* network are likely to be conserved in other insect species that have been used to study segmentation, such as *Tribolium*, *Nasonia vitripennis*, and *Oncopeltus fasciatus*? And how might the *Drosophila* network differ from that of its sequentially segmenting ancestors?

The cross-regulatory interactions that we found between the timer genes might be quite widely conserved in insect segmentation. Activation of *D* by Cad, repression of *cad* by Opa, and repression of *D* by Opa are all consistent with a segment addition zone that is subdivided into a posterior region that expresses Cad and D and an anterior region that expresses Opa, as seen for example in *Tribolium* (***Clark and Peel, 2018***). However, repression of *cad* by D would need to be reconciled with the sustained expression of both *cad* and *D* in the posterior segment addition zone. Intriguingly, some of the timer gene cross-regulatory interactions may even be important for regulating expression dynamics in completely different developmental contexts, given that Opa has recently been found to repress *D* during the temporal patterning of *Drosophila* intermediate neural progenitors (***Abdusselamoglu et al., 2019***).

The different components of the *Drosophila* terminal system seem to have acquired their posterior patterning roles at different times: posterior *tll* expression is found across diverse holometabolan species (***Schroder et al., 2000***; ***Lynch et al., 2006***; ***Wilson and Dearden, 2009***; ***García-Solache et al., 2010***; ***Lemke et al., 2010***; ***Klomp et al., 2015***) although not in hemipterans (***Weisbrod***

et al., 2013; *Bickel et al., 2013*), whereas *hkb* and *tor* appear to have been recruited to terminal patterning roles more recently (*García-Solache et al., 2010*; *Kittelmann et al., 2013*; *Duncan et al., 2013*). In *Tribolium*, *tll* is expressed downstream of *tor* (as in *Drosophila*), and *tor* RNAi embryos fail to express *cad* and *wg* in the posterior of the embryo, resulting in AP truncation (*Schoppmeier and Schröder, 2005*). In *Nasonia*, *tll* RNAi results in a reduction of posterior *cad*, as well as in gap gene misregulation that disrupts much of abdominal segmentation (*Lynch et al., 2006*). It will be instructive to test whether these losses of *cad* expression in *Tribolium* and *Nasonia* are mediated by ectopic expression of Opa, as we found for *tll*$^-$ and *tor*$^-$ mutants in *Drosophila*. If so, it would suggest that the initial spatial regulation of the timer gene network by Tll in the posterior blastoderm might be conserved across holometabolan embryos, despite their varying modes of development.

So, how *does* timer gene regulation differ between sequentially segmenting embryos (which establish a persistent segment addition zone) and simultaneously segmenting embryos like *Drosophila*? One key difference is likely to be the role of a posterior Wnt signalling centre: there is evidence from many different sequentially segmenting species that Wnt signalling is important for activating *cad* expression and maintaining the segment addition zone (reviewed in *Clark et al., 2019*), whereas we found that timer gene expression was unaffected in *Drosophila wg*$^-$ mutants, at least during our stages of interest. In addition, it seems probable that timer gene cross-regulation of *opa* is important in sequentially segmenting species, with this having been lost from the *Drosophila* lineage during the evolution of simultaneous patterning.

If we modify the *Drosophila* timer gene network to incorporate these additional features (*Appendix 4*), we can see how appropriate segment addition zone dynamics might naturally emerge (*Figure 8—figure Supplement 1*). It therefore seems plausible that the cross-regulatory interactions between the *Drosophila* timer genes may represent an evolutionary vestige of a "dynamical module" that was originally involved in axial elongation (*Clark and Peel, 2018*; *Clark, 2021*). Functional experiments in sequentially segmenting species will be necessary to test this hypothesis.

Materials and Methods

Table 1. Key Resources table

Reagent type (species) or resource	Designation	Source or reference	Identifiers	Additional information
gene (*Drosophila melanogaster*)	*caudal* (*cad*)	FlyBase	FLYB:FBgn0000251	
gene (*D. melanogaster*)	*Dichaete* (*D*)	FlyBase	FLYB:FBgn0000411	
gene (*D. melanogaster*)	*engrailed* (*en*)	FlyBase	FLYB:FBgn0000577	
gene (*D. melanogaster*)	*even-skipped* (*eve*)	FlyBase	FLYB:FBgn0000606	
gene (*D. melanogaster*)	*forkhead* (*fkh*)	FlyBase	FLYB:FBgn0000659	
gene (*D. melanogaster*)	*huckebein* (*hkb*)	FlyBase	FLYB:FBgn0261434	
gene (*D. melanogaster*)	*muscle segment homeobox* (*msh*)	FlyBase	FLYB:FBgn0000492	
gene (*D. melanogaster*)	*odd-paired* (*opa*)	FlyBase	FLYB:FBgn0003002	
gene (*D. melanogaster*)	*sloppy-paired* (*slp*)	FlyBase	FLYB:FBgn0003430	
gene (*D. melanogaster*)	*tailless* (*tll*)	FlyBase	FLYB:FBgn0003720	
gene (*D. melanogaster*)	*torso* (*tor*)	FlyBase	FLYB:FBgn0003733	
gene (*D. melanogaster*)	*wingless* (*wg*)	FlyBase	FLYB:FBgn0284084	
strain, strain background (*D. melanogaster*)	Oregon-R	Bloomington Drosophila Stock Center	BDSC:5; RRID:BDSC_5	"wild-type"

Continued on next page

Reagent type (species) or resource	Designation	Source or reference	Identifiers	Additional information
strain, strain background (*Escherichia coli*)	One Shot BL21 Star (DE3)	ThermoFisher Scientific	C601003	chemically competent cells
genetic reagent (*D. melanogaster*)	cad[3]	Bloomington Drosophila Stock Center	BDSC:5316; FLYB:FBal0001531; RRID:BDSC_5316	gift from H. Skaer
genetic reagent (*D. melanogaster*)	cad[2] FRT40A	Bloomington Drosophila Stock Center	BDSC:7091; FLYB:FBal0001530; FLYB:FBti0002071; RRID:BDSC_7091	
genetic reagent (*D. melanogaster*)	D[r72]	Bloomington Drosophila Stock Center	BDSC:8858 FLYB:FBal0086878; RRID:BDSC_8858	gift from S. Russell
genetic reagent (*D. melanogaster*)	fkh[6]	Bloomington Drosophila Stock Center	BDSC:545; FLYB:FBal0004012; RRID:BDSC_545	gift from K. Roeper
genetic reagent (*D. melanogaster*)	hkb[A321R1]	Bloomington Drosophila Stock Center	BDSC:2059; FLYB:FBal0031495; RRID:BDSC_2059	
genetic reagent (*D. melanogaster*)	opa[8]	Bloomington Drosophila Stock Center	BDSC:5335; FLYB:FBal0013272; RRID:BDSC_5335	
genetic reagent (*D. melanogaster*)	Df(3R)Exel6217	Bloomington Drosophila Stock Center	BDSC:7695; FLYB:FBab0038272; RRID:BDSC_7695	deficiency covering the *tll* locus
genetic reagent (*D. melanogaster*)	tor[XR1]	***Sprenger et al., 1989***	FLYB:FBal0016988; RRID:BDSCXXXX	Gift from T. Johnson
genetic reagent (*D. melanogaster*)	wg[l-8]	Bloomington Drosophila Stock Center	BDSC:5351; FLYB:FBal0018500; RRID:BDSC_5351	
genetic reagent (*D. melanogaster*)	CyO, hb-lacZ	Bloomington Drosophila Stock Center	BDSC:6650; FLYB:FBba0000025; FLYB:FBti0002621, RRID:BDSC_6650	
genetic reagent (*D. melanogaster*)	TM6C, twi-lacZ	Bloomington Drosophila Stock Center	BDSC:7251; FLYB:FBba0000071; FLYB:FBti0010595; RRID::BDSC_7251	
genetic reagent (*D. melanogaster*)	TM3, hb-lacZ	Bloomington Drosophila Stock Center	BDSC:78357; FLYB:FBba0000047; FLYB:FBti0010581; RRID:BDSC_78357	gift from S. Russell
genetic reagent (*D. melanogaster*)	hsFLP	Bloomington Drosophila Stock Center	BDSC:6; FLYB:FBti0002044; RRID:BDSC_6	
genetic reagent (*D. melanogaster*)	ovoD1 FRT40A	Bloomington Drosophila Stock Center	BDSC:2121; FLYB:FBtp0000359; FLYB:FBti0002071; RRID:BDSC_2121	no longer listed in BDSC

Continued on next page

Reagent type (species) or resource	Designation	Source or reference	Identifiers	Additional information
antibody	anti-D (rabbit poly-clonal)	***Soriano and Russell, 1998***		(1:10)
antibody	anti-Hkb (rat poly-clonal)	***Ashyraliyev et al., 2009***		(1:100)
antibody	anti-Opa (guinea-pig polyclonal)	this paper		(1:5000)
antibody	anti-Tll (rabbit poly-clonal)	***Kosman et al., 1998***		(1:100)
antibody	anti-guinea pig Alexa Fluor 647 (goat poly-clonal)	Invitrogen	Cat#:A-21450; RRID:AB_2735091	(1:500)
antibody	anti-rabbit Alexa Fluor 488 (goat poly-clonal)	Invitrogen	Cat#:A-11034; RRID:AB_2576217	(1:500)
antibody	anti-rabbit Alexa Fluor 555 (goat poly-clonal)	Invitrogen	Cat#:A-21429; RRID:AB_2535850	(1:500)
antibody	anti-rat Alexa Fluor 488 (goat polyclonal)	Invitrogen	Cat#:A-11006; RRID:AB_2534074	(1:500)
recombinant DNA reagent	FI01113 (clone)	Drosophila Genomics Resource Center	DGRC:1623347; RRID:DGRC_1623347	opa cDNA
recombinant DNA reagent	Gateway pDONR221 (plasmid)	ThermoFisher Scien-tific	Cat#:12536017	
recombinant DNA reagent	Gateway pET-DEST42 (plasmid)	ThermoFisher Scien-tific	Cat#:12276010	
sequence-based reagent	*cad*	Molecular Instru-ments	HCR v3.0 probes	designed to target NCBI:NM_134301.4
sequence-based reagent	*cad*-Intron	Molecular Instru-ments	HCR v3.0 probes	designed to target NCBI:NT_033779.5: 20771910-20781798
sequence-based reagent	*D*	Molecular Instru-ments	HCR v3.0 probes	designed to target NCBI:NM_001274901.1
sequence-based reagent	*en*	Molecular Instru-ments	HCR v3.0 probes	designed to target NCBI:NM_078976.4
sequence-based reagent	*eve*	Molecular Instru-ments	HCR v3.0 probes	designed to target NCBI:NM_078946.4
sequence-based reagent	*fkh*	Molecular Instru-ments	HCR v3.0 probes	designed to target NCBI:NM_001300645.1
sequence-based reagent	*hkb*	Molecular Instru-ments	HCR v3.0 probes	designed to target NCBI:NM_079497.4
sequence-based reagent	*msh*	Molecular Instru-ments	HCR v3.0 probes	designed to target NCBI:NM_057976.3
sequence-based reagent	*opa*	Molecular Instru-ments	HCR v3.0 probes	designed to target NCBI:NM_079504.4
sequence-based reagent	*slp*	Molecular Instru-ments	HCR v3.0 probes	designed to target NCBI:NM_057382.3
sequence-based reagent	*tll*	Molecular Instru-ments	HCR v3.0 probes	designed to target NCBI:NM_079857.4

Continued on next page

Reagent type (species) or resource	Designation	Source or reference	Identifiers	Additional information
sequence-based reagent	*wg*	Molecular Instruments	HCR v3.0 probes	designed to target NCBI:NM_078778.5
sequence-based reagent	*lacZ*	Molecular Instruments	HCR v3.0 probes	designed to target NCBI:NC_000913.3: c366305-363231
sequence-based reagent	B1-5 Alexa Fluor 488	Molecular Instruments	HCR amplifiers	amplifiers coordinated with probes
sequence-based reagent	B1-5 Alexa Fluor 514	Molecular Instruments	HCR amplifiers	amplifiers coordinated with probes
sequence-based reagent	B1-5 Alexa Fluor 546	Molecular Instruments	HCR amplifiers	amplifiers coordinated with probes
sequence-based reagent	B1-5 Alexa Fluor 594	Molecular Instruments	HCR amplifiers	amplifiers coordinated with probes
sequence-based reagent	B1-5 Alexa Fluor 647	Molecular Instruments	HCR amplifiers	amplifiers coordinated with probes
sequence-based reagent	opaDM-F	this paper	PCR primers	AAAAAGCAGGCTTCGA AGGAGATAGAACCATG AACGCCTTCATTGAGC
sequence-based reagent	opaA-R	this paper	PCR primers	AGAAAGCTGGGTTGTC GTAGCCGTGGGATG
sequence-based reagent	attB1adap-F	this paper	PCR primers	GGGGACAAGTTTGTAC AAAAAAGCAGGCT
sequence-based reagent	attB2adap-R	this paper	PCR primers	GGGGACCACTTTGTAC AAGAAAGCTGGGT
commercial assay or kit	Gatweway BP Clonase II	ThermoFisher Scientific	Cat#:11789020	
commercial assay or kit	Gateway LR Clonase II	ThermoFisher Scientific	Cat#:11791020	
pepdtide, recombinant protein	Phusion Plus DNA Polymerase	ThermoFisher Scientific	Cat#:F630S	
chemical compound, drug	Overnight Express Instant TB Medium	Novagen	Cat#:71491-3	
chemical compound, drug	Ni-NTA Agarose	Qiagen	Cat#:30210	
other	Normal Goat Serum blocking solution	Vector Laboratories	Cat#:S-1000-20	
other	DAPI stain	Invitrogen Scientific	Cat#:D1306	(1 ng/μL)
other	#1.5 coverslips	Corning	Cat#:2980-224	
other	SlowFade Gold AntiFade Mountant	ThermoFisher Scientific	Cat#:S36940	

Drosophila husbandry and genetics

Stock maintenance and embryo fixation (20 minutes with 4% formaldehyde in PBS) was performed as described in **Sullivan et al.** (**2000**). "Wild-type" flies were Oregon-R. The mutant alleles used were $wg^{l\text{-}8}$ (Bloomington #5351), cad^{3} (gift from H. Skaer), cad^{2} (Bloomington #7091), D^{r72} (gift from S. Russell), opa^{8} (Bloomington #5340), tor^{XR1} (gift from T. Johnson), $hkb^{[A321R1]}$ (Bloomington #2059), Df(3R)Exel6217 (Bloomington #7695, a deficiency covering the *tll* locus), and fkh^{6} (gift from K. Roeper). Mutant lines obtained from the Bloomington *Drosophila* Stock Centre were verified by cuticle preparations as described in **Sullivan et al.** (**2000**). The tll^{-} opa^{-} double mutant was

generated by the Cambridge Fly Facility by recombining Df(3R)Exel6217 and *opa*^{8}. Mutants were balanced over marked balancer chromosomes expressing *lacZ* during early embryogenesis: *CyO*, *hb-lacZ* (Bloomington #6650) for the 2nd chromosome and *TM6C*, *twi-lacZ Sb*^{1} *Tb*^{1} (Bloomington #7251) or *TM3*, *hb-lacZ Sb*^{1} (gift from S. Russell) for the 3rd.

cad^{-} germline clones were generated using the heatshock induced FLP/FRT system as described in ***Selva and Stronach*** (***2007***). Briefly, 8 vials of 30 *cad*^{2} *FRT40A* / *CyO* virgin females (Bloomington #7091) were each crossed with 10 *hsFLP w*; *ovoD1 FRT40A* / *CyO* males (constructed by crossing Bloomington #6 *hsFLP w*; *Adv* / *CyO* females with Bloomington #2121 *ovoD1 FRT40A* / *CyO*, but note that #2121 is no longer listed in Bloomington). Adults were flipped to new vials every two days, resulting in a total of ∼100 vials. When crawling L3 larvae were visible, vials were heatshocked at 37° C in a waterbath for 1 hour, allowed to recover at 25° C for 24 hours, then heatshocked again at 37° C for 1 hour. Approximately 600 non-*CyO* virgin females (all presumably with *cad*^{2} / *cad*^{2} ovaries) were collected from the heatshocked vials and crossed with ∼300 *cad*^{3} / *CyO*, *hb-lacZ* males. Resulting embryos without *lacZ* expression lacked both maternal and zygotic *cad* (*cad*$^{m-z-}$), while embryos with *lacZ* expression were paternal rescues (*cad*$^{m-z+}$). Zygotic *cad* mutants (*cad*$^{m+z-}$) were offspring from *cad*^{3}/ *CyO*, *hb-lacZ* parents that lacked *lacZ* expression; note that this genotype is also heterozygous for maternal *cad*.

Opa antibody generation

Clone FI01113 containing Opa coding sequence was obtained from the Drosophila Genomics Resource Center. Gateway attB primers were designed to express 386 amino acids from the N-terminus of Opa (amino acids 3-389), spanning the zinc finger region in the centre of the protein. The forward primer included a Shine-Dalgarno sequence; the reverse primer was designed to be in-frame with the C-terminal fusion of the Gateway expression vector pET-DEST42 (ThermoFisher Scientific). A two stage PCR procedure was used to obtain a final amplicon carrying the attB-sequences at each end of the N-terminal opa sequence.

Primers for the first amplification were:

opaDM-F: AAAAAGCAGGCTTCGAAGGAGATAGAACCATGAACGCCTTCATTGAGC

opaA-R: AGAAAGCTGGGTTGTCGTAGCCGTGGGATG

Overlapping primers for the second amplification to complete the attB regions were:

attB1adap-F: GGGGACAAGTTTGTACAAAAAAGCAGGCT

attB2adap-R: GGGGACCACTTTGTACAAGAAAGCTGGGT

The attB-opa amplicon was obtained by PCR with Phusion proofreading polymerase (ThermoFisher Scientific), using primers opaDM-F and opaA-R. This first amplicon was diluted 1000-fold, then Phusion PCR was repeated with primers attB1adap-F and attB2adap-R. This attB-opa amplicon was recombined into Gateway donor vector pDONR (ThermoFisher Scientific), using the BP Clonase II kit (ThermoFisher Scientific). Plasmid DNA from a sequence-verified clone was then recombined into pET-DEST42, using the LR Clonase II kit (ThermoFisher Scientific).

For expression of the fusion protein, plasmid DNA was transformed into One Shot BL21 Star (DE3) chemically competent E. coli (ThermoFisher Scientific). Opa protein was expressed in two ways, firstly by IPTG induction of exponentially growing cells (0.75 mM IPTG for 2.75 hours), secondly by overnight culture in TB Overnight Express (Novagen). The Opa fusion protein in pET-DEST42 had a C-terminal 6-His tag. Protein was purified from bacterial pellets, each from 100 ml of cells induced in IPTG or TB Overnight Express. Purification was carried out using Ni-NTA Agarose (Qiagen), under 8 M urea denaturing conditions according to the manufacturer's protocol. Purified protein was dialysed against water then concentrated using an Amicon Ultra-Ultracel 5 kDa centrifugal filter (Millipore). Antibodies were raised in two guinea pigs by Eurogentec.

HCR in situ hybridisation and antibody staining

Prior to staining, fixed embryos stored in methanol were put through a rehydration series of 5 minutes each at 75%, 50%, and 25% methanol in PBS + 0.1% Tween-20, then washed 3 times with

PBS + 0.1% Tween-20.

HCR in situ hybridisation was performed using probes and hairpins produced by Molecular Instruments, following the protocol for whole-mount fruit fly embryos included in ***Choi et al., 2016***, adapted for v3.0 probes as described in ***Choi et al., 2018***. In addition, the percentage of dextran sulphate in the probe hybridisation and amplification buffers was reduced from 10% w/v to 5% w/v, to reduce viscosity and allow the embryos to settle more easily in the tube. A 20 minute postfix step (4% formaldehyde in 5x SSC + 0.1% Tween-20) was added at the end of the protocol to stabilise the signal.

For antibody staining following HCR, embryos were incubated for 30 minutes in blocking solution [5% Normal Goat Serum (Vector Laboratories) in 5x SSC + 0.1% Triton X-100], at room temperature with rocking. Embryos were then incubated overnight in preabsorbed primary antibody diluted in blocking solution, at 4° C with rocking. Embryos were washed 4 times for 15 minutes in 5x SSC + 0.1% Triton X-100, at room temperature with rocking, then incubated for 30 minutes in blocking solution, at room temperature with rocking. Embryos were then incubated for 2 hours with fluorescently labeled secondary antibody diluted in blocking solution, at room temperature with rocking. Embryos were washed 4 times for 15 minutes then 1 time for 30 minutes with 5x SSC + 0.1% Triton X-100, at room temperature with rocking. Antibody staining without prior HCR was performed as above with the exception that PBS was used instead of 5x SSC. Primary antibodies were guinea pig anti-Opa (this work) at 1:5000, rabbit anti-Dichaete (***Soriano and Russell, 1998***) at 1:10, rabbit anti-Tll (***Kosman et al., 1998***) at 1:100, and rat anti-Hkb (***Ashyraliyev et al., 2009***) at 1:100. Secondary antibodies were goat anti-guinea pig Alexa Fluor 647 (Invitrogen A-21450), goat anti-rabbit Alexa Fluor 488 (Invitrogen A-11034), goat anti-rabbit Alexa Fluor 555 (Invitrogen A-21429), and goat anti-rat Alexa Fluor 488 (Invitrogen A-11006), diluted 1:1 with 100% glycerol for storage and used 1:500.

Following HCR and/or antibody staining, embryos were incubated for 30 minutes with 1 ng/μL DAPI (ThermoFisher Scientific) in 5x SSC + 0.1% Tween-20, at room temperature with rocking, then washed 3 times for 30 minutes in 5x SSC + 0.1% Tween-20, at room temperature with rocking. Prior to mounting, embryos were stored in 1.5 mL tubes in SlowFade Gold Antifade Mountant (ThermoFisher Scientific).

Microscopy

Embryos were mounted in SlowFade Gold Antifade Mountant (ThermoFisher) on glass microscope slides (Thermo Scientific) with #1.5 coverslips (Corning). #1.5 coverslips were used as bridges to prevent embryos from being squashed. Clear nail varnish was used to seal the edges of the slide.

Microscopy was performed on an Olympus FV3000 confocal microscope at the Department of Zoology Imaging Facility (University of Cambridge). Acquired images were 12-bit, with a 1024x768 scan format and a 2 μs/pixel dwell time. Whole embryo images were acquired using an Olympus UPlanSApo 30x 1.05 NA silicon immersion oil objective, a physical pixel size of 0.47 μm x 0.47 μm, and a Z-stack step size of 1.5 μm. The close-ups in ***Figure 1*** and ***Figure 3*** were acquired using an Olympus UPlanSApo 60x 1.3 NA silicon immersion oil objective, a physical pixel size of 0.21 μm x 0.21 μm, and a Z-stack step size of 0.8 μm. Each Z-stack was specified so as to span from just above the top surface of the focal embryo through to the middle of its yolk.

In each experiment, embryos had been stained for up to four transcripts and/or proteins of interest plus nuclei, generally using Alexa Fluor 488, Alexa Fluor 546, Alexa Fluor 594, Alexa Fluor 647, and DAPI. (For mutant experiments, a *lacZ* probe or a probe to a gene covered by a deficiency was additionally labelled with one of these same fluorophores, so that homozygous mutant embryos could be easily identified.) All imaging channels were acquired sequentially, to minimise cross-talk. The laser lines and collection windows were: 405 laser and 443-472 nm window for DAPI; 488 laser and 500-536 nm window for Alexa Fluor 488; 561 laser and 566-584 nm window for Alexa Fluor 546 or Alexa Fluor 555; 594 laser and 610-631 nm window for Alexa Fluor 594; 640 laser and 663-713 nm window for AlexaFluor 647. Alexa Fluor 514 (514 laser and 519-540 nm window) was used in

place of Alexa Fluor 488 for a round of HCR experiments carried out when the 488 laser was awaiting repair. When necessary, a transmitted light channel was also collected, to allow for embryo staging based on the progress of cellularisation.

Image analysis and figure preparation

Embryo staging was based on Bownes stages (***Bownes, 1975***; ***Campos-Ortega and Hartenstein, 1997***), with subdivision of particular stages into substages where necessary (details in ***Appendix 1***). Fiji (***Schindelin et al., 2012***) was used for routine inspection of imaging data and certain image adjustments (details in ***Appendix 2***). Image processing and analysis scripts were written in Python 3 (www.python.org), using the libraries `NumPy` (***Harris et al., 2020***), `SciPy` (***Virtanen et al., 2020***), `scikit-image` (***van der Walt et al., 2014***), and `matplotlib` (***Hunter, 2007***); see ***Appendix 2*** for details. Figures were assembled in Affinity Designer (Serif Europe). Embryo outlines were drawn manually in Affinity. Image look-up tables (LUTs) were either chosen from the "ChrisLUTs" LUT package for ImageJ (Christophe Leterrier and Scott Harden; github.com/cleterrier/ChrisLUTs; "NeuroCyto LUTs" update site in Fiji), or generated for custom colours using a macro provided by Nicolás De Francesco (github.com/ndefrancesco).

Models and simulations

Models (see)were implemented in python using `NumPy` (***Harris et al., 2020***), and outputs were plotted using `matplotlib` (***Hunter, 2007***). See ***Appendix 4*** for details.

List of figure supplements

- ***Figure 1—figure Supplement 1***. Single channel images.
- ***Figure 2—figure Supplement 1***. Additional single channel images.
- ***Figure 2—figure Supplement 2***. Additional early stage embryos.
- ***Figure 2—figure Supplement 3***. D antibody staining in embryos from stage 4 to stage 6.
- ***Figure 2—figure Supplement 4***.: Expression dynamics of timer gene transcripts and proteins.
- ***Figure 3—figure Supplement 1***. Single channel images.
- ***Figure 4—figure Supplement 1***. Timer gene expression traces from timer gene mutants, relative to wild-type.
- ***Figure 4—figure Supplement 2***. Full-length *opa* expression traces from timer gene mutants.
- ***Figure 4—figure Supplement 3***. Additional characterisation of $cad^{m\text{-}z\text{-}}$, $cad^{m\text{-}z+}$, and $cad^{m+z\text{-}}$ mutants.
- ***Figure 4—figure Supplement 4***. Timer gene expression in wg^{-} mutants at stage 6.
- ***Figure 4—figure Supplement 5***. Timer gene expression in opa^{-}, tll^{-}, and tll^{-} opa^{-} embryos at stage 6.
- ***Figure 4—figure Supplement 6***. Morphological differences between wild-type and $cad^{m\text{-}z\text{-}}$ blastoderms.
- ***Figure 5—figure Supplement 1***. Expression of *tll* and *hkb* in wild-type embryos from stage 2 to stage 6.
- ***Figure 5—figure Supplement 2***. Single channel images.
- ***Figure 5—figure Supplement 3***. Expression dynamics of *tll* and *hkb* transcripts.
- ***Figure 5—figure Supplement 4***. Relative expression dynamics of Tll protein and *tll* transcript.
- ***Figure 5—figure Supplement 5***. Relative expression dynamics of Hkb, Tll and Opa proteins.
- ***Figure 5—figure Supplement 6***. Examples of source imaging data for supplementary plots.
- ***Figure 6—figure Supplement 1***. Timer gene expression traces from terminal mutants, relative to wild-type.
- ***Figure 6—figure Supplement 2***. Expression of *tll* in wild-type and hkb^{-} embryos from stage 5.5 to stage 7.
- ***Figure 7—figure Supplement 1***. Terminal gene expression traces from $cad^{m\text{-}z\text{-}}$, tll^{-} and hkb^{-} mutants, relative to wild-type.

- ***Figure 7—figure Supplement 2***. Timer gene expression traces from *fkh*$^{-}$ mutants, relative to wild-type.
- ***Figure 7—figure Supplement 3***. *wg* and *cad* expression in *fkh*$^{-}$ mutants at stages 6 and 7.
- ***Figure 7—figure Supplement 4***. Abnormal morphogenesis in *cad*$^{m\text{-}z\text{-}}$ and *fkh*$^{-}$ mutants.
- ***Figure 8—figure Supplement 1***. Simulation of a hypothetical timer gene network for sequential segmentation.

List of source data files

- ***Figure 2—source data 1***. Expression trace source data.
- ***Figure 4—source data 1***. Expression trace source data.
- ***Figure 5—source data 1***. Expression trace source data.
- ***Figure 5—source data 2***. Measurements of the size of the posterior *tll* expression domain at stage 5.2 and stage 5.5.
- ***Figure 6—source data 1***. Expression trace source data.
- ***Figure 7—source data 1***. Expression trace source data.
- **Figure 2—figure Supplement 4—source data 1**. Expression trace source data.
- **Figure 4—figure Supplement 6—source data 2**. Measurements of wild-type and *cad*$^{m\text{-}z\text{-}}$ blastoderms.
- **Figure 5—figure Supplement 3—source data 3**. Expression trace source data .
- **Figure 5—figure Supplement 4—source data 4**. Expression trace source data.
- **Figure 5—figure Supplement 5—source data 5**. Expression trace source data.
- ***Appendix 2—Figure 1—source data 1***. Sample image stack and image analysis scripts.
- ***Appendix 2—Figure 1—source data 2***. List of source image files for all figures.

List of appendices

- ***Appendix 1***. Embryo staging and substaging criteria.
- ***Appendix 2***. Image processing and analysis.
- ***Appendix 3***. Evidence for proposed cross-regulatory interactions between Tll, Hkb, Fkh, Wg, Cad, D, and Opa.
- ***Appendix 4***. Model and simulation details.

Acknowledgements

This project was made possible by Michael Akam, who provided laboratory space, resources, encouragement, and helpful feedback on the manuscript. We are grateful to Ken Siggens for generating the guinea pig anti-Opa antibody, and to Simon Collier at the Department of Genetics Fly Facility (University of Cambridge) for creating the *tll- opa*$^{-}$ double mutant. We thank the Imaging Facility at the Department of Zoology (University of Cambridge) for confocal imaging support, and members of the *Drosophila* community for various fly lines and reagents. EC thanks Angela DePace for hosting him in her group while work on this project was ongoing. Stocks and materials obtained from the Bloomington Drosophila Stock Center (NIH P40OD018537) and the Drosophila Genomics Resource Center (NIH 2P40OD010949) were used in this study. Information from FlyBase (***Larkin et al., 2021***) was invaluable.

Materials availability statement

Aliquots of the new Opa antibody are available from EC on request. The new *tll*$^{-}$ *opa*$^{-}$ double mutant is available from EC on request.

Data availability statement

All necessary data are included in the main text, appendices, and supplementary information. The confocal imaging dataset on which this study is based is freely available to download from the

BioImage Archive (http://www.ebi.ac.uk/bioimage-archive; ***Ellenberg et al., 2018***; ***Sarkans et al., 2018***) under accession number S-BIAD582. This 335 GB dataset contains multiplexed image stacks of more than 800 individual embryos, including 12 different genotypes and over 50 different genotype / gene product combinations. Image analysis code is provided in ***Appendix 2—Figure 1—source data 1***. A list of the corresponding image file(s) within the dataset for all figure panels within the main text, appendices, and supplementary information is provided in ***Appendix 2—Figure 1—source data 2***. Source Data files are provided for the expression traces in the main and supplementary figures.

Funding statement

EC was supported by a BBSRC Research Grant (BB/P009336/1), a Junior Research Fellowship from Trinity College, Cambridge, and an EMBO postdoctoral fellowship (EMBO ALTF 383-2018). MAB was supported by the Deutsche Forschungsgemeinschaft (DFG Research Fellowship BE 6732/1-1), the Isaac Newton Trust (Research Grant) and the University of Cambridge Department of Zoology. MB was supported by a PhD studentship from the Wellcome Trust (220019/Z/19/Z).

Competing interests statement

The authors declare no competing interests.

References

Abdusselamoglu MD, Eroglu E, Burkard TR, Knoblich JA. The transcription factor odd-paired regulates temporal identity in transit-amplifying neural progenitors via an incoherent feed-forward loop. eLife. 2019; 8:e46566.

Akam M. The molecular basis for metameric pattern in the Drosophila embryo. Development. 1987; 101(1):1–22.

Aleksic J, Ferrero E, Fischer B, Shen SP, Russell S. The role of Dichaete in transcriptional regulation during Drosophila embryonic development. BMC genomics. 2013; 14:861.

Ashyraliyev M, Siggens K, Janssens H, Blom J, Akam M, Jaeger J. Gene circuit analysis of the terminal gap gene huckebein. PLoS computational biology. 2009; 5(10):e1000548.

Baker NE. Localization of transcripts from the wingless gene in whole Drosophila embryos. Development. 1988; 103(2):289–298.

Baker NE. Molecular cloning of sequences from wingless, a segment polarity gene in Drosophila: the spatial distribution of a transcript in embryos. The EMBO Journal. 1987; 6(6):1765–1773.

Bate CM. Embryogenesis of an insect nervous system. I. A map of the thoracic and abdominal neuroblasts in Locusta migratoria. Journal of Embryology and Experimental Morphology. 1976; 35(1):107–123.

Baumgartner S, Bopp D, Burri M, Noll M. Structure of two genes at the gooseberry locus related to the paired gene and their spatial expression during Drosophila embryogenesis. Genes & Development. 1987; 1(10):1247–1267.

Baumgartner S, Noll M. Network of interactions among pair-rule genes regulating paired expression during primordial segmentation of Drosophila. Mechanisms of Development. 1990; 33(1):1–18.

Benedyk MJ, Mullen JR, DiNardo S. odd-paired: a zinc finger pair-rule protein required for the timely activation of engrailed and wingless in Drosophila embryos. Genes & Development. 1994; 8(1):105–117.

Bhat KM, Farkas G, Karch F, Gyurkovics H, Gausz J, Schedl P. The GAGA factor is required in the early Drosophila embryo not only for transcriptional regulation but also for nuclear division. Development. 1996; 122(4):1113–1124.

Bickel RD, Cleveland HC, Barkas J, Jeschke CC, Raz AA, Stern DL, Davis GK. The pea aphid uses a version of the terminal system during oviparous, but not viviparous, development. EvoDevo. 2013; 4(1):10.

Biffar L, Stollewerk A. Conservation and evolutionary modifications of neuroblast expression patterns in insects. Developmental Biology. 2014; 388(1):103–116.

Birkholz O, Rickert C, Berger C, Urbach R, Technau GM. Neuroblast pattern and identity in the Drosophila tail region and role of doublesex in the survival of sex-specific precursors. Development. 2013; 140(8):1830–1842.

Bownes M. A photographic study of development in the living embryo of Drosophila melanogaster. Journal of Embryology and Experimental Morphology. 1975; 33(3):789–801.

Brena C, Akam M. An analysis of segmentation dynamics throughout embryogenesis in the centipede Strigamia maritima. BMC biology. 2013; 11:112.

Bronner G, Jackle H. Control and function of terminal gap gene activity in the posterior pole region of the Drosophila embryo. Mechanisms of Development. 1991; 35(3):205–211.

Bronner G, Jackle H. Regulation and function of the terminal gap gene huckebein in the Drosophila blastoderm. International Journal of Developmental Biology. 1996; 40(1):157–165.

Bronner G, Chu-LaGraff Q, Doe CQ, Taubert H, Jackie H. Spl/egr-like zinc-finger protein required for endoderm specification and germ-layer formation in Drosophila. Nature. 1994; 369:664–8.

Brown JL, Sonoda S, Ueda H, Scott MP, Wu C. Repression of the Drosophila fushi tarazu (ftz) segmentation gene. The EMBO journal. 1991; 10(3):665–674.

Cadigan KM, Grossniklaus U, Gehring WJ. Localized expression of sloppy paired protein maintains the polarity of Drosophila parasegments. Genes & Development. 1994; 8(8):899–913.

Campos-Ortega JA, Hartenstein V. The Embryonic Development of Drosophila Melanogaster. Springer Berlin / Heidelberg; 1997.

Casanova J, Struhl G. Localized surface activity of torso, a receptor tyrosine kinase, specifies terminal body pattern in Drosophila. Genes & Development. 1989; 3(12B):2025–2038.

Casanova J. Pattern formation under the control of the terminal system in the Drosophila embryo. Development. 1990; 110:621–8.

Casanova J, Llimargas M, Greenwood S, Struhl G. An oncogenic form of human raf can specify terminal body pattern in Drosophila. Mechanisms of Development. 1994; 48(1):59–64.

Chapman RF, Simpson SJ, Douglas AE. The Insects: Structure and Function. Cambridge University Press; 2013.

Choi HMT, Calvert CR, Husain N, Huss D, Barsi JC, Deverman BE, Hunter RC, Kato M, Lee SM, Abelin ACT, Rosenthal AZ, Akbari OS, Li Y, Hay BA, Sternberg PW, Patterson PH, Davidson EH, Mazmanian SK, Prober DA, van de Rijn M, et al. Mapping a multiplexed zoo of mRNA expression. Development. 2016; 143(19):3632–3637.

Choi HMT, Schwarzkopf M, Fornace ME, Acharya A, Artavanis G, Stegmaier J, Cunha A, Pierce NA. Third-generation in situ hybridization chain reaction: multiplexed, quantitative, sensitive, versatile, robust. Development. 2018; 145(12):dev165753.

Chou Tb, Perrimon N. The autosomal FLP-DFS technique for generating germline mosaics in Drosophila melanogaster. Genetics. 1996; 144(4):1673–1679.

Chung S, Kim S, Andrew DJ. Uncoupling apical constriction from tissue invagination. eLife. 2017; 6:e22235.

Clark E. Dynamic patterning by the Drosophila pair-rule network reconciles long-germ and short-germ segmentation. PLoS biology. 2017; 15(9):e2002439.

Clark E. Time and space in segmentation. Interface Focus. 2021; 11(3):20200049.

Clark E, Akam M. Odd-paired controls frequency doubling in Drosophila segmentation by altering the pair-rule gene regulatory network. eLife. 2016; 5:e18215.

Clark E, Peel AD. Evidence for the temporal regulation of insect segmentation by a conserved sequence of transcription factors. Development. 2018; p. dev.155580.

Clark E, Peel AD, Akam M. Arthropod segmentation. Development. 2019; 146(18):dev170480.

Copf T, Schröder R, Averof M. Ancestral role of caudal genes in axis elongation and segmentation. Proceedings of the National Academy of Sciences of the United States of America. 2004; 101(51):17711–17715.

Costa M, Wilson ET, Wieschaus E. A putative cell signal encoded by the folded gastrulation gene coordinates cell shape changes during Drosophila gastrulation. Cell. 1994; 76(6):1075–1089.

Davis GK, Patel NH. Short, long, and beyond: molecular and embryological approaches to insect segmentation. Annual Review of Entomology. 2002; 47:669–699.

Demerec M. Biology of Drosophila. New York: John Wiley and Sons, Inc.; 1950.

Diaz RJ, Harbecke R, Singer JB, Pignoni F, Janning W, Lengyel JA. Graded effect of tailless on posterior gut development: molecular basis of an allelic series of a nuclear receptor gene. Mechanisms of Development. 1996; 54(1):119–130.

DiNardo S. Development of embryonic pattern in D. melanogaster as revealed by accumulation of the nuclear engrailed protein. Cell. 1985; 43(1):59–69.

DiNardo S, O'Farrell PH. Establishment and refinement of segmental pattern in the Drosophila embryo: spatial control of engrailed expression by pair-rule genes. Genes & Development. 1987; 1(10):1212–1225.

Doe CQ. Molecular markers for identified neuroblasts and ganglion mother cells in the Drosophila central nervous system. Development. 1992; 116(4):855–863.

Duffy JB, Perrimon N. The Torso Pathway in Drosophila: Lessons on Receptor Tyrosine Kinase Signaling and Pattern Formation. Developmental Biology. 1994; 166(2):380–395.

Duncan EJ, Benton MA, Dearden PK. Canonical terminal patterning is an evolutionary novelty. Developmental Biology. 2013; 377(1):245–261.

El-Sherif E, Zhu X, Fu J, Brown SJ. Caudal Regulates the Spatiotemporal Dynamics of Pair-Rule Waves in Tribolium. PLoS Genetics. 2014; 10(10):e1004677.

Ellenberg J, Swedlow JR, Barlow M, Cook CE, Sarkans U, Patwardhan A, Brazma A, Birney E. A call for public archives for biological image data. Nature Methods. 2018; 15(11):849–854.

Farkas G, Gausz J, Galloni M, Reuter G, Gyurkovics H, Karch F. The Trithorax-like gene encodes the Drosophila GAGA factor. Nature. 1994; 371(6500):806–808.

Fjose A, McGinnis WJ, Gehring WJ. Isolation of a homoeo box-containing gene from the engrailed region of Drosophila and the spatial distribution of its transcripts. Nature. 1985; 313(6000):284–289.

Foe VE. Mitotic domains reveal early commitment of cells in Drosophila embryos. Development. 1989; 107(1):1–22.

Frasch M, Hoey T, Rushlow C, Doyle H, Levine M. Characterization and localization of the even-skipped protein of Drosophila. The EMBO journal. 1987; 6(3):749–759.

Freeland DE, Kuhn DT. Expression patterns of developmental genes reveal segment and parasegment organization of D. melanogaster genital discs. Mechanisms of Development. 1996; 56(1-2):61–72.

Fujimi TJ, Hatayama M, Aruga J. Xenopus Zic3 controls notochord and organizer development through suppression of the Wnt/β-catenin signaling pathway. Developmental Biology. 2012; 361(2):220–231.

García-Solache M, Jaeger J, Akam M. A systematic analysis of the gap gene system in the moth midge Clogmia albipunctata. Developmental Biology. 2010; 344(1):306–318.

Gaskill MM, Gibson TJ, Larson ED, Harrison MM. GAF is essential for zygotic genome activation and chromatin accessibility in the early Drosophila embryo. eLife. 2021; 10:e66668.

Gaul U, Weigel D. Regulation of Krüppel expression in the anlage of the Malpighian tubules in the Drosophila embryo. Mechanisms of Development. 1991; 33:57–67.

Goldstein RE. Huckebein repressor activity in Drosophila terminal patterning is mediated by Groucho. Development. 1999; 126(17):3747–55.

Goyal Y, Schüpbach T, Shvartsman SY. A quantitative model of developmental RTK signaling. Developmental Biology. 2018; 442(1):80–86.

Graham V, Khudyakov J, Ellis P, Pevny L. SOX2 functions to maintain neural progenitor identity. Neuron. 2003; 39(5):749–765.

Greenwood S, Struhl G. Different levels of Ras activity can specify distinct transcriptional and morphological consequences in early Drosophila embryos. Development. 1997; 124(23):4879–4886.

Grossniklaus U, Pearson RK, Gehring WJ. The Drosophila sloppy paired locus encodes two proteins involved in segmentation that show homology to mammalian transcription factors. Genes & Development. 1992; 6(6):1030–1051.

Gutjahr T, Patel NH, Li X, Goodman CS, Noll M. Analysis of the gooseberry locus in Drosophila embryos: gooseberry determines the cuticular pattern and activates gooseberry neuro. Development. 1993; 118(1):21–31.

Harbecke R. The segmentation gene Krüppel of Drosophila melanogaster has homeotic properties. Genes & Development. 1989; 3(1):114–22.

Harris CR, Millman KJ, van der Walt SJ, Gommers R, Virtanen P, Cournapeau D, Wieser E, Taylor J, Berg S, Smith NJ, Kern R, Picus M, Hoyer S, van Kerkwijk MH, Brett M, Haldane A, Del Río JF, Wiebe M, Peterson P, Gérard-Marchant P, et al. Array programming with NumPy. Nature. 2020; 585(7825):357–362.

Harrison MM, Li XY, Kaplan T, Botchan MR, Eisen MB. Zelda binding in the early Drosophila melanogaster embryo marks regions subsequently activated at the maternal-to-zygotic transition. PLoS genetics. 2011; 7(10):e1002266.

Harrison SD, Travers AA. The tramtrack gene encodes a Drosophila finger protein that interacts with the ftz transcriptional regulatory region and shows a novel embryonic expression pattern. The EMBO journal. 1990; 9(1):207–216.

de las Heras JM, Casanova J. Spatially distinct downregulation of Capicua repression and tailless activation by the Torso RTK pathway in the Drosophila embryo. Mechanisms of Development. 2006; 123(6):481–486.

Hoch M, Pankratz MJ. Control of gut development by fork head and cell signaling molecules in Drosophila. Mechanisms of Development. 1996; 58(1-2):3–14.

Hoey T, Doyle HJ, Harding K, Wedeen C, Levine M. Homeo box gene expression in anterior and posterior regions of the Drosophila embryo. Proceedings of the National Academy of Sciences. 1986; 83(13):4809–4813.

Hou XS, Melnick MB, Perrimon N. Marelle acts downstream of the Drosophila HOP/JAK kinase and encodes a protein similar to the mammalian STATs. Cell. 1996; 84(3):411–419.

Houtmeyers R, Souopgui J, Tejpar S, Arkell R. The ZIC gene family encodes multi-functional proteins essential for patterning and morphogenesis. Cellular and Molecular Life Sciences. 2013; 70(20):3791–3811.

Huang A, Rupprecht JF, Saunders TE. Embryonic geometry underlies phenotypic variation in decanalized conditions. eLife. 2020; 9:e47380.

Hughes CL, Kaufman TC. Hox genes and the evolution of the arthropod body plan1. Evolution & Development. 2002; 4(6):459–499.

Hunter JD. Matplotlib: A 2D graphics environment. Computing in Science & Engineering. 2007; 9(3):90–95.

Häder T, La Rosée A, Ziebold U, Busch M, Taubert H, Jäckle H, Rivera-Pomar R. Activation of posterior pair-rule stripe expression in response to maternal caudal and zygotic knirps activities. Mechanisms of Development. 1998; 71(1-2):177–186.

Ingham P, Martinez-Arias A, Lawrence PA, Howard K. Expression of engrailed in the parasegment of Drosophila. Nature. 1985; 317(6038):634–636.

Jaeger J. The gap gene network. Cellular and Molecular Life Sciences. 2011; 68(2):243–274.

Jaeger J, Surkova S, Blagov M, Janssens H, Kosman D, Kozlov KN, Manu, Myasnikova E, Vanario-Alonso CE, Samsonova M, Sharp DH, Reinitz J. Dynamic control of positional information in the early Drosophila embryo. Nature. 2004; 430(6997):368–371.

Janssen R. Gene expression suggests double-segmental and single-segmental patterning mechanisms during posterior segment addition in the beetle Tribolium castaneum. The International Journal of Developmental Biology. 2014; 58(5):343–347.

Janssens H, Crombach A, Richard Wotton K, Cicin-Sain D, Surkova S, Lu Lim C, Samsonova M, Akam M, Jaeger J. Lack of tailless leads to an increase in expression variability in Drosophila embryos. Developmental Biology. 2013; 377(1):305–317.

Jarial MS. Ultrastructure of the anal organ of Drosophila larva with reference to ion transport. Tissue & Cell. 1987; 19:559–75.

Jaynes JB, Fujioka M. Drawing lines in the sand: even skipped et al. and parasegment boundaries. Developmental Biology. 2004; 269(2):609–622.

Johnson HE, Djabrayan NJV, Shvartsman SY, Toettcher JE. Optogenetic Rescue of a Patterning Mutant. Current Biology. 2020; p. S0960982220309118.

Johnson HE, Toettcher JE. Signaling Dynamics Control Cell Fate in the Early Drosophila Embryo. Developmental Cell. 2019; 48(3):361–370.e3.

Joshi P, Darr AJ, Skromne I. CDX4 regulates the progression of neural maturation in the spinal cord. Developmental Biology. 2019; 449(2):132–142.

Jürgens G, Wieschaus E, Nüsslein-Volhard C, Kluding H. Mutations affecting the pattern of the larval cuticle inDrosophila melanogaster. Wilhelm Roux's archives of developmental biology. 1984; 193(5):283–295.

Jürgens G. Segmental organisation of the tail region in the embryo of Drosophila melanogaster: A blastoderm fate map of the cuticle structures of the larval tail region. Roux's Archives of Developmental Biology. 1987; 196(3):141–157.

Jürgens G, Weigel D. Terminal versus segmental development in the Drosophila embryo: the role of the homeotic gene fork head. Roux's Archives of Developmental Biology. 1988; 197(6):345–354.

Keenan SE, Avdeeva M, Yang L, Alber DS, Wieschaus EF, Shvartsman SY. Dynamics of Drosophila endoderm specification. Proceedings of the National Academy of Sciences. 2022; 119(15):e2112892119.

Keenan SE, Blythe SA, Marmion RA, Djabrayan NJV, Wieschaus EF, Shvartsman SY. Rapid Dynamics of Signal-Dependent Transcriptional Repression by Capicua. Developmental Cell. 2020; 52(6):794–801.e4.

Keränen SVE, Fowlkes CC, Luengo Hendriks CL, Sudar D, Knowles DW, Malik J, Biggin MD. Three-dimensional morphology and gene expression in the Drosophila blastoderm at cellular resolution II: dynamics. Genome Biology. 2006; 7(12):R124.

Kittelmann S, Ulrich J, Posnien N, Bucher G. Changes in anterior head patterning underlie the evolution of long germ embryogenesis. Developmental Biology. 2013; 374(1):174–184.

Klingler M, Erdélyi M, Szabad J, Nüsslein-Volhard C. Function of torso in determining the terminal anlagen of the Drosophila embryo. Nature. 1988; 335(6187):275–277.

Klomp J, Athy D, Kwan CW, Bloch NI, Sandmann T, Lemke S, Schmidt-Ott U. A cysteine-clamp gene drives embryo polarity in the midge Chironomus. Science. 2015; 348(6238):1040–1042.

Kornberg T, Sidén I, O'Farrell P, Simon M. The engrailed locus of Drosophila: in situ localization of transcripts reveals compartment-specific expression. Cell. 1985; 40(1):45–53.

Koromila T, Gao F, Iwasaki Y, He P, Pachter L, Gergen JP, Stathopoulos A. Odd-paired is a pioneer-like factor that coordinates with Zelda to control gene expression in embryos. eLife. 2020; 9:e59610.

Kosman D, Small S, Reinitz J. Rapid preparation of a panel of polyclonal antibodies to Drosophila segmentation proteins. Development Genes and Evolution. 1998; 208(5):290–294.

Kuhn DT, Chaverri JM, Persaud DA, Madjidi A. Pair-rule genes cooperate to activate en stripe 15 and refine its margins during germ band elongation in the D. melanogaster embryo. Mechanisms of development. 2000; 95(1-2):297–300.

Kuhn DT, Sawyer M, Packert G, Turenchalk G, Mack JA, Sprey TE, Gustavson E, Kornberg TB. Development of the D. melanogaster caudal segments involves suppression of the ventral regions of A8, A9 and A10. Development. 1992; 116:11–20.

Kuhn D, Turenchalk G, Mack JA, Packert G, Kornberg TB. Analysis of the genes involved in organizing the tail segments of the Drosophila melanogaster embryo. Mechanisms of Development. 1995; 53(1):3–13.

La Rosee A. Mechanism and Bicoid-dependent control of hairy stripe 7 expression in the posterior region of the Drosophila embryo. The EMBO Journal. 1997; 16(14):4403–4411.

Larkin A, Marygold SJ, Antonazzo G, Attrill H, Dos Santos G, Garapati PV, Goodman JL, Gramates LS, Millburn G, Strelets VB, Tabone CJ, Thurmond J, FlyBase Consortium. FlyBase: updates to the Drosophila melanogaster knowledge base. Nucleic Acids Research. 2021; 49(D1):D899–D907.

Lawrence PA, Johnston P, Macdonald P, Struhl G. Borders of parasegments in Drosophila embryos are delimited by the fushi tarazu and even-skipped genes. Nature. 1987; 328(6129):440–442.

Lawrence PA, Martinez-Arias A, Gardner RL, Lawrence PA. The cell lineage of segments and parasegments in Drosophila. Philosophical Transactions of the Royal Society of London B, Biological Sciences. 1985; 312(1153):83–90.

Lee JJ, von Kessler DP, Parks S, Beachy PA. Secretion and localized transcription suggest a role in positional signaling for products of the segmentation gene hedgehog. Cell. 1992; 71(1):33–50.

Lemke S, Busch SE, Antonopoulos DA, Meyer F, Domanus MH, Schmidt-Ott U. Maternal activation of gap genes in the hover fly Episyrphus. Development. 2010; 137(15):2604–2604.

Levine M, Harding K, Wedeen C, Doyle H, Hoey T, Radomska H. Expression of the Homeo Box Gene Family in Drosophila. Cold Spring Harbor Symposia on Quantitative Biology. 1985; 50(0):209–222.

Li WX. Functions and mechanisms of receptor tyrosine kinase Torso signaling: Lessons from Drosophila embryonic terminal development. Developmental Dynamics. 2005; 232(3):656–672.

Li Xy, MacArthur S, Bourgon R, Nix D, Pollard DA, Iyer VN, Hechmer A, Simirenko L, Stapleton M, Luengo Hendriks CL, Chu HC, Ogawa N, Inwood W, Sementchenko V, Beaton A, Weiszmann R, Celniker SE, Knowles DW, Gingeras T, Speed TP, et al. Transcription factors bind thousands of active and inactive regions in the Drosophila blastoderm. PLoS biology. 2008; 6(2):e27.

Liang HL, Nien CY, Liu HY, Metzstein MM, Kirov N, Rushlow C. The zinc-finger protein Zelda is a key activator of the early zygotic genome in Drosophila. Nature. 2008; 456(7220):400–403.

Lim B, Fukaya T, Heist T, Levine M. Temporal dynamics of pair-rule stripes in living Drosophila embryos. Proceedings of the National Academy of Sciences of the United States of America. 2018; 115(33):8376–8381.

Lohs-Schardin M, Cremer C, Nüsslein-Volhard C. A fate map for the larval epidermis of Drosophila melanogaster: localized cuticle defects following irradiation of the blastoderm with an ultraviolet laser microbeam. Developmental Biology. 1979; 73(2):239–255.

Lord PCW, Lin MH, Hales KH, Storti RV. Normal Expression and the Effects of Ectopic Expression of the Drosophila muscle segment homeobox (msh) Gene Suggest a Role in Differentiation and Patterning of Embryonic Muscles. Developmental Biology. 1995; 171(2):627–640.

Lu X, Li JM, Elemento O, Tavazoie S, Wieschaus EF. Coupling of zygotic transcription to mitotic control at the Drosophila mid-blastula transition. Development. 2009; 136(12):2101–2110.

Luengo Hendriks CL, Keränen SVE, Fowlkes CC, Simirenko L, Weber GH, DePace AH, Henriquez C, Kaszuba DW, Hamann B, Eisen MB, Malik J, Sudar D, Biggin MD, Knowles DW. Three-dimensional morphology and gene expression in the Drosophila blastoderm at cellular resolution I: data acquisition pipeline. Genome Biology. 2006; 7(12):R123.

Lynch JA, Olesnicky EC, Desplan C. Regulation and function of tailless in the long germ wasp Nasonia vitripennis. Development Genes and Evolution. 2006; 216(7-8):493–498.

Ma Y, Niemitz EL, Nambu PA, Shan X, Sackerson C, Fujioka M, Goto T, Nambu JR. Gene regulatory functions of Drosophila fish-hook, a high mobility group domain Sox protein. Mechanisms of Development. 1998; 73(2):169–182.

MacArthur S, Li XY, Li J, Brown JB, Chu HC, Zeng L, Grondona BP, Hechmer A, Simirenko L, Keränen SVE, Knowles DW, Stapleton M, Bickel P, Biggin MD, Eisen MB. Developmental roles of 21 Drosophila transcription factors are determined by quantitative differences in binding to an overlapping set of thousands of genomic regions. Genome Biology. 2009; 10(7):R80.

Macdonald PM, Ingham P, Struhl G. Isolation, structure, and expression of even-skipped: a second pair-rule gene of Drosophila containing a homeo box. Cell. 1986; 47(5):721–734.

Macdonald PM, Struhl G. A molecular gradient in early Drosophila embryos and its role in specifying the body pattern. Nature. 1986; 324(6097):537–545.

Mahoney PA, Lengyel JA. The zygotic segmentation mutant tailless alters the blastoderm fate map of the Drosophila embryo. Developmental Biology. 1987; 122(2):464–470.

Martinez-Arias A, Lawrence PA. Parasegments and compartments in the Drosophila embryo. Nature. 1985; 313(6004):639–642.

Matsuda R. Morphology and Evolution of the Insect Abdomen: With Special Reference to Developmental Patterns and Their Bearings Upon Systematics. Pergamon Press; 1976.

McDaniel SL, Gibson TJ, Schulz KN, Fernandez Garcia M, Nevil M, Jain SU, Lewis PW, Zaret KS, Harrison MM. Continued Activity of the Pioneer Factor Zelda Is Required to Drive Zygotic Genome Activation. Molecular Cell. 2019; 74(1):185–195.e4.

Meijering EH, Niessen WJ, Viergever MA. Quantitative evaluation of convolution-based methods for medical image interpolation. Medical Image Analysis. 2001; 5(2):111–126.

Merzdorf CS. Emerging roles for zic genes in early development. Developmental Dynamics. 2007; 236(4):922–940.

Mlodzik M, Fjose A, Gehring WJ. Isolation of caudal, a Drosophila homeo box-containing gene with maternal expression, whose transcripts form a concentration gradient at the pre-blastoderm stage. The EMBO Journal. 1985; 4(11):2961–2969.

Mlodzik M, Gehring WJ. Expression of the caudal gene in the germ line of Drosophila: Formation of an RNA and protein gradient during early embryogenesis. Cell. 1987; 48(3):465–478.

Mlodzik M, Gehring WJ. Hierarchy of the genetic interactions that specify the anteroposterior segmentation pattern of the Drosophila embryo as monitored by caudal protein expression. Development. 1987; 101:421–435.

Mohler J, Vani K. Molecular organization and embryonic expression of the hedgehog gene involved in cell-cell communication in segmental patterning of Drosophila. Development. 1992; 115(4):957–971.

Mohler J. Spatial regulation of segment polarity gene expression in the anterior terminal region of the Drosophila blastoderm embryo. Mechanisms of Development. 1995; 50(2-3):151–161.

Moran E, Jimenez G. The Tailless Nuclear Receptor Acts as a Dedicated Repressor in the Early Drosophila Embryo. Molecular and Cellular Biology. 2006; 26(9):3446–3454.

Moshe A, Kaplan T. Genome-wide search for Zelda-like chromatin signatures identifies GAF as a pioneer factor in early fly development. Epigenetics & Chromatin. 2017; 10(1):33.

Mukherjee S, Luedeke DM, McCoy L, Iwafuchi M, Zorn AM. SOX transcription factors direct TCF-independent WNT/β-catenin responsive transcription to govern cell fate in human pluripotent stem cells. Cell Reports. 2022; 40(8):111247.

Murgan S, Kari W, Rothbächer U, Iché-Torres M, Mélénec P, Hobert O, Bertrand V. Atypical Transcriptional Activation by TCF via a Zic Transcription Factor in C. elegans Neuronal Precursors. Developmental Cell. 2015; 33(6):737–745.

Nambu PA, Nambu JR. The Drosophila fish-hook gene encodes a HMG domain protein essential for segmentation and CNS development. Development. 1996; 122(11):3467–3475.

Nasiadka A, Krause HM. Kinetic analysis of segmentation gene interactions in Drosophila embryos. Development. 1999; 126(7):1515–1526.

Nasiadka A, Dietrich BH, Krause HM. Anterior-posterior patterning in the Drosophila embryo. In: *Advances in Developmental Biology and Biochemistry*, vol. 12 Elsevier; 2002.p. 155–204.

Nien CY, Liang HL, Butcher S, Sun Y, Fu S, Gocha T, Kirov N, Manak JR, Rushlow C. Temporal coordination of gene networks by Zelda in the early Drosophila embryo. PLoS genetics. 2011; 7(10):e1002339.

Nusslein-Volhard C, Frohnhofer HG, Lehmann R. Determination of anteroposterior polarity in Drosophila. Science. 1987; 238(4834):1675–1681.

Olesnicky EC, Brent AE, Tonnes L, Walker M, Pultz MA, Leaf D, Desplan C. A caudal mRNA gradient controls posterior development in the wasp Nasonia. Development. 2006; 133(20):3973–3982.

Panovska-Griffiths J, Page KM, Briscoe J. A gene regulatory motif that generates oscillatory or multiway switch outputs. Journal of the Royal Society, Interface. 2013; 10(79):20120826.

Parks S, Wieschaus E. The Drosophila gastrulation gene concertina encodes a Gα-like protein. Cell. 1991; 64(2):447–458.

Perez-Carrasco R, Barnes CP, Schaerli Y, Isalan M, Briscoe J, Page KM. Combining a Toggle Switch and a Repressilator within the AC-DC Circuit Generates Distinct Dynamical Behaviors. Cell Systems. 2018; 6(4):521–530.e3.

Perkins LA, Perrimon N. The molecular genetics of tail development in Drosophila melanogaster. In Vivo. 1991; 5(5):521–531.

Pignoni F, Steingrimsson E, JA L. bicoid and the terminal system activate tailless expression in the early Drosophila embryo. Development. 1992; 115:239–251.

Pignoni F, Baldarelli RM, Steingrimsson E, Diaz RJ, Patapoutian A, Merriam JR, Lengyel JA. The Drosophila gene tailless is expressed at the embryonic termini and is a member of the steroid receptor superfamily. Cell. 1990; 62(1):151–163.

Pourebrahim R, Houtmeyers R, Ghogomu S, Janssens S, Thelie A, Tran HT, Langenberg T, Vleminckx K, Bellefroid E, Cassiman JJ, Tejpar S. Transcription Factor Zic2 Inhibits Wnt/β-Catenin Protein Signaling. The Journal of Biological Chemistry. 2011; 286(43):37732–37740.

Read D, Levine M, Manley JL. Ectopic expression of the Drosophila tramtrack gene results in multiple embryonic defects, including repression of even-skipped and fushi tarazu. Mechanisms of Development. 1992; 38(3):183–195.

Reinitz J, Levine M. Control of the initiation of homeotic gene expression by the gap genes giant and tailless in Drosophila. Developmental Biology. 1990; 140(1):57–72.

Rijsewijk F, Schuermann M, Wagenaar E, Parren P, Weigel D, Nusse R. The Drosophila homology of the mouse mammary oncogene int-1 is identical to the segment polarity gene wingless. Cell. 1987; 50(4):649–657.

Rivera-Pomar R, Lu X, Perrimon N, Taubert H, Jäckle H. Activation of posterior gap gene expression in the Drosophila blastoderm. Nature. 1995; 376(6537):253–256.

van Rooijen C, Simmini S, Bialecka M, Neijts R, van de Ven C, Beck F, Deschamps J. Evolutionarily conserved requirement of Cdx for post-occipital tissue emergence. Development. 2012; 139(14):2576–2583.

Russell SR, Sanchez-Soriano N, Wright CR, Ashburner M. The Dichaete gene of Drosophila melanogaster encodes a SOX-domain protein required for embryonic segmentation. Development. 1996; 122(11):3669–3676.

Sackerson C, Fujioka M, Goto T. The even-skipped locus is contained in a 16-kb chromatin domain. Developmental Biology. 1999; 211(1):39–52.

Sarkans U, Gostev M, Athar A, Behrangi E, Melnichuk O, Ali A, Minguet J, Rada JC, Snow C, Tikhonov A, et al. The BioStudies database—one stop shop for all data supporting a life sciences study. Nucleic acids research. 2018; 46(D1):D1266–D1270.

Sato T, Denell RE. Segmental identity of caudal cuticular features of Drosophila melanogaster larvae and its control by the bithorax complex. Developmental Biology. 1986; 116(1):78–91.

Schindelin J, Arganda-Carreras I, Frise E, Kaynig V, Longair M, Pietzsch T, Preibisch S, Rueden C, Saalfeld S, Schmid B, Tinevez JY, White DJ, Hartenstein V, Eliceiri K, Tomancak P, Cardona A. Fiji: an open-source platform for biological-image analysis. Nature Methods. 2012; 9(7):676–682.

Schmidt-Ott U, Sander K, Technau GM. Expression of engrailed in embryos of a beetle and five dipteran species with special reference to the terminal regions. Roux's Archives of Developmental Biology. 1994; 203(6):298–303.

Schmied C, Jambor HK. Effective image visualization for publications–a workflow using open access tools and concepts. F1000Research. 2020; 9:1373.

Schoppmeier M, Schröder R. Maternal Torso Signaling Controls Body Axis Elongation in a Short Germ Insect. Current Biology. 2005; 15(23):2131–2136.

Schroder R, Eckert C, Wolff C, Tautz D. Conserved and divergent aspects of terminal patterning in the beetle Tribolium castaneum. Proceedings of the National Academy of Sciences. 2000; 97(12):6591–6596.

Schroeder MD, Greer C, Gaul U. How to make stripes: deciphering the transition from non-periodic to periodic patterns in Drosophila segmentation. Development. 2011; 138(14):3067–3078.

Schulz C, Schröder R, Hausdorf B, Wolff C, Tautz D. A caudal homologue in the short germ band beetle Tribolium shows similarities to both, the Drosophila and the vertebrate caudal expression patterns. Development Genes and Evolution. 1998; 208(5):283–289.

Schulz C, Tautz D. Zygotic caudal regulation by hunchback and its role in abdominal segment formation of the Drosophila embryo. Development. 1995; 121:1023–1028.

Selva EM, Stronach BE. Germline clone analysis for maternally acting Drosophila hedgehog components. Methods in Molecular Biology. 2007; 397:129–144.

da Silva SM, Vincent JP. Oriented cell divisions in the extending germband of Drosophila. Development. 2007; 134(17):3049–3054.

Singer JB, Harbecke R, Kusch T, Reuter R, Lengyel JA. Drosophila brachyenteron regulates gene activity and morphogenesis in the gut. Development. 1996; 22:3707–18.

Smits CM, Shvartsman SY. The design and logic of terminal patterning in Drosophila. In: *Current Topics in Developmental Biology*, vol. 137 Academic Press; 2020.p. 193–217.

Snodgrass RE. Principles of Insect Morphology. McGraw-Hill Book Company, Incorporated; 1935.

Soluri IV, Zumerling LM, Payan Parra OA, Clark EG, Blythe SA. Zygotic pioneer factor activity of Odd-paired/Zic is necessary for late function of the Drosophila segmentation network. eLife. 2020; 9:e53916.

Soriano NS, Russell S. The Drosophila SOX-domain protein Dichaete is required for the development of the central nervous system midline. Development. 1998; 125(20):3989–3996.

Spirov AV, Timakin DL, Reinitz J, Kosman D. Experimental Determination of Drosophila Embryonic Coordinates by Genetic Algorithms, the Simplex Method, and Their Hybrid. In: Goos G, Hartmanis J, van Leeuwen J, Cagnoni S, editors. *Real-World Applications of Evolutionary Computing*, vol. 1803 Springer Berlin / Heidelberg; 2000.p. 97–106.

Spirov AV, Vanario-Alonso CE, Spirova EN, Holloway DM. Experimental Determination of Intrinsic Drosophila Embryo Coordinates by Evolutionary Computation. In: Ngom A, Formenti E, Hao JK, Zhao XM, van Laarhoven T, editors. *Pattern Recognition in Bioinformatics* Springer Berlin / Heidelberg; 2013. p. 126–137.

Sprenger F, Stevens LM, Nüsslein-Volhard C. The Drosophila gene torso encodes a putative receptor tyrosine kinase. Nature. 1989; 338(6215):478–483.

Stevanovic M, Drakulic D, Lazic A, Ninkovic DS, Schwirtlich M, Mojsin M. SOX Transcription Factors as Important Regulators of Neuronal and Glial Differentiation During Nervous System Development and Adult Neurogenesis. Frontiers in Molecular Neuroscience. 2021; 14:654031.

Strecker TR, Kongsuwan K, Lengyel JA, Merriam JR. The zygotic mutant tailless affects the anterior and posterior ectodermal regions of the Drosophila embryo. Developmental Biology. 1986; 113(1):64–76.

Strecker TR, Merriam JR, Lengyel JA. Graded requirement for the zygotic terminal gene, tailless, in the brain and tail region of the Drosophila embryo. Development. 1988; 102:721–34.

Sullivan W, Ashburner M, Hawley RS. Drosophila protocols. Cold Spring Harbor Laboratory Press; 2000.

Surkova S, Kosman D, Kozlov K, Manu, Myasnikova E, Samsonova AA, Spirov A, Vanario-Alonso CE, Samsonova M, Reinitz J. Characterization of the Drosophila segment determination morphome. Developmental Biology. 2008; 313(2):844–862.

Sweeton D, Parks S, Costa M, Wieschaus E. Gastrulation in Drosophila: the formation of the ventral furrow and posterior midgut invaginations. Development. 1991; 112(3):775–789.

Tabata T, Eaton S, Kornberg TB. The Drosophila hedgehog gene is expressed specifically in posterior compartment cells and is a target of engrailed regulation. Genes & Development. 1992; 6(12B):2635–2645.

Tashiro S, Michiue T, Higashijima S, Zenno S, Ishimaru S, Takahashi F, Orihara M, Kojima T, Saigo K. Structure and expression of hedgehog, a Drosophila segment-polarity gene required for cell-cell communication. Gene. 1993; 124(2):183–189.

Trivedi V, Choi HMT, Fraser SE, Pierce NA. Multidimensional quantitative analysis of mRNA expression within intact vertebrate embryos. Development. 2018; 145(1):dev156869.

Tsurumi A, Xia F, Li J, Larson K, LaFrance R, Li WX. STAT is an essential activator of the zygotic genome in the early Drosophila embryo. PLoS genetics. 2011; 7(5):e1002086.

Turner FR, Mahowald AP. Scanning electron microscopy of Drosophila melanogaster embryogenesis: III. Formation of the head and caudal segments. Developmental Biology. 1979; 68(1):96–109.

Vincent BJ, Staller MV, Lopez-Rivera F, Bragdon MDJ, Pym ECG, Biette KM, Wunderlich Z, Harden TT, Estrada J, DePace AH. Hunchback is counter-repressed to regulate even-skipped stripe 2 expression in Drosophila embryos. PLoS genetics. 2018; 14(9):e1007644.

Virtanen P, Gommers R, Oliphant TE, Haberland M, Reddy T, Cournapeau D, Burovski E, Peterson P, Weckesser W, Bright J, van der Walt SJ, Brett M, Wilson J, Millman KJ, Mayorov N, Nelson ARJ, Jones E, Kern R, Larson E, Carey CJ, et al. SciPy 1.0: fundamental algorithms for scientific computing in Python. Nature Methods. 2020; 17(3):261–272.

van der Walt S, Schönberger JL, Nunez-Iglesias J, Boulogne F, Warner JD, Yager N, Gouillart E, Yu T, scikit-image contributors. scikit-image: image processing in Python. PeerJ. 2014; 2:e453.

Weigel D, Jurgens G, Klingler M, Jackle H. Two gap genes mediate maternal terminal pattern information in Drosophila. Science. 1990; 248(4954):495–498.

Weigel D, Jürgens G, Küttner F, Seifert E, Jäckle H. The homeotic gene fork head encodes a nuclear protein and is expressed in the terminal regions of the Drosophila embryo. Cell. 1989; 57(4):645–658.

Weisbrod A, Cohen M, Chipman AD. Evolution of the insect terminal patterning system—Insights from the milkweed bug, Oncopeltus fasciatus. Developmental Biology. 2013; 380(1):125–131.

Wilson MJ, Dearden PK. Tailless patterning functions are conserved in the honeybee even in the absence of Torso signaling. Developmental Biology. 2009; 335(1):276–287.

Wu LH, Lengyel JA. Role of caudal in hindgut specification and gastrulation suggests homology between Drosophila amnioproctodeal invagination and vertebrate blastopore. Development. 1998; 125:2433–42.

Yan R, Small S, Desplan C, Dearolf CR, Darnell JE. Identification of a Stat gene that functions in Drosophila development. Cell. 1996; 84(3):421–430.

Zhong Y, Herrera-Úbeda C, Garcia-Fernàndez J, Li G, Holland PWH. Mutation of amphioxus Pdx and Cdx demonstrates conserved roles for ParaHox genes in gut, anus and tail patterning. BMC Biology. 2020; 18(1):68.

Appendix 1

Embryo staging and selection

Briefly, embryos younger than stage 5 were staged to a nuclear cycle based on their nuclear density (stage 4.1 = nuclear cycle 10; stage 4.2 = nuclear cycle 11; stage 4.3 = nuclear cycle 12; stage 4.4 = nuclear cycle 13), while embryos older than stage 5 were staged by the progress of morphogenesis, the presence of mitotic domains (***Foe, 1989***), and/or the appearance of terminal segment-polarity stripes. Stage 5 itself was divided into 5 substages, stage 5.1 to stage 5.5, which can be differentiated from one another on the basis of *wg* expression, *D* expression, *eve* expression, or the progress of cellularisation (***Appendix 1—Figure 1***; for most stains, we relied on *wg* and/or *D* expression). ***Appendix 1—Table 1*** describes our staging criteria and also notes how our stage 5 classification scheme maps onto the 8 "temporal equivalence" classes used in ***Surkova et al.*** (***2008***), and the 4 "phases" used in ***Schroeder et al.*** (***2011***).

Expression patterns in embryos of the same (sub)stage and genotype generally looked remarkably similar; each phenotype we describe was observed in multiple individual embryos (biological replicates) and was consistent across different stain combinations (experiments). Occasional obviously atypical embryos (e.g., very small, or with abnormal patterns of mitotic division) were identified by visual inspection and discarded from the dataset. Any repeat scans of a given embryo were also discarded from the dataset to avoid pseudoreplication and artefacts from photo-bleaching. Embryos with the same stain combination were generally sourced from a single experiment; stainings were only repeated and/or combined when this was necessary to improve the coverage of stages. Embryos of all orientations were examined when characterising mutant phenotypes, but only laterally oriented embryos were selected for figure preparation and quantitative analysis. In most figures, a single representative embryo and/or expression trace is shown for any given (sub)stage. In some figures (***Figure 4***; ***Figure 6***; ***Figure 7***, ***Figure 4—figure Supplement 1***; ***Figure 4—figure Supplement 2***; ***Figure 5—figure Supplement 3***; ***Figure 6—figure Supplement 1***; ***Figure 7—figure Supplement 1***; ***Figure 7—figure Supplement 2***), expression traces from 2-4 embryos of the same stage and genotype are overlaid on the same axes to show the qualitative consistency of each phenotype across individuals. These sets of embryos were manually selected to be close matches in stage and orientation, since both factors influence the shape of the resulting expression trace.

Appendix 1—table 1: Embryo staging and substaging criteria used in this work. Bownes stages 4, 5, 8 and 11 (***Bownes, 1975***) are further divided into substages, as described, based on the expression patterns of *wg*, *D* and *eve*, or the progression of cellularisation. For each stage 5 substage, the corresponding "temporal equivalence class(es)" (***Surkova et al., 2008***) or "phase" (***Schroeder et al., 2011***) are also listed for comparison. Note that the subdivision of a continuous developmental process into discrete time-classes is convenient for analysis but biologically somewhat arbitrary; there are no sharp boundaries between the substages we have defined.

stage	criteria	Surkova	Schroeder
1 to 3	same as Bownes (1975).		
4.1	syncytial blastoderm nuclear cycle 10 (judged by number/density of nuclei).		
4.2	syncytial blastoderm nuclear cycle 11 (judged by number/density of nuclei).		
4.3	syncytial blastoderm nuclear cycle 12 (judged by number/density of nuclei).		
4.4	syncytial blastoderm nuclear cycle 13 (judged by number/density of nuclei).		
5.1	*wg*: not present. *D*: broad trunk domain, head domain not well established (mainly nuclear dots). *eve*: broad trunk expression, may have some AP modulation. blastoderm morphology: round, early-looking nuclei.	T1	phase 1
5.2	*wg*: head and posterior domain expression just starting (mainly nuclear dots). *D*: head domain established, trunk domain still uniform. *eve*: not yet a regular 7 stripe pattern. blastoderm morphology: no invagination of plasma membrane.	T2-3	phase 2
5.3	*wg*: head and posterior domains established; wg0 and wg1 forming. *D*: broad trunk domain becoming fainter in the middle. No tail domain. *eve*: regular 7 stripe pattern but stripes still fuzzy and broad. blastoderm morphology: plasma membrane invaginating.	T4-T5	phase 2
5.4	*wg*: wg0 and wg1 well established; trunk stripes (mainly odd-numbered) just appearing. *D*: tail domain appearing laterally with similar intensity to trunk expression; anterior and posterior halves of the trunk domain are well-separated; trunk expression is becoming more modulated. *eve*: 7 well separated but still symmetrical stripes. blastoderm morphology: membranes have reached the bottom of the nuclei.	T6-7	phase 3
5.5	*wg*: segmental pattern clearly developing (both odd-numbered and even-numbered stripes), though may not be fully established. *D*: tail domain is more established and has separated from the trunk; trunk expression is starting to fade and neuroectoderm expression is just appearing, including a bright anterior-ventral stripe. *eve*: anterior stripes narrowing to 2-cell wide late element expression; posterior stripes becoming AP graded as they transition to the late element. blastoderm morphology: elongated nuclei.	T8	phase 4
6	*wg*: regular segmental stripes. *D*: tail domain strong; trunk expression (except dorsal saddle) fading; neuroectoderm expression developing but not yet uniform across the AP axis. *eve*: all 7 stripes have narrowed, faint secondary stripes present. blastoderm morphology: signs of gastrulation and/or cephalic furrow formation; by late stage 6 pole cells moving dorsally and dorsal crumpling present.		
7	same as Bownes (1975).		
8.1	mitotic domain 4 dividing.		
8.2	wg14 absent/weak, en15 absent.		
8.3	wg14 present, en15 absent/weak.		
8.4	wg14 present, en15 present.		
9	same as Bownes (1975).		
10	same as Bownes (1975).		
11.1	wg15 present, en16 absent.		
11.2	wg15 present, en16 present.		
12+	same as Bownes (1975).		

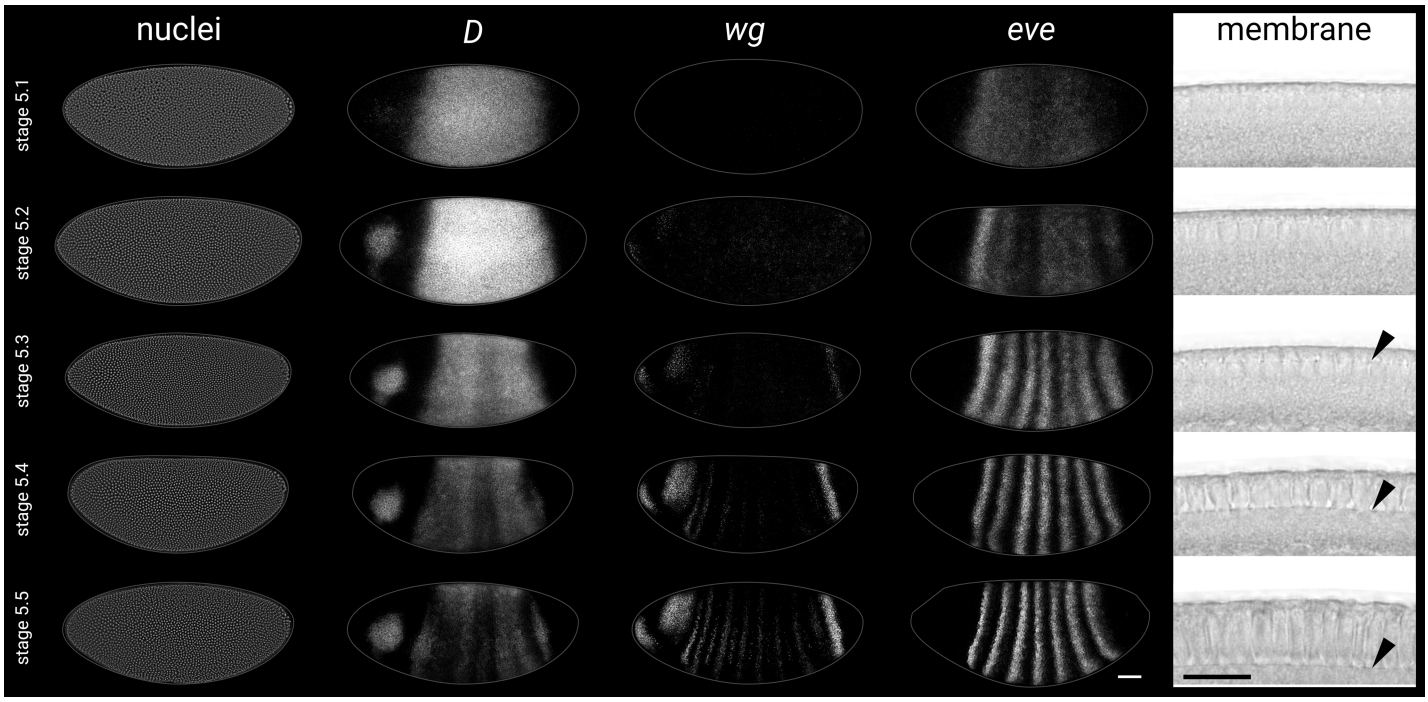

Appendix 1—figure 1: Substaging scheme for stage 5 embryos. Representative gene expression patterns and blastoderm morphology for each of the 5 substages in our substaging scheme for stage 5 (nuclear cycle 14). See ***Appendix 1—Table 1*** for details. Rightmost column shows transmitted light images of a sagittal view of the dorsal blastoderm surface (imaged on a confocal microscope); black arrowheads point to the invaginating plasma membrane. All embryos are anterior left, dorsal up, lateral view. Scale bars = 50 μm (whole embryos), 20 μm (membrane close-ups); grey lines show embryo outlines. Note that the 5 images in each row are not all sourced from the same embryo.

Appendix 2

Initial image processing

Initial processing of raw image stacks was carried out to detect, rotate, mask, and crop each focal embryo (***Appendix 2—Figure 1***A-E, ***Appendix 2—Figure 1—source data 1*** script 1). Briefly, a "height map" of a given z-stack was built up by thresholding a maximum projection of z range $0 : i$ for increasing values of i, and summing these together to produce an image showing the topography of any embryos within the field of view (***Appendix 2—Figure 1***B). Local peaks within a truncated version of this image were detected and then used as the seeds for a watershed segmentation to separate touching embryos, while "low-lying" background areas were masked (***Appendix 2—Figure 1***C). Because all images were centred on a specific embryo of interest, the convex hull of the central segmented region was used as the embryo mask (***Appendix 2—Figure 1***D). The major axis of the embryo mask was used to determine the orientation of this focal embryo, and the image was rotated accordingly so as to align its AP axis with the horizontal. The embryo mask was then dilated slightly, before being used to crop the image and mask non-embryo background (***Appendix 2—Figure 1***E). This process was first applied to all images in batch, and then the resulting masks were inspected for accuracy. Any images with unsatisfactory masks were reprocessed individually, with manual parameter adjustment at the image segmentation step to correct the mask. Processed images were then flipped horizontally and/or vertically as necessary, to yield a consistent "anterior left, dorsal up" orientation.

Extraction of quantitative expression traces

Laterally oriented embryos of the appropriate stages and genotypes were then selected for the extraction of quantitative AP expression traces (***Appendix 2—Figure 1***F-L, ***Appendix 2—Figure 1—source data 1*** scripts 2 and 3). Previous studies have tended to use percentage egg length to quantify AP expression profiles (e.g., ***Pignoni et al., 1990***; ***Surkova et al., 2008***; ***Janssens et al., 2013***), but percentage egg length is not a perfect proxy for the AP axis, due to the embryo's curvilinear intrinsic coordinate system (***Spirov et al., 2000***; ***Luengo Hendriks et al., 2006***; ***Spirov et al., 2013***). Percentage egg length measurements for expression domains near the poles are also potentially unreliable because they depend on the degree of flattening of a mounted embryo, given that a z-projection of a squashed embryo will exaggerate the size of the termini compared to a z-projection of an unsquashed embryo, due to the different curvature in z. We therefore decided to use a heuristic approach to approximate a curved trace along the lateral surface of the embryo, using guidance from embryo morphology.

Briefly, DAPI (nuclei)-derived height maps were used to define thin embryo "shells" (~18 μm thick), which tracked the blastoderm surface in 3D and contained most of the gene expression signal (***Appendix 2—Figure 1***F,G). A mean z-projection of the voxels within this shell region was then saved as a multichannel 2D image (***Appendix 2—Figure 1***H). Next, the dorsal and ventral borders of the embryo mask were used to create a "DV map" for this image by interpolation (***Appendix 2—Figure 1***I), and 30% of the DV axis, corresponding to the mid-lateral part of the embryo, was selected for quantification (***Appendix 2—Figure 1***J). (As each embryo had a slightly different DV orientation on the slide, the selected DV range had to be adjusted manually for each image, so that the centre of the selected region consistently intersected with a DV position corresponding to the centre of the *D* head domain. This DV adjustment was important because the positions and expression intensities of most AP expression domains vary along the DV axis (***Luengo Hendriks et al., 2006***). A 3D spline was fitted along the middle of the DV region of interest, using z values from the height

map. To improve the consistency of the traces, the posterior endpoint of the spline was anchored close to a pixel coordinate marking the transition between the posterior midgut primordium and the pole cells, which was selected manually for each image. Cumulative distance along the spline was calculated in 3D using the Pythagorean theorem, accounting for the anisotropy of the z axis relative to the x and y. The total AP distance along the spline was normalised to 1, where 0 = the anterior tip of the embryo mask, and 1 = the beginning of the pole cells. Expression intensity traces were extracted for each channel by running a sliding window of 1% AP length (roughly 1 nuclear diameter) along the spline, with each window angled normal to the xy orientation of the spline (so as to avoid generating artificial expression overlaps from slanted posterior domains), and bounded dorsally and ventrally by the DV region of interest (***Appendix 2—Figure 1***K). Each extracted trace (***Appendix 2—Figure 1***J) consisted of 500 measurements separated by a distance of 0.2% AP length.

The expression intensity traces in ***Figure 3*** (solid plotted lines) were calculated by moving a sliding window with a width of 25 pixels (~1 nuclear diameter) across the x axis of the rectangular region of interest and measuring the average intensity at 1 pixel intervals. Nuclear foci for *opa* and the *cad* intronic probe were identified by detecting local peaks above a threshold intensity; the dashed plotted lines in ***Figure 3***B are density plots for the x coordinates of the detected foci.

Normalised expression plots

When comparing traces from embryos of different stages to examine the dynamics of gene expression, all traces from a particular experimental sample were normalised to the range 0-1 as a group [i.e., for each channel, normalised values = (original values - min(group)) / (max(group) - min(group)]. When comparing traces from individual embryos of the same stage to examine the positioning of expression domains within and between genotypes, each trace was normalised to the range 0-1 individually [i.e., normalised values = (original values - min(individual) / (max(individual) - min(individual)]. In D^- mutants, expression levels were severely reduced across the entire AP axis, and so the normalised expression traces were multiplied by a small constant to dampen them. In most cases, expression traces are presented without any further adjustments. In ***Figure 4—figure Supplement 1***B, additional plots show "aligned traces", in which each trace has been shifted anteriorly or posteriorly by a small amount so that the position of the anterior border of the *wg* posterior domain coincides in all traces. The aligned plots are useful for assessing any changes to the relative positioning of particular domains (as opposed to their absolute positional variation across different embryos).

Embryo images

A list of source image files for all figure panels within the main text, appendices, and supplementary information is provided in ***Appendix 2—Figure 1—source data 2***. Unless otherwise stated, all images of embryos are maximum intensity projections of confocal z-stacks of the upper half of the embryo. Fiji was used to adjust image brightness and contrast, in accordance with guidelines presented by ***Schmied and Jambor*** (***2020***). Image gamma was adjusted to 0.1 for all *opa* transcript stains, due to the extremely bright transcriptional foci. Embryos from the same round of staining and imaging are presented using the same brightness and contrast values; unless otherwise noted, this holds for any embryos within a given figure that share the same genotype and combination of stains. To correct for uneven illumination from the 405 laser, the DAPI (nuclei) signal from each blastoderm stage embryo was flattened by applying a Gaussian filter with $\sigma = 6$, and then dividing the original image by the new blurred image.

In ***Figure 1***B; stage 8.1, the inset shows a maximum intensity projection from the surface to the midline of the embryo. In ***Figure 1***B; stage 11.1, the inset shows a single section of a z-stack that was rotated -45° around the x axis using the ImageJ plug-in `TransformJ` (***Meijering et al., 2001***) using the "Quintic B-Spline" method for interpolation. In ***Figure 3***, the curved surface of the embryo was flattened in Fiji by reslicing each channel along the long axis of the embryo (output spacing 0.206 μm), manually masking the region of interest with a segmented line ("spline fit" checked) of width 130 pixels, using the "Straighten" tool to process the entire stack, then reslicing the stack (output spacing 0.206 μm) and re-merging the channels to return to the original view. Average projections (DAPI [nuclei] and Opa channels) or maximum projections (HCR channels) were then generated for a z-range spanning from the top of the embryo to just below the nuclei.

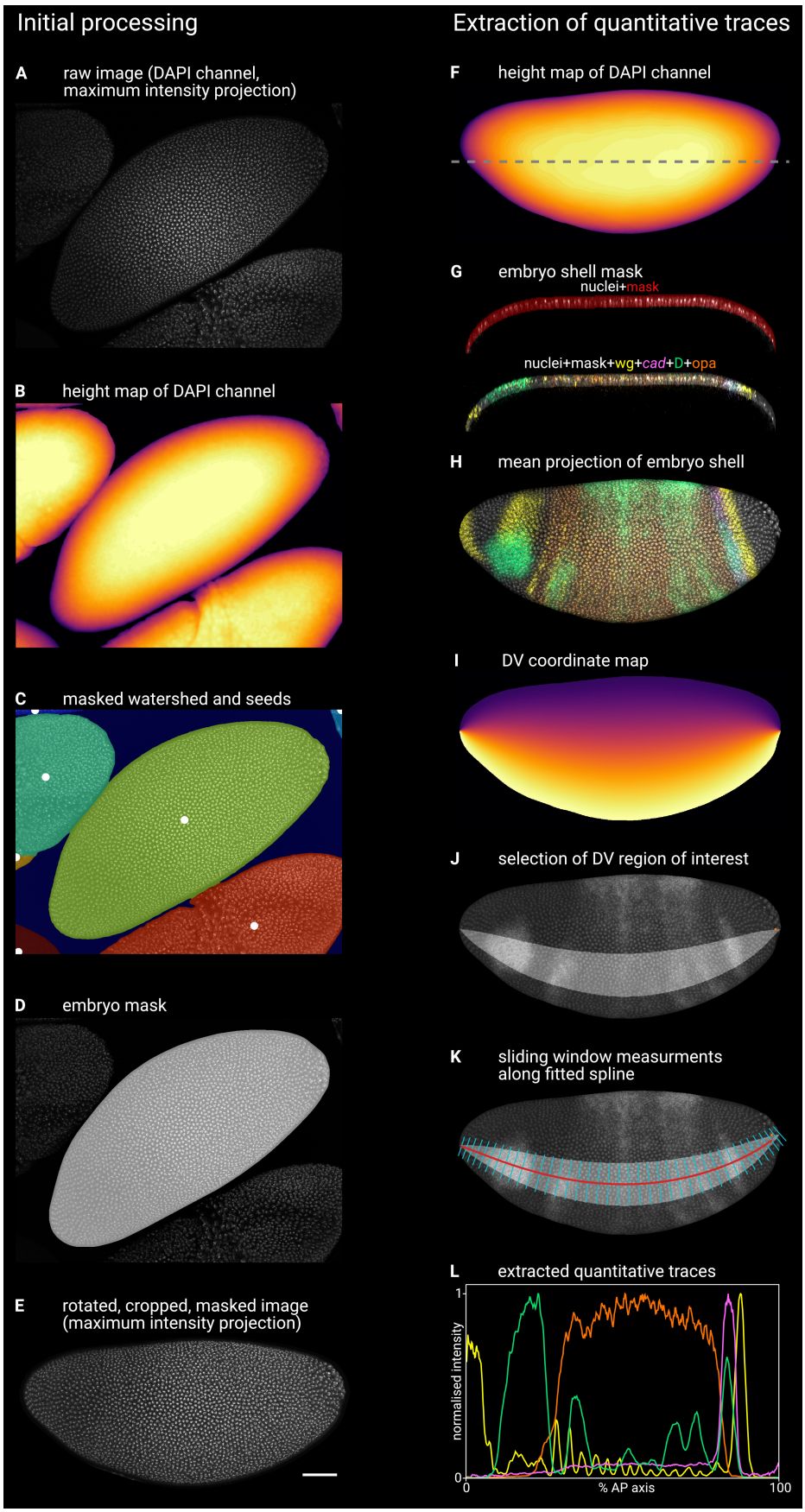

Appendix 2—figure 1: Illustration of image processing steps. (Caption continued on next page.)

Appendix 2—figure 1: Timer gene expression in timer gene mutants (continued). Left column illustrates the initial processing of raw confocal data to generate single embryo stacks; right column illustrates the extraction of quantitative expression intensity traces from the processed stacks (see text for additional details and explanation). **A**: maximum z-projection of the DAPI (nuclei) channel of the raw multi-channel stack. **B**: height map generated from the smoothed DAPI (nuclei) channel, where the colour of the pixel (yellow=high, black=low) indicates the height of the embryo surface. **C**: watershed segmentation of the (inverted) height map, in which local peaks (white dots) indicate the watershed seeds, each segmented region is overlaid by a different colour, and the low-lying background area is masked (dark blue). **D**: the 2D mask for the focal embryo (light grey), overlaid on the maximum z-projection of the DAPI (nuclei) channel. **E**: a maximum z-projection of the DAPI (nuclei) channel after image rotation, cropping, masking, and manual flipping. **F**: height map of the embryo z-stack, as in B. Dashed line marks the location of the xz plane shown in G. **G**: an xz (frontal) section through the embryo, showing the embryo "shell mask" overlaid on the DAPI (nuclei) channel (top) or on a merge of all 5 imaging channels (bottom). Note that the vast majority of the transcriptional signal is contained within the shell mask. **H**: a 5-channel merge showing a mean z-projection of the 3D region defined by the embryo shell mask. **I**: a map of the DV coordinates assigned to the embryo z-projection by interpolating between the dorsal and ventral boundaries of the embryo mask. **J**: a region of interest (light grey area) defined by a specific range of DV coordinates. The range spans 30% of the DV axis and is selected to intersect with the round *D* domain in the head. Note the manually input coordinate (orange dot at the posterior of the embryo) marking the beginning of the pole cell region. **K**: the red line shows a 2D projection of a 3D spline fitted to the centre of the DV region of interest (x and y coordinates) and the corresponding values from the height map (z coordinates). The cyan lines are normal to the spline in x and y. Expression traces are extracted from the image by running a sliding window (width = 1% of the length of the spline in 3D, anterior and posterior boundaries normal to the spline, dorsal and ventral boundaries defined by the DV region of interest) along the spline and recording the mean intensity of each image channel. **L**: the quantitative expression traces extracted from the image, after normalising each trace to the 0-1 range.

Appendix 2—figure 1—source data 1. Sample image stack and image analysis scripts.

Appendix 2—figure 1—source data 2. List of source image files for all figures.

Appendix 3

Justification for gene regulatory network topology

The detailed reasoning for the topology of the gene regulatory network in ***Figure 8***A is presented in ***Appendix 3—Table 1***. This table summarises and discusses the experimental evidence relevant to each potential pairwise interaction between the genes in the network, drawing on the expression data from this study as well as a comprehensive survey of the existing literature on *Drosophila* posterior terminal patterning.

Appendix 3—table 1. Evidence for proposed cross-regulatory interactions between Tll, Hkb, Fkh, Wg, Cad, D, and Opa. For every pairwise combination of input factor (Tll, Hkb, Fkh, Cad, D, Opa) and potential target gene (*tll*, *hkb*, *fkh*, *wg*, *cad*, *D*, *opa*), the inferred regulatory interaction (activation / repression / none / undetermined) is listed, accompanied by a summary of the relevant experimental evidence and line of reasoning.

Input	Target	Interaction	Evidence and discussion
Tll	*tll*	none	Tll is a dedicated repressor (***Moran and Jimenez, 2006***) so is unlikely to autoactivate, and sustained expression in wild-type (***Figure 5—figure Supplement 1***) precludes strong autorepression. Indirect activation is a possibility, but one would need to look at a *tll*$^{-}$ allele that still makes transcript to assess whether *tll* transcription is affected in *tll*$^{-}$ mutants.
Tll	*hkb*	none	*hkb* is transcribed within the Tll domain (***Figure 5—figure Supplement 1***), therefore Tll does not repress *hkb*. The *hkb* expression domain is a similar size in wild-type and *tll*$^{-}$ embryos (***Figure 7***B), therefore Tll is not required to (indirectly) activate *hkb*.
Tll	*fkh*	(indirect) activation	*fkh* is transcribed across the Tll domain in wild-type and *hkb*$^{-}$ embryos (***Figure 7***A,B; ***Figure 7—figure Supplement 1***A), and the *fkh* domain is reduced (to the size of the *hkb* domain) in *tll*$^{-}$ embryos (***Figure 7***A,B; ***Figure 7—figure Supplement 1***B). Activation from Tll is presumed to be indirect as Tll is a dedicated repressor (***Moran and Jimenez, 2006***).
Tll	*wg*	none	*wg* is transcribed within the Tll domain in wild-type embryos (***Figure 5***B) and in *hkb*$^{-}$ mutants (***Figure 7***A,B; ***Figure 7—figure Supplement 1***A), therefore Tll does not repress *wg*. Tll is necessary for *wg* expression (*wg* expression is lost in *tll*$^{-}$ mutants and is posteriorly shifted in *hkb*$^{-}$ mutants, correlating with the altered Tll domain; ***Figure 7***A,B; ***Figure 7—figure Supplement 1***A), but this activation seems to be indirect (via Fkh) as Tll is a dedicated repressor (***Moran and Jimenez, 2006***), and the presence of Tll-positive, Hkb-negative territory is not sufficient to activate *wg* in *fkh*$^{-}$ or *cad*$^{m-z-}$ genotypes (***Figure 7***; ***Figure 7—figure Supplement 1***B).
Tll	*cad*	(weak) repression	*cad* transcription overlaps the graded anterior edge of the Tll domain throughout most of the blastoderm stage in wild-type embryos (***Figure 5***), indicating that Tll does not strongly repress *cad*. However, *cad* is still repressed in (Tll-positive, Fkh-positive) posterior tissue in *hkb*$^{-}$ mutants (***Figure 6***E-G), suggesting that *cad* must be repressed by either Tll or Fkh (or both). As *cad* expression is largely normal in *fkh*$^{-}$ mutants (***Figure 7***C,D), it seems likely that Tll does indeed repress *cad*, albeit more weakly than Tll represses other targets such as *D* and *opa*. Investigation of *cad* expression in *fkh*$^{-}$ *hkb*$^{-}$ double mutants would be informative for isolating the role of Tll in *cad* regulation.

Continued on next page

Input	Target	Interaction	Evidence and discussion
Tll	*D*	repression	The graded posterior border of the *D* domain is anticorrelated with Tll levels in wild-type embryos, and the *D* tail domain appears only after *tll* expression in this region decline (***Figure 5***A). The *D* posterior boundary shifts posteriorly in *tll*$^{-}$ mutants, and also in *hkb*$^{-}$ mutants, apparently because the *tll* domain is reduced (***Figure 6***C-H). *D* expression is normal in *fkh*$^{-}$ mutants (***Figure 7***C,D), indicating that the repressive effect of Tll is not mediated by Fkh. It is currently unclear whether the *D* tail domain has the same regulatory logic / sensitivity to Tll as does the *D* trunk domain; investigation of *D* enhancer regions will be informative.
Tll	*opa*	repression	*opa* is excluded from the Tll domain in wild-type (***Figure 5***A), and the posteriorly shifting *opa* boundary (***Figure 3***B) correlates with the posteriorly shifting dynamics of the Tll domain (***Figure 5—figure Supplement 3***; ***Figure 5—figure Supplement 4***). The *opa* boundary is shifted posteriorly in *tll*$^{-}$ mutants, and also in *hkb*$^{-}$ mutants, apparently because the *tll* domain is reduced (***Figure 6***C-H). *opa* expression is normal in *fkh*$^{-}$ mutants (***Figure 7***C,D), indicating that the repressive effect of Tll is not mediated by Fkh.
Hkb	*tll*	(indirect) activation	*tll* is coexpressed with Hkb (***Figure 5—figure Supplement 1***), therefore Hkb does not repress *tll*. The *tll* domain is reduced in *hkb*$^{-}$ mutants (***Figure 6***F,H), but as Hkb is a repressor (***Goldstein, 1999***) and *tll* expression is affected anterior to the Hkb domain, this *hkb*$^{-}$dependent activation of *tll* is presumably indirect. *tll* expression also persists longer in *hkb*$^{-}$ mutants (***Figure 6—figure Supplement 2***), but again the Hkb-dependent effect on *tll* (in this case, late repression) is presumably indirect.
Hkb	*hkb*	none	Hkb is a repressor (***Goldstein, 1999***) so is unlikely to autoactivate. Sustained *hkb* expression in wild-type embryos (***Figure 5—figure Supplement 1***) precludes strong autorepression. Indirect activation is a possibility, but one would need to look at a *hkb*$^{-}$ allele that still makes transcript to assess whether *hkb* transcription is affected in *hkb*$^{-}$ mutants.
Hkb	*fkh*	(indirect) activation	*fkh* is transcribed across the Hkb domain (***Figure 7—figure Supplement 1***B), therefore Hkb does not repress *fkh*. *fkh* is still expressed within the *hkb* domain in *tll*$^{-}$ mutants (***Figure 7***A,B), indicating that Hkb can activate *fkh* independently of Tll. As Hkb is a repressor (***Goldstein, 1999***), this activation is presumably indirect.
Hkb	*wg*	repression	The *wg* posterior boundary abuts the Hkb anterior boundary in wild-type embryos (***Figure 5***B), and *wg* expression extends to the posterior pole in *hkb*$^{-}$ mutants (***Figure 6***E,G; ***Figure 7***A,B).
Hkb	*cad*	repression	*cad* is not expressed within the Hkb domain from early stage 5 in wild-type embryos (***Figure 5***; ***Figure 5—figure Supplement 2***), and clearance of *cad* expression from the posterior pole is delayed in *hkb*$^{-}$ mutants (***Figure 6***E; ***Figure 7***A,B). *cad* remains repressed from the Hkb domain in *tll*$^{-}$ mutants (***Figure 6***C,D,G; ***Figure 7***A,B), indicating that Hkb represses *cad* independently of Tll. In addition, *cad* expression is largely normal in *fkh*$^{-}$ mutants throughout blastoderm stages (***Figure 7***C,D), suggesting that *cad* repression is not mediated by Fkh. Examining *cad* expression in *tll*$^{-}$ *fkh*$^{-}$ double mutants would be helpful to confirm whether Hkb represses *cad* independently of both Tll and Fkh.
Hkb	*D*	repression	*D* expression is excluded from the Hkb domain in *tll*$^{-}$ mutants (***Figure 6***D). Examining *D* expression in *tll*$^{-}$*fkh*$^{-}$ double mutants would be helpful to confirm whether this repression is independent of Fkh.
Hkb	*opa*	repression	*opa* expression is excluded from the Hkb domain in *tll*$^{-}$ mutants (***Figure 6***D). Examining *opa* expression in *tll*$^{-}$*fkh*$^{-}$ double mutants would be helpful to confirm whether this repression is independent of Fkh.

Continued on next page

Input	Target	Interaction	Evidence and discussion
Fkh	*tll*	none	*tll* expression precedes Fkh expression in wild-type (***Figure 5—figure Supplement 1***; ***Weigel et al., 1989***; extended imaging dataset), therefore Fkh is not required to activate *tll*. Tll and Fkh are co-expressed throughout stage 5 (***Figure 7***A,B; extended imaging dataset), indicating that Fkh does not repress *tll*. In addition, although we did not examine *tll* expression in *fkh*$^{-}$ mutants, *tll*-dependent patterning of *D* and *opa* appears normal in *fkh*$^{-}$ mutants (***Figure 7***C,D), indicating that *tll* expression is unlikely to be perturbed. It would be useful to examine *tll* expression in *fkh*$^{-}$ mutants to confirm this.
Fkh	*hkb*	none	*hkb* expression precedes Fkh expression in wild-type (***Figure 5—figure Supplement 1***; ***Weigel et al., 1989***; extended imaging dataset), therefore Fkh is not required to activate *hkb*. Hkb and Fkh are coexpressed throughout stage 5 (***Figure 7—figure Supplement 1***B; extended imaging dataset), indicating that Fkh does not repress *hkb*. It would be useful to examine *hkb* expression in *fkh*$^{-}$ mutants to confirm it looks normal.
Fkh	*fkh*	none	Sustained Fkh expression in wild-type embryos (***Figure 7***A; ***Weigel et al., 1989***; extended imaging dataset) suggests autorepression is unlikely. It would be useful to examine *fkh* expression in *fkh*$^{-}$ mutants to assess whether autoactivation occurs.
Fkh	*wg*	activation	*wg* is only expressed in Fkh-positive, Hkb-negative territory in wild-type embryos (***Figure 5***B), and *wg* expression is strongly reduced in *fkh*$^{-}$ mutants (***Figure 7***C,D; ***Figure 7—figure Supplement 3***; ***Figure 7—figure Supplement 4***) and also *cad*$^{m-z-}$ mutants (***Figure 4***A,B; ***Figure 7***A; ***Figure 4—figure Supplement 3***A), which have reduced *fkh* expression (***Figure 7***A,B).
Fkh	*cad*	undetermined	The posterior *cad* boundary consistently abuts the anterior *fkh* boundary, for example in wild-type embryos, *tll*$^{-}$ mutants, and *hkb*$^{-}$ mutants (***Figure 7***A,B). However, *cad* expression is largely normal in *fkh*$^{-}$ mutants throughout stage 5 (***Figure 7***C,D), with a possible posterior expansion after gastrulation (***Figure 7—figure Supplement 3***). Because we think that Tll both represses *cad* and (indirectly) activates *fkh*, it is unclear whether Fkh indeed has no effect on *cad*, or alternatively whether Fkh and Tll repress *cad* redundantly. Misexpression of Fkh in the tail region would be informative.
Fkh	*D*	undetermined	Unclear, as Fkh is only ever expressed in territories expressing *D* repressors Tll or Hkb (***Figure 7***A,B). Misexpression of Fkh in segmental territories would be informative.
Fkh	*opa*	undetermined	Unclear, as Fkh is only ever expressed in territories expressing *opa* repressors Tll or Hkb (***Figure 7***A,B). Misexpression of Fkh in segmental territories would be informative.
Cad	*tll*	none	The *tll* domain emerges from Cad-positive territory (***Figure 5***A), therefore Cad does not repress *tll*. *tll* is expressed normally in *cad*$^{m-z-}$ mutants (***Figure 7***A,B), therefore Cad is not required to activate *tll*.
Cad	*hkb*	none	The *hkb* domain emerges from Cad-positive territory (***Figure 2***; ***Figure 5***B), therefore Cad does not repress *hkb*. *hkb* is expressed normally in *cad*$^{m-z-}$ mutants (***Figure 7—figure Supplement 1***B), therefore Cad is not required to activate *hkb*.
Cad	*fkh*	activation	*fkh* expression is strongly reduced in *cad*$^{m-z-}$ mutants, even though *tll* and *hkb* expression is largely normal (***Figure 7***A,B; ***Figure 7—figure Supplement 1***).
Cad	*wg*	none	Although the *wg* posterior domain is lost in *cad*$^{m-z-}$ mutants (***Figure 4***A,B; ***Figure 4—figure Supplement 3***A), this phenotype is likely mediated by the loss of *fkh* expression in these embryos (***Figure 7***A,B), because the *wg* posterior domain is also lost in *fkh*$^{-}$ mutants (***Figure 7***C,D; ***Figure 7—figure Supplement 3***; ***Figure 7—figure Supplement 4***) and these have normal *cad* expression (***Figure 7***C,D). In addition, *wg* expression persists posterior to the *cad* domain throughout germband extension in wild-type, after broad blastoderm Cad expression has decayed (***Figure 2***).

Continued on next page

Input	Target	Interaction	Evidence and discussion
Cad	*cad*	none	The persistent expression of *cad* in the tail in both wild-type embryos and *cad*$^{m-z-}$ mutants (***Figure 4***C) is inconsistent with both direct autorepression and direct autoactivation. We interpret the delayed clearance of *cad* from the trunk in *cad*$^{m-z-}$ mutants (***Figure 4***C) as due to the lower levels of *D* in this genotype (***Figure 4***C), rather than due to direct autoregulation.
Cad	*D*	activation	*D* expression emerges within Cad-positive territory in both the trunk and the tail in wild-type embryos (***Figure 2***), indicating that Cad does not repress *D*. Reduced *D* levels in the trunk of *cad*$^{m-z-}$ embryos (***Figure 4***C), dorsal loss of *D* tail expression in *cad*$^{m-z-}$ embryos (***Figure 4***; ***Figure 4—figure Supplement 3***A), and late loss of *D* tail expression in *cad*$^{m+z-}$ embryos (***Figure 4—figure Supplement 3***B) all indicate that Cad activates *D*. However, additional activators of *D* must exist, given that *D* expression is reduced rather than completely lost in *cad*$^{m-z-}$ embryos.
Cad	*opa*	none	*opa* is transcribed strongly across the trunk while Cad levels are still high in wild-type embryos (***Figure 2***; ***Figure 2—figure Supplement 4***), and *opa* expression later invades the *cad* tail domain from the anterior (***Figure 3***B), indicating that Cad does not repress *opa*. *opa* is expressed largely normally in *cad*$^{m-z-}$ mutants (***Figure 4***A; ***Figure 4—figure Supplement 2***; though note the AP modulation), indicating that Cad is not required to activate *opa*.
D	*tll*	undetermined	There is a subtle anterior shift and expansion of the posterior terminal fate map in *D*$^{-}$ mutants (***Figure 4***A,B; ***Figure 4—figure Supplement 2***), which can be most easily explained by supposing that D represses *tll*. Although we did not examine *tll* expression in *D*$^{-}$ mutants, *tll* and *D* are expressed in opposing gradients during stage 4.4 (nuclear cycle 13) in wild-type embryos (***Figure 5***A), and it seems plausible that mutual repression between *tll* and *D* could help to scale the AP pattern. Investigation of *tll* expression in *D*$^{-}$ mutants and misexpression of D in the posterior of the embryo would both be informative experiments.
D	*hkb*	undetermined	Unclear, as domains of *D* and *hkb* expression are distinct (***Figure 5***). Misexpression of D in the posterior of the embryo would be informative.
D	*fkh*	undetermined	Unclear, as domains of *D* and *fkh* expression are distinct (***Figure 2***; ***Figure 7***A,B). Although we did not examine *fkh* expression in *D*$^{-}$ mutants, the *wg* posterior domain is activated normally in *D*$^{-}$ mutants (***Figure 4***A,B) suggesting that *fkh* expression is unlikely to be strongly affected. Misexpression of D in the posterior of the embryo would be informative.
D	*wg*	undetermined	Unclear, as domains of *D* and *wg* expression are distinct (***Figure 2***). The *wg* posterior domain looks essentially normal in *D*$^{-}$ mutants (***Figure 4***A,B). Misexpression of D in the posterior of the embryo would be informative.
D	*cad*	repression	*cad* expression ceases in the trunk as D levels increase in wild-type embryos (***Figure 2***; ***Figure 2—figure Supplement 3***; ***Figure 2—figure Supplement 4***), while *cad* expression persists in some parts of the trunk in *D*$^{-}$ mutants (***Figure 4***A). The anterior border of the *cad* tail domain correlates with the earlier position of the posterior border of the *D* trunk domain in wild-type, *hkb*$^{-}$ mutants, *tll*$^{-}$ mutants, and *tll*$^{-}$ *opa*$^{-}$ mutants (***Figure 2***; ***Figure 6***; ***Figure 4—figure Supplement 5***; extended imaging dataset).
D	*D*	undetermined	We were unable to assess possible autoregulatory effects, as *D* transcript levels were strongly reduced in the *D*$^{-}$ mutants we examined (***Figure 4***A), presumably due to nonsense-mediated decay.

Continued on next page

Input	Target	Interaction	Evidence and discussion
D	*opa*	none	*opa* expression emerges from D-positive territory in the trunk in wild-type (***Figure 2***; ***Figure 2—figure Supplement 3***; ***Figure 2—figure Supplement 4***), and *opa* expression is largely normal in D^- mutants (***Figure 4***A; ***Figure 4—figure Supplement 2***), indicating that D neither represses nor activates *opa*. The *opa* posterior border is shifted slightly anteriorly in D^- mutants (***Figure 4—figure Supplement 2***), but this is likely to be an indirect effect mediated by Tll, or possibly by Cad.
Opa	*tll*	undetermined	Unclear, as the domains of *opa* and *tll* expression are distinct (***Figure 5***A). Misexpression of Opa in the posterior of the embryo would be informative.
Opa	*hkb*	undetermined	Unclear, as domains of *opa* and *hkb* expression are distinct (***Figure 5***). Misexpression of Opa in the posterior of the embryo would be informative.
Opa	*fkh*	undetermined	Unclear, as domains of *opa* and *fkh* expression are distinct (***Figure 5***; ***Figure 7***A,B). Misexpression of Opa in the posterior of the embryo would be informative.
Opa	*wg*	undetermined	Unclear, as domains of *opa* and (posterior) *wg* expression are distinct (***Figure 2***). Interestingly, Opa activates the segmental *wg* stripes in the trunk (***Benedyk et al., 1994***), but Opa/Zic is a Wnt antagonist in other developmental contexts (***Pourebrahim et al., 2011***; ***Fujimi et al., 2012***; ***Murgan et al., 2015***). Misexpression of Opa in the posterior of the embryo would be informative.
Opa	*cad*	repression	The anterior border of the *cad* tail domain retracts in wild-type embryos as Opa levels increase (***Figure 3***B), suggesting that Opa represses *cad*. Repression of *cad* by Opa is also suggested by the late repression of the ectopic *cad* expression present in the trunk of D^- mutants (***Figure 4***A; extended imaging dataset), and by the late repression of the *cad* posterior domain in tll^- mutants, which overlaps with *opa* expression (***Figure 6***C,G; ***Figure 4—figure Supplement 5***).
Opa	*D*	repression	In wild-type embryos, *D* expression in the trunk decreases as Opa levels increase (***Figure 2***; ***Figure 2—figure Supplement 4***), and the anterior border of the *D* tail domain lines up with the Opa posterior border (***Figure 3***A). In opa^- mutants, *D* expression in the trunk persists for longer and *D* expression in the tail is strengthened (***Figure 4***A,B; ***Figure 4—figure Supplement 5***), indicating that Opa represses *D*. In addition, a *D* tail domain does not emerge in tll^- mutants, which misexpress *opa* anterior to the Hkb domain (***Figure 6***C,D,G), but a tail-like *D* domain does emerge in tll^- opa^- double mutants (***Figure 4—figure Supplement 5***).
Opa	*opa*	none	Sustained *opa* expression in wild-type embryos (***Figure 2***; ***Figure 2—figure Supplement 4***) and normal expression of *opa* in opa^- mutants (***Figure 4***A; ***Figure 4—figure Supplement 2***; ***Figure 4—figure Supplement 5***) indicate that strong autoregulatory effects are unlikely, at least within our period of interest.

Appendix 4

Model and simulation details

In ***Figure 8***, the *Drosophila* AP axis is modelled as four discrete regions, where region 1 represents the trunk, region 2 represents the tail, region 3 represents the hindgut primordium, and region 4 represents the posterior midgut primordium. Each region receives hard-coded inputs from `Tll` and `Hkb`, logical variables that can take the values 0 (no expression), 1 (weak expression), or 2 (strong expression). Region 1 remains free of both `Tll` and `Hkb` expression across all four timepoints $(0, 0, 0, 0)$. Region 2 experiences weak, transient `Tll` expression $(1, 1, 0, 0)$ and no `Hkb` expression $(0, 0, 0, 0)$. Region 3 experiences rapidly established strong `Tll` expression $(1, 2, 2, 2)$ and transient weak `Hkb` expression $(1, 1, 0, 0)$. Region 4 experiences rapidly established strong `Tll` expression $(1, 2, 2, 2)$ and persistent strong `Hkb` expression $(2, 2, 2, 2)$.

In addition to `Tll` and `Hkb`, each region can express `Fkh`, `Wg`, `Cad`, `D`, and `Opa`, logical variables that can take one of either three (0, 1, 2) or two (0, 1) possible values, as defined by their regulatory logic:

```
Fkh = 1 if (Tll + Hkb) > 1 and (Cad + Fkh) > 0; else Fkh = 0.
Wg = 1 if Fkh > 0 and Hkb < 2; else Wg = 0.
Cad = 1 if D < 2 and Opa < 2 and Hkb < 2 and Tll < 2; else Cad = 0.
D = 2 if Opa < 2 and Tll < 1 and Hkb < 1 and Cad > 0; D = 1 if Opa < 2 and Tll < 1
    and Hkb < 1 and Cad < 1; else D = 0.
Opa = 2 if Hkb < 2 and Tll < 1 and Opa > 0; Opa = 1 if Hkb < 2 and Tll < 1 and Opa
    < 1; else Opa = 0.
```

Thus, `Fkh` is only expressed when combined `Tll` and `Hkb` levels are high, and `Cad` must initially be present for `Fkh` expression to become established. `Wg` is expressed when `Fkh` is present but `Hkb` levels are low. `Cad` is on by default but repressed by strong `D`, strong `Opa`, strong `Tll` or strong `Hkb`. `D` can be repressed by strong `Opa` or any amount of `Hkb` or `Tll`, and `Cad` must be present for `D` to be expressed strongly. Finally, `Opa` can only be repressed by `Tll` or strong `Hkb`, but it must transit through weak expression before it reaches high levels. This last condition represents the observation that Opa protein is synthesised relatively slowly (***Figure 2—figure Supplement 4***; ***Clark and Akam, 2016***; ***Soluri et al., 2020***).

Each simulation begins at $t0$ with `Cad` ubiquitously expressed, and then proceeds through 3 iterations ($t1$-$t3$) in which the expression of `Fkh`, `Wg`, `Cad`, `D`, and `Opa` is synchronously updated based on the current state of the region. $t0$ represents stage 4, $t1$ represents early stage 5, $t2$ represents mid stage 5, and $t3$ represents stage 6. Over the course of a simulation, expression dynamics within each region are shaped both by the (potentially dynamic) inputs from `Tll` and `Hkb`, and by cross-regulation between the other factors. The limited number of expression updates reflects the rapid development of the *Drosophila* blastoderm, which limits the number of regulatory links (i.e., temporally distinct rounds of protein synthesis or decay) within any particular dynamical causal chain (***Nasiadka and Krause, 1999***). Mutant genotypes are simulated by keeping the relevant factor(s) turned off for all timepoints.

Genotype-by-genotype explanation of simulation output

This section explains the simulated patterning dynamics of each genotype in terms of their underlying regulatory logic. For the wild-type simulation, all expression changes across timepoints $t1 - t3$ are explained. For the mutant genotypes, only the differences from the wild-type simulation are explained. ***Appendix 4—Table 1*** lists the key properties of the simu-

lated expression patterns in each genotype, and, for each prediction, provides figure cross-references to real embryo data showing the same thing.

Wild-type (***Figure 8***C): At $t1$, all three timer genes have begun to be expressed, but they are differentially repressed by the terminal gap genes; D and Opa are more sensitive to Tll and so are repressed everywhere but region 1, while Cad is only repressed in region 4, due to the strong Hkb expression there. Fkh has been activated in regions 3 and 4 due to strong combined Hkb and Tll expression, together with activation from Cad.

At $t2$, the Cad expression domain has refined from both the anterior and the posterior. In region 1 it has been repressed by D, and in region 3 it has been repressed by the strengthening of Tll expression. Wg has been activated by Fkh in region 3, but remains repressed in region 4 by strong Hkb expression.

At $t3$, D has been repressed in region 1 by the strong Opa expression that has built up over time. Finally, D and Opa have been de-repressed in region 2, due to the previous clearance of Tll.

fkh^{-} (***Figure 8***D): due to the absence of Fkh, Wg is never activated in region 3.

cad$^{m\text{-}z}$ (***Figure 8***E): due to the absence of Cad, Fkh is never activated in regions 3-4, and Wg in turn is never activated in region 3. D is also expressed less strongly, both in region 1 and in region 2.

D^{-} (***Figure 8***F): due to the absence of D, Cad expression persists longer in region 1, although it is later repressed by Opa.

opa^{-} (***Figure 8***G): due to the absence of Opa, D is not repressed completely in region 1. The residual D expression in region 1 is weaker than in region 2, because only region 2 receives activation from Cad.

tor^{-} (***Figure 8***H, modelled as a *hkb*$^{-}$ *tll*$^{-}$ double mutant): in the absence of Tll and Hkb input, all regions behave exactly like region 1.

hkb^{-} (***Figure 8***I): due to the absence of Hkb, Cad expression persists for longer in region 4 and Wg is de-repressed. There is also a delay in Fkh and (therefore) Wg expression, which does not affect the final expression pattern.

tll^{-} (***Figure 8***J): due to the absence of Tll, the expression of all three timer genes is posteriorly expanded and the size of the Fkh domain is reduced. An assumption of graded early Hkb expression that represses D more anteriorly than Cad and Opa is necessary to explain the transient Cad expression in region 3: Cad is first repressed by D in regions 1 and 2, and only later by Opa in region 3. Because Fkh is not expressed outside the Hkb domain, Wg is never expressed.

tll^{-} *opa*$^{-}$ (***Figure 8***K): patterning resembles the *tll*$^{-}$ mutant through $t2$, but diverges at $t3$ due to the absence of Opa. Specifically, Cad expression in region 3 is allowed to persist, and D expression is de-repressed in region 3 after the clearance of Hkb. Weak D expression also persists in regions 1 and 2, similar to region 1 in *opa*$^{-}$ mutants.

Modified model for sequential segmentation

In ***Figure 8—figure Supplement 1***, the AP axis of a sequentially segmenting species is modelled as a growing array of "cells" with a Wg signalling centre at the posterior end, as in ***Clark, 2021***. The domain starts at one cell long at $t0$, then adds a cell each iteration by duplicating the most posterior cell. The range of effective Wg signalling is finite (in this case, 8 cells from the posterior signalling centre), so the zone of Wg signalling moves posteriorly with

time. Each cell may express Cad, D, and Opa, which are Boolean variables with the following regulatory logic:

```
Cad = 0 if Opa > 0 or (D > 0 and Wg < 1); else Cad = 1.
D = 0 if Opa > 0; else D = 1.
Opa = 0 if Cad > 0; else Opa = 1.
```

Thus, Cad is repressed by Opa and D but can be coexpressed with D in the presence of Wg signalling, D is repressed by Opa, and Opa is repressed by Cad. At each iteration, expression in each cell is updated synchronously, based on the current state of the cell.

Appendix 4—table 1: Cross-references for simulation output and corresponding expression data. For each simulated genotype, the "prediction / observation" column lists noteworthy behaviours of the system that were both predicted by the model and observed in real embryos. The relevant simulation timepoint(s) are listed, along with figure references for the corresponding expression data, and the stages of the embryos / expression traces shown. wt = wild-type; Fig = Figure; SFig = figure Supplement.

genotype	t	prediction / observation	corresponding data	stage(s)
wt	$t0$	*cad* expressed ubiquitously	Fig 2, SFig 2.2,2.4,5.3	4.4
wt	$t0$	Nested domains of *tll* and *hkb* already established	SFig 5.1	4.4
wt	$t0$	Expression of other factors either absent or just beginning	Fig2	4.4
wt	$t1$	*fkh* expressed where *tll* (and *hkb*) expression is strong	Fig 7A,B, SFig 7.1	5.4
wt	$t1$	*cad* clearing from posterior pole	Fig 2, SFig 2.4,5.3	5.2
wt	$t1$	*D* and *opa* expressed in trunk, complementary to *tll*	Fig 5A	5.2
wt	$t1$	Posterior *wg* not yet established	Fig 5B	5.2
wt	$t2$	*tll* domain retracts / narrows over time	Fig 5, SFig 5.3,5.4,5.5	5.2-5.5
wt	$t2$	*wg* expressed in *tll*-positive, *hkb*-negative territory	Fig 5B	5.4
wt	$t2$	*cad* clears from trunk and *tll* domain, expressed in between *D*/*opa* to the anterior and *tll*/*wg* to the posterior	Fig 2,3A,5	5.4-5.5
wt	$t2$	A gap opens up between the *tll* and *D*/*opa* domains	Fig 5A	5.2-5.5
wt	$t2$	A gap opens up between the *hkb* and *cad* domains	Fig 5B	5.3-5.5
wt	$t2$	*opa*/Opa expression builds up in the trunk over time	Fig 2,3, SFig 2.4,5.3,5.5	5.1-5.6
wt	$t3$	*D* expression clears from the trunk	Fig 2, SFig 2.3,2.4	6
wt	$t3$	*D* expression appears in the tail, coexpressed with *cad*	Fig 2,3A SFig 2.3,2.4	5.5-6
wt	$t3$	New *opa* expression appears within the tail, overlapping *cad*	Fig 3B	5.5-6
fkh^{-}	$t2$,$t3$	Posterior *wg* domain absent, patterning otherwise normal	Fig 7C,D	5.5
cad^{m-z-}	$t1$	Early *D* expression is weaker than wt	Fig 4C	5.2
cad^{m-z-}	$t1$-$t3$	*fkh* expression severely reduced	Fig 7A,B	5.4
cad^{m-z-}	$t2$-$t3$	Posterior *wg* domain absent	Fig 4A,B,7A,B, SFig 4.3	5.2-6
cad^{m-z-}	$t3$	Tail *D* expression reduced compared to wt	Fig 4, SFig 4.3	5.4-6
cad^{m-z-}	$t0$-$t3$	*tll*, *hkb*, and *opa* expression normal	Fig 4,7A,B, SFig 4.2,7.1	5.4-5.5
D^{-}	$t2$	*cad* expression persists longer in the trunk	Fig 4A,B	5.5
opa^{-}	$t3$	Weak *D* expression persists longer in the trunk	Fig 4A, SFig 4.5	5.5-6
tor^{-}	$t1$-$t3$	Expression of *cad*, *D*, and *opa* extends to the posterior pole	Fig 6B,G	5.2-5.5
tor^{-}	$t2$	*cad* expression clears from the embryo at the normal time	Fig 6B	5.4
tor^{-}	$t3$	*D* expression clears from the embryo at the normal time	Fig 6B	5.5
tor^{-}	$t2$-$t3$	The posterior *wg* domain is absent	Fig 6B	5.2-5.5
hkb^{-}	$t2$-$t3$	The posterior *wg* domain extends to the posterior pole	Fig 6E,G,7A,B	5.4-5.5
hkb^{-}	$t1$	*cad* expression persists longer in the posterior of the embryo	Fig 6E,G,7A,B	5.4
tll^{-}	$t1$-$t3$	The size of the *fkh* domain is reduced	Fig 7A,B	5.4
tll^{-}	$t1$-$t3$	*cad*, *D* and *opa* expression is posteriorly expanded	Fig 6C,D,G SFig 4.5	5.3-6
tll^{-}	$t1$-$t3$	*cad* and *opa* share a posterior border, *D* is slightly more anterior	Fig 6C,D, SFig 6.1	5.3-5.5
tll^{-}	$t2$	A transient *cad* stripe is expressed anterior to the *hkb* domain	Fig 6C,D, SFig 4.5	5.3-6
tll^{-}	$t3$	The *cad* stripe is repressed and there is no posterior *D* domain	Fig 6C, SFig 4.5	6
tll^{-} *opa*$^{-}$	$t3$	There is persistent posterior *cad* expression and a posterior *D* domain, unlike in *tll*$^{-}$	SFig 4.5	6

.

Figure 1—figure supplement 1. **A**: individual *wg*, *en* and DAPI (nuclei) channels from the two-channel and three-channel merges shown in ***Figure 1***A, plus two additional embryos (stage 5.2 and stage 5.4) showing *wg* and *en* expression at earlier stages. **B**: individual *slp*, *eve* and DAPI (nuclei) channels from the two-channel and three-channel merges shown in ***Figure 1***B. Embryo orientations as described for ***Figure 1***. Scale bars = 50 μm; grey lines show embryo outlines.

.

Figure 2—figure supplement 1. Additional single channel images. Individual DAPI (nuclei) and *wg* channels from the two-channel merges shown in the leftmost column of ***Figure 2***. All embryos are anterior left, dorsal up. Stages 4.3-6 show lateral views, stage 8.2 is a dorsolateral view. Scale bar = 50 μm; grey lines show embryo outlines.

.

Figure 2—figure supplement 2. Additional early stage embryos. Timer gene expression and DAPI (nuclei) staining in young wild-type embryos; note the weak, patchy *D* expression at stage 4.2. All embryos are anterior left, dorsal up, lateral view. Scale bar = 50 μm; grey lines show embryo outlines.

.

Figure 2—figure supplement 3. D antibody staining in embryos from stage 4 to stage 6. As the D antibody gave high background staining in the yolk, the D protein channel shows a mean z-projection of a thin 3D "shell" tracking the embryo surface, which significantly improved the signal:background ratio (see ***Appendix 2***). All embryos are anterior left, dorsal up, lateral view. Scale bar = 50 μm; grey lines show embryo outlines.

.

Figure 2—figure supplement 4. Expression dynamics of timer gene transcripts and proteins. **A-C**: quantitative expression traces (0-100% AP axis) from individual embryos of different ages, to convey the spatiotemporal dynamics of timer gene expression within the early embryo. The line colour of a given stage is the same across all plots (see legend at bottom left of figure). All traces in a given plot are from embryos from the same tube, imaged with the same microscope settings in the same imaging session. **A**: expression traces from a *wg*/*cad*/*opa*/*D* HCR (see example source embryos in ***Figure 2***). **B**: expression traces from a *wg*/*cad-Intron*/*opa*/Opa combined HCR and antibody stain (see example source embryos in ***Figure 3***). **C**: expression traces from a D antibody stain (see example source embryos in ***Figure 2—figure Supplement 3***). **D**: a rough approximation of timer gene expression dynamics at 50-60% AP axis, using normalised intensity measurements from the traces in A (*cad*, *D* and *opa* transcripts), B (Opa protein), C (D protein), and Figure 2B from ***Surkova et al., 2008*** (Cad protein). Note the transcript/protein time lags for expression peaks and troughs.

.

Figure 3—figure supplement 1. Single channel images. Individual channels from the two-channel and multi-channel merges shown in ***Figure 3***. All embryos are anterior left, dorsal up, lateral view. Scale bars = 50 μm (embryo posteriors), 20 μm (boxed close-ups); grey lines show embryo outlines.

.

Figure 4—figure supplement 1. Timer gene expression traces from timer gene mutants, relative to wild-type. **A**, **B**: plots showing quantitative expression traces (67.5-97.5% AP axis) from multiple stage 5.5 embryos, individually normalised to the range 0-1. Leftmost column shows traces from wild-type embryos (coloured lines); remaining columns show traces from *cad*$^{m-z-}$, *D*$^{-}$ or *opa*$^{-}$ mutants (coloured lines) overlaid on the same wild-type traces shown in the leftmost column (grey lines). **A**: traces without any alignment step; locations of borders / domains represent their absolute position along the AP axis. Note the loss of the *wg* posterior domain in *cad*$^{m-z-}$ mutants, the slight anterior shift and expansion of the fate map in *D*$^{-}$ mutants, and the stronger *D* tail domain in *opa*$^{-}$ mutants. **B**: all traces have been aligned with each other so that the *cad* posterior border from each embryo lines up with the others (see ***Appendix 2***). Note the broadened *cad* domain in *D*$^{-}$ mutants and the broadened *D* tail domain in *opa*$^{-}$ mutants. Note also the slightly increased distance between *opa* and *wg* in *D*$^{-}$ mutants. Source data is the same as ***Figure 4***.

.

Figure 4—figure supplement 2. Full-length *opa* expression traces from timer gene mutants. Plots showing quantitative expression traces (0-100% AP axis) from multiple stage 5.5 embryos, individually normalised to the range 0-1. Top left plot shows *opa* expression in wild-type embryos (orange lines); other plots show *opa* expression from *cad*$^{m-z-}$, *D*$^{-}$ or *opa*$^{-}$ mutants (orange lines) overlaid on the same wild-type traces shown in the top left plot (grey lines). Note the marked AP modulation of *opa* expression in the *cad*$^{m-z-}$ mutants, and the anteriorly shifted position of the *opa* posterior border in *D*$^{-}$ mutants. Source data is the same as ***Figure 4***.

.

Figure 4—figure supplement 3. Additional characterisation of *cad*$^{m-z-}$, *cad*$^{m-z+}$, and *cad*$^{m+z-}$ mutants. **A**: *wg*, *D* and *msh* expression in wild-type and *cad*$^{m-z-}$ mutants. Transmitted light images of a sagittal section through the dorsal membrane surface (used for embryo staging) are shown at top right; black arrowheads mark the invagination of the plasma membrane. Note the early / ectopic expression of *msh* in the *cad*$^{m-z-}$ mutants, especially in the posterior of the embryo. **B**: *wg*, *cad* and *D* expression in wild-type and *cad*$^{m+z-}$ (zygotic) mutants. Note the normal *D* expression in the *cad*$^{m+z-}$ mutant at stage 6 but the absence of the *D* tail domain in the *cad*$^{m+z-}$ mutant at stage 8 (white arrowheads). **C**: *wg*, *cad* and *D* expression in a *cad*$^{m-z-}$ mutant (top) compared to a paternally rescued *cad*$^{m-z+}$ mutant (bottom, note the *lacZ* expression in the head from the *hb-lacZ* marked balancer). Note that the *D* tail domain is rescued in the *cad*$^{m-z+}$ mutant (white arrowheads). The posterior *wg* expression domain is also partially rescued (white arrows), as is the segmental pattern. *cad* and *D* expression resembles the *cad*$^{m-z-}$ mutant. All embryos are anterior left, dorsal up. All embryos except the dorsolateral stage 8 wild-type embryo in B are lateral views. Scale bars = 50 μm (whole embryos), 20 μm (membrane close-ups); grey lines show embryo outlines.

.

Figure 4—figure supplement 4. Timer gene expression in *wg*$^{-}$ mutants at stage 6. Left column shows a multi-channel merge; other columns show individual channels. (Note that the *wg*$^{-}$ embryo pictured is slightly younger than the wild-type embryo and so does not show the same pattern of weak pair-rule *cad* stripes in the trunk. Older *wg*$^{-}$ embryos express these stripes as normal.) Both embryos are anterior left, dorsal up, lateral view. Scale bar = 50 μm; grey lines show embryo outlines.

.

Figure 4—figure supplement 5. Timer gene expression in *opa*$^-$, *tll*$^-$, and *tll*$^-$ *opa*$^-$ embryos at stage 6. Individual *cad*, *D*, and *opa* channels are shown for each genotype, as well as two-channel merges with *wg*. Multi-channel merges with and without the DAPI (nuclei) channel are also shown in the left column. White arrowheads point to the *D* tail domain – note that it is expanded in the *opa*$^-$ mutant, absent in the *tll*$^-$ mutant, and "rescued" (though posteriorly shifted) in the *tll*$^-$*opa*$^-$ mutant. Note also that the *cad* tail domain is slightly broader than normal at this stage in the *opa*$^-$ mutant, weak/fading in the *tll*$^-$ mutant, and partially rescued (though again, posteriorly shifted) in the *tll*$^-$ *opa*$^-$ mutant. All embryos are anterior left, dorsal up, lateral or ventrolateral views. Scale bar = 50 μm; grey lines show embryo outlines.

.

Figure 4—figure supplement 6. Morphological differences between wild-type and *cad*$^{m\text{-}z\text{-}}$ blastoderms. **A**: DAPI (nuclei) staining from a wild-type vs a *cad*$^{m\text{-}z\text{-}}$ embryo. The *cad*$^{m\text{-}z\text{-}}$ embryo is bigger and broader in the xy maximum projection, and shows a dimple in the surface in the xy (frontal) and zy (transverse) sections. **B**: scatter plot showing the AP (x-axis) and DV (y-axis) lengths of the embryo masks for n=78 wild-type embryos and n=73 *cad*$^{m\text{-}z\text{-}}$ embryos; note that the *cad*$^{m\text{-}z\text{-}}$ measurements are on average larger, particularly in DV. **C**: violin plots comparing the AP length, DV length, and fineness ratio (AP length / DV length) for the embryos in B. The rightmost violin plot compares the thickness in the z-axis (top surface of the embryo to mid-yolk) for a separate set of n=29 wild-type embryos and n=29 *cad*$^{m\text{-}z\text{-}}$ embryos. Horizontal lines on the violin plots mark minimum, mean and maximum values. Measurements were taken from embryos sourced from a variety of different imaging sessions and there should be no systematic differences in mounting technique. The means of all measurements shown in the violin plots are significantly different (two-tailed t-test). AP length: wild-type mean 503.5 μm, *cad*$^{m\text{-}z\text{-}}$ mean 512.3 μm; $t = -3.12$, $p = 0.002$. DV length: wild-type mean 217.9 μm, *cad*$^{m\text{-}z\text{-}}$ mean 244.8 μm; $t = -9.76$, $p = 1.0x10^{-17}$. Fineness ratio: wild-type mean 2.32, *cad*$^{m\text{-}z\text{-}}$ mean 2.10; $t = 8.11$, $p = 1.7x10^{-13}$. Thickness in z: wild-type mean 72.8 μm, *cad*$^{m\text{-}z\text{-}}$ mean 65.0 μm; $t = 3.27$, $p = 0.002$. Scale bar = 50 μm.

.

Figure 5—figure supplement 1. Expression of *tll* and *hkb* in wild-type embryos from stage 2 to stage 6. The adjusted ("adj.") images for the stage 2-4.3 embryos have altered brightness and contrast to better show the early expression of *tll* and *hkb*. All embryos are anterior left, dorsal up, lateral view. Scale bar = 50 μm; grey lines show embryo outlines.

.

Figure 5—figure supplement 2. Single channel images. Individual channels from the two-channel and three-channel merges shown in ***Figure 5***. All embryos are anterior left, dorsal up, lateral view. Scale bar = 50 μm; grey lines show embryo outlines.

.

Figure 5—figure supplement 3. Expression dynamics of *tll* and *hkb* transcripts. **A**,**B**: quantitative expression traces (0-100% AP axis) from individual embryos of different ages, to convey the spatiotemporal dynamics of gene expression within the early embryo. All traces in a given plot are from embryos from the same tube imaged with the same microscope settings in the same imaging session. The stage corresponding to each line colour is shown in the legends below the plots (colours are consistent between plots). **A**: expression traces from a *tll*/*cad*/*D*/*opa* HCR (see example source embryos in ***Figure 5***A). Note the posterior retraction of the *tll* boundary between stages as well as the rise and fall in *tll* expression levels. **B**: expression traces from a *tll*/*cad*/*wg*/*hkb* HCR (see example source embryos in ***Figure 5***B). Note the greater posterior retraction of the *tll* border compared to *hkb*, and the more pronounced fall in expression levels over stage 5.

.

Figure 5—figure supplement 4. Relative expression dynamics of Tll protein and *tll* transcript. **A**,**B**: quantitative expression traces (0-100% AP axis) from individual embryos of different ages, to convey the relative expression (A) or spatiotemporal dynamics (B) of gene expression within the early embryo (an example source embryo is shown in ***Figure 5—figure Supplement 6***A). All traces in a given plot are from embryos from the same tube imaged in the same imaging session with the same microscope settings. Legends for gene products (A) or embryo stages (B) are shown below the plots. **A**: *tll*/Tll/*eve* traces from individual embryos of different ages; note the time lag for Tll protein levels compared to *tll* transcript, as well as the relative positions of their posterior domain borders at stage 5.4 and stage 5.5. **B**: the same data as in A, except that plots are grouped by gene product rather than by embryo. Note the different temporal dynamics of Tll protein compared to *tll* transcript, and the posterior retraction of both posterior domain borders. The *eve* channel was used for embryo staging; note that the stripes in older embryos are more refined and have shifted anteriorly across the blastoderm.

.

Figure 5—figure supplement 5. Relative expression dynamics of Hkb, Tll and Opa proteins. **A**,**B**: quantitative expression traces (0-100% AP axis) from individual embryos of different ages, to convey the relative expression (A) or spatiotemporal dynamics (B) of Hkb, Tll and Opa protein expression within the early embryo (an example source embryo is shown in ***Figure 5—figure Supplement 6***B). All traces in a given plot are from embryos from the same tube imaged in the same imaging session with the same microscope settings. Legends for gene products (A) or embryo stages (B) are shown below the plots. **A**: Hkb/Tll/Opa expression from individual embryos of different ages; note the nested domain of Tll and Hkb and the correlation between the Tll and Opa borders. **B**: the same data as in A, except that plots are grouped by protein rather than by embryo. In all plots, the Opa channel has been linearly unmixed from the Hkb channel to remove bleedthrough signal from Hkb in the poles of the embryo.

.

Figure 5—figure supplement 6. Examples of source imaging data for supplementary plots. **A**, **B**: examples of individual embryos from the imaging datasets used to extract the expression traces shown in ***Figure 5—figure Supplement 4*** (A) and ***Figure 5—figure Supplement 5*** (B). **A**: Tll antibody/*tll* HCR/*eve* HCR. **B**: Tll/Hkb/Opa antibody stain. Both embryos are anterior left, dorsal up, lateral view. Scale bar = 50 μm; grey lines show embryo outlines.

.

Figure 6—figure supplement 1. Timer gene expression traces from terminal system mutants, relative to wild-type. **A**, **B**: plots showing quantitative expression traces (75-100% AP axis) from multiple stage 5.5 embryos, individually normalised to the range 0-1. Leftmost column shows traces from wild-type embryos (coloured lines); remaining columns show traces from *tor*$^{-}$, *tll*$^{-}$ or *hkb*$^{-}$ mutants (coloured lines) overlaid on the same wild-type traces shown in the leftmost column (grey lines). **A**: in *tor*$^{-}$ mutants, note the loss of spatial patterning. In *tll*$^{-}$ mutants, note the posterior shifts of the *cad*, *D*, and *opa* posterior boundaries and the loss of the posterior *wg* domain. In *hkb*$^{-}$ mutants, note the posterior shifts of all boundaries and the extension of the posterior *wg* domain to the posterior pole. **B**: note the posterior shift of the *tll* boundary in *hkb*$^{-}$ mutants, in addition to the posterior shifts of the *cad*, *D*, and *opa* boundaries also seen in for the *hkb*$^{-}$ mutants in A. Source data is the same as ***Figure 6***.

.

Figure 6—figure supplement 2. Expression of *tll* in wild-type and *hkb*$^{-}$ embryos from stage 5.5 to stage 7. Note that the posterior domain persists for longer in the *hkb*$^{-}$ mutants, and ectopic expression appears at the anterior pole. All embryos are anterior left, dorsal up, lateral views. Scale bar = 50 μm; grey lines show embryo outlines.

.

Figure 7—figure supplement 1. Terminal gene expression traces from *cad*$^{m\text{-}z\text{-}}$, *tll*$^{-}$ and *hkb*$^{-}$ mutants, relative to wild-type. **A**, **B**: plots showing quantitative expression traces (75-100% AP axis) from multiple stage 5.4 and stage 5.5 embryos, individually normalised to the range 0-1. Leftmost column shows traces from wild-type embryos (coloured lines); remaining columns show traces from *cad*$^{m\text{-}z\text{-}}$, *tll*$^{-}$ or *hkb*$^{-}$ mutants (coloured lines) overlaid on the same wild-type traces shown in the leftmost column (grey lines). **A**: in *cad*$^{m\text{-}z\text{-}}$ mutants, note the severe reduction in *fkh* levels, the loss of the posterior *wg* domain, and the persistence of *cad* expression in the trunk. In *tll*$^{-}$ mutants, note the reduced size of the *fkh* domain and the posterior shift of the *cad* domain. In *hkb*$^{-}$ mutants, note the reduced sizes of the *tll* and *fkh* domains, the posterior shifts of the *wg* and *cad* domains, and the total (*wg*) or partial (*cad*) derepression of expression in the posterior of the embryo. **B**: a similar combination of genes is shown, with *hkb* in place of *cad*. Note that the size of the *hkb* domain is unaffected in either *cad*$^{m\text{-}z\text{-}}$ or *tll*$^{-}$ mutants. The *tll*$^{-}$ traces in both A and B are taken from a single *wg*/*cad*/*hkb*/*fkh* stain. Source data fis the same as ***Figure 7***.

.

Figure 7—figure supplement 2. Timer gene expression traces from *fkh*$^{-}$ mutants, relative to wild-type. Plots showing quantitative expression traces (67.5-97.5% AP axis) from multiple stage 5.5 embryos, individually normalised to the range 0-1. Left column shows traces from wild-type embryos (coloured lines); right column shows traces from *fkh*$^{-}$ mutants (coloured lines) overlaid on the same wild-type traces shown on the left (grey lines). Note the loss of the *wg* posterior domain in *fkh*$^{-}$ mutants. Source data is the same as ***Figure 7***.

.

Figure 7—figure supplement 3. *wg* and *cad* expression in *fkh*$^{-}$ mutants at stages 6 and 7. Black arrowheads mark the posterior *wg* domain (severely reduced in *fkh*$^{-}$ mutants). White arrowheads mark the *cad* tail domain. In the stage 6 wild-type embryo, note the additional *cad* domain posteriorly abutting the posterior *wg* domain (white arrow). This domain (corresponding to presumptive Malpighian tubules and proximal posterior midgut; ***Harbecke, 1989***) is absent in stage 6 *fkh*$^{-}$ mutants. In *fkh*$^{-}$ mutants, new *cad* expression instead appears later, at the posterior edge of the tail domain (white arrow in the stage 7 embryo, pointing at prominent transcriptional foci). MD1 = mitotic domain 1 (used for embryo staging). All embryos are anterior left, dorsal up, lateral or ventrolateral views. Scale bar = 50 μm; grey lines show embryo outlines.

.

Figure 7—figure supplement 4. Abnormal morphogenesis in *cad*$^{m\text{-}z\text{-}}$ and *fkh*$^{-}$ mutants. *wg* expression and DAPI (nuclei) staining from wild-type, *cad*$^{m\text{-}z\text{-}}$ mutant and *fkh*$^{-}$ mutant embryos at stage 6, stage 7 and stage 8. Embryos were staged by the presence of mitotic domain 1 (MD1, stage 7) or mitotic domain 4 (MD4, stage 8). Note the delayed proctodaeal invagination seen in both *cad*$^{m\text{-}z\text{-}}$ and *fkh*$^{-}$ mutants relative to wild-type embryos. Note also the epithelial buckling in *fkh*$^{-}$ mutants (arrowheads at stage 6 and stage 7), reminiscent of *folded gastrulation* (*fog*$^{-}$) mutants (***Sweeton et al., 1991***). Both *cad*$^{m\text{-}z\text{-}}$ and *fkh*$^{-}$ mutants also mostly lack the posterior *wg* domain (arrows). All embryos are anterior left, dorsal up, lateral or dorsolateral views. Scale bar = 50 μm; grey lines show embryo outlines.

.

Figure 8—figure supplement 1. Simulation of a hypothetical timer gene network for sequential segmentation. **A**: Arrow diagram showing a hypothetical timer gene network for sequential segmentation. Pointed arrowheads represent activation; flat arrowheads represent repression. Solid arrows are interactions taken from the *Drosophila* timer gene network in ***Figure 8***A; dotted arrows are two additional interactions that might be present in sequentially segmenting species. The arrow from Wg to Cad supposes that Wg signalling from a posterior signalling centre activates *cad* expression, even in the presence of D. [Note that both Sox and Zic transcription factors can have different regulatory effects in the presence or absence of Wnt signalling, via molecular interactions with β-catenin and TCF (***Pourebrahim et al., 2011***; ***Murgan et al., 2015***; ***Mukherjee et al., 2022***)]. The arrow from Cad to Opa completes an "AC-DC circuit" network motif (***Panovska-Griffiths et al., 2013***; ***Perez-Carrasco et al., 2018***) between the timer genes. **B**: simulation output from a model of the network in A operating in a scenario of posterior Wg signalling and AP axial growth (see ***Appendix 4***). Each plot shows axial expression of the logical variables `Wg`, `Cad`, `D`, and `Opa` at a different timepoint in the simulation ($t0$-$t30$). The position of the `Wg` signalling centre (dark yellow rectangle) marks the posterior of the elongating AP axis; the spatial extent of `Wg` signalling is also shown (light yellow rectangle). Close to the posterior `Wg` signalling centre, `Cad` is activated by `Wg`, in turn activating `D` and keeping `Opa` repressed. Further away from the signalling centre, repression of `Cad` by `D` kicks in. `Cad` turns off, repression of `Opa` is lifted, and `Opa` in turn represses both `Cad` and `D`. Combined with the axial elongation of the tissue, this scenario produces posteriorly-shifting wavefront dynamics (the transition between `Cad`/`D` and `Opa` expression moves posteriorly across the axis over time), similar to those found in *Tribolium* (***Clark and Peel, 2018***).